# Characterisation of High Modulus Asphalt (EME) Mixes, focussing on Flexural Response and Fatigue

By

Barend Hendrik Botes

**Dissertation**

Submitted to the Department of Civil Engineering,
Faculty of Engineering, University of Stellenbosch
In fulfilment for the degree

**Master of Engineering**

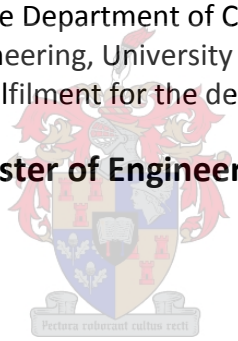


**Supervisor**
Prof Kim Jenkins PhD
SANRAL Chair in Pavement Engineering
Faculty of Engineering
Department of Civil Engineering

**Co-Supervisor**
Me Chantal Rudman
Faculty of Engineering
Department of Civil Engineering

December 2016

# DECLARATION

By submitting this thesis electronically, I declare that the entirety of the work contained therein is my own, original work, that I am the sole author thereof (save to the extent explicitly otherwise stated), that reproduction and publication thereof by Stellenbosch University will not infringe any third party rights and that I have not previously in its entirety or in part submitted it for obtaining any qualification.

Signature: .....

Date: .....

# SUMMARY

The road construction industry is faced with the challenge of designing and constructing high performance asphalt materials to meet the ever growing demand of increasing traffic volumes and axle loadings. EME (Enrobés à Module Elevé) or simply high modulus asphalt was developed in France in the mid-seventies. EME asphalt provides a high performance material for the use in heavy duty pavements. EME asphalt has a very high resistance in terms of permanent deformation as well as a stiffness surpassing that of standard mixes used in base layers. EME mixes also have a good resistance to fatigue due to the high binder content of the mix.

Numerous studies have investigated the fatigue resistance of hot-mix asphalt (HMA) mixtures, with limited research into EME mixes on the basis of its material properties and structural responses. In this study, a Four Point Beam fatigue apparatus was used to measure the fatigue response of a certain EME mix at various strain values (50, 100, 175, 250 με) and temperatures (10 and 40˚C) under a pulse frequency of 10Hz. Both a haversine and sinusoidal loading profile was investigated in terms of the Four Point Beam Test (4PBT). In this regard, it was concluded that sinusoidal loading was the only viable loading option. At low temperatures and high strain values, haversine loading caused premature failure in a number of beam specimens. This conclusion was confirmed with the help of a numerical analysis, done in ABAQUS FAE, in order to investigate initial tensile stresses in the beam specimens with the application of both loading profiles.

Witczak, et al. (2013) indicated that during the sinusoidal test, the deflection pattern is sinusoidal, bending the beam specimen in both directions. The neutral axis of the beam stays unchanged during the test, as it remains in the original position halfway between the two extreme deflection positions. During the haversine test, the deflection pattern is haversine, bending the beam with the same peak-to-peak magnitude as the sinusoidal test but only in one direction. Because of the static force component in the load signal and the viscous character of the material, creep (permanent deformation) will occur in the beam, causing the neutral axis of the beam to shift downwards after a few loading cycles. After the shift of the neutral axis the original haversine loading pattern will become a sinusoidal loading pattern with respect to the new neutral axis. This phenomenon was confirmed through the applied loading outputs from the 4PBT.

Using the Four Point Beam apparatus, frequency-temperature sweeps were done at pulse frequencies of 0.5, 1, 2, 5 and 10 Hz with conditioning temperatures ranging from 10˚C to 40˚C at 5˚C intervals. The frequency and temperature sweeps were done to develop the stiffness Master Curves, in order to create a framework for predicting stiffness versus loading time relationship for the investigated EME asphaltic material.

In this study, principles regarding EME, findings on the flexural fatigue performance and discussions of data as well as recommendations and conclusions are made. The recommendations serves as a vital part of the research study as EME testing, in South Africa, has not yet been conducted on the scale in which it is covered during this study. The recommendations would thus be helpful with regards to future testing and research on the subject.

# OPSOMMING

Die pad konstruksiebedryf word gekonfronteer met die uitdaging om hoë werks verrigtende asfalt materiale, wat die steeds groeiende toename in verkeers volumes en as-laste kan hanteer, te onwerp en bou. EME (Enrobés à Module Elevé) of bloot hoëmodulus asfalt is in die middel sewentigerjare in Frankryk ontwikkel. EME asfalt bied 'n hoë verrigtende materiaal vir die gebruik in swaar belaste paaie. EME asfalt het ‘n baie hoë weerstand in terme van permanente vervorming asook ‘n styfheid wat dié van standard mengsels, wat in basislae gebruik word, oortref. EME mengsels bied 'n goeie weerstand teen vermoeiing as gevolg van die hoë bindstof inhoud wat in hierdie mengsels gevind word.

Verskeie studies is al ingestel om die weerstand teen vermoeing, van warm-mengsel asfalt (HMA), te ondersoek. Slegs ‘n beperkte hoeveelheid navorsing, in terme van EME op grond van sy materiaal eienskappe en strukturele reaksie, is al gedoen. In hierdie studie is ‘n Vier Punt Buig apparaat gebruik om die vermoeing van ‘n gegewe EME mengsel, by verskeie spannings (50, 100, 175, 250 με) en temperatuur waardes (10 en 40°C) onder ‘n pols frekwensie van 10 Hz, te ondersoek. Beide ‘n haversine en sinusvormige laai profiel is ondersoek, in terme van die Vier Punt Buig Toets (4PBT). In hierdie verband is daar tot die gevolgtrekking gekom dat die sinusvormige laai profiel die enigste haalbare opsie is. By die lae temperature en hoë spanning waardes het die haversine laai profiel voortydige faling in ‘n aantal van die balk monsters veroorsaak. Hierdie gevolgtrekking is bevestig met die hulp van ‘n numeries analise, wat in ABAQUS FAE gedoen is, ten einde die aanvanklike trek spanning in die balk monsters met die toepassing van beide laai profiele te ondersoek.

Witczak, et al. (2013) het aangedui dat tydens die sinusvormige toets, die defleksie patroon sinusvormig is, die balk word dus in buide rigtings gebuig. Die neutral as van die balk bly onveranderd, halfpad tussen die twee uiterste defleksie posisies. Gedurende die haversine toets, is die defleksie patroon haversine, die balk buig dus met dieselfde piek-tot-piek grootte as die sinusvormige toets maar slegs in een rigting. As gevolg van die statiese krag komponent in die las sein en die viskeuse karakter van die materiaal, vind kruip (permanente vervorming) plaas in die balk. Hierdie veroorsaak dan dat die neutrale as van die balk, na afloop van 'n paar laai siklusse, afwaarts skuif. Na aanloop van die verskuiwing van die neutrale as, verander die oorspronklike haversine laai patroon na 'n sinusvormige laai patroon, ten opsigte van die nuwe

neutrale as. Hierdie verskynsel is bevestig deur gebruik te maak van die toepassing laai uitsette van die 4PBT.

Deur gebruik te maak van die Vier Punt Buig apparaat, is ferkwensie-temperatuur “sweeps” gedoen by pols frekwensies van 0.5, 1, 2, 5 en 10 Hz met kondisionerings temperature wat wissel van 10°C tot 40°C op 5˚C intervalle. Die frekwensie en temperatuur “sweeps” is gedoen om die styfheid Meester Kurwes te ontwikkel, ten einde 'n raamwerk vir die voorspelling van styfheid teen laai tyd verhouding, vir die EME asfalt materiaal te ontwikkel.

In hierdie studie word, beginsels rakende EME, bevindings oor die buig vermoeing eienskappe en besprekings van data asook aanbevelings en gevolgtrekkings gemaak. Die aanbevelings dien as 'n belangrike deel van die navorsingstudie, aangesien toetse op EME, nog nie in Suid-Afrika op die skaal gedoen is waarop dit in hierdie studie gedoen is nie. Die aanbevelings sal dus nuttig wees met betrekking tot toekomstige toetse en navorsing wat oor die onderwerp handel.

# ACKNOWLEDGEMENTS

I gratefully acknowledge the following people:

- Prof Kim Jenkins for selfless contribution of time, support, assistance and unrelenting knowledge he shared throughout the span of the project. The friendliness, support and motivation was not taken for granted.

- Me Chantal Rudman for the sound advice and guidance she gave me throughout the project. The selfless support she gave towards the project is greatly appreciated.

- Royal HaskoningDHV (Pty) Ltd, and especially Johan van Heerden and Imran Amien for their guidance with respect to the tests done for the project as well as the time they contributed towards the project.

- All the laboratory staff at Much Asphalt as well as Colin Brooks for the preparation and compaction of the slab specimens as used in the project.

- To my parents (Ben and Elriëtte Botes) for laying the foundation for my success as well as their unending love, encouragement and financial support.

- To my girlfriend Christel Smit for her patience, support and love throughout the years.

- Last but not least to the Almighty Lord, for blessing me with the talents and people in my life that make me who I am.

# TABLE OF CONTENT

**CHAPTER THREE**



**CHAPTER FOUR**

# LIST OF FIGURES

# LIST OF TABLES

# LIST OF GRAPHS

# LIST OF ABREVIATIONS

| | | |
|---|---|---|
| 4PBT | : | Four Point Beam Testing |
| AASHTO | : | American Association of State Highway and Transportation Officials |
| AFNOR | : | Association Française de Normalisation |
| ASTM | : | American Society for Testing and Materials |
| BRD | : | Bulk Relative Density |
| CSIR | : | Council for Scientific and Industrial Research |
| EME | : | Enrobés à Module Elevé |
| GHG | : | Greenhouse Gas |
| HiMA | : | High Modulus Asphalt |
| HMA | : | Hot Mix Asphalt |
| IPC | : | Industrial Process Control |
| ITSM | : | Indirect Tensile Stiffness Modulus |
| LCPC | : | Laboratoire Central des Ponts et Chaussées |
| LVDT | : | Linear Variable Differential Transducer |
| OAPEC | : | Organization of Arab Petroleum Exporting Countries |
| PCG | : | Presse à Cisaillement Giratoire |
| PG | : | Performance Grading |
| PV | : | Plateau Value |
| R&B | : | Ring and Ball |
| RDEC | : | Ratio of Dissipated Energy Change |
| RTFOT | : | Rolling Thin-Film Oven Test |
| SANRAL | : | South African National Roads Agency Limited |
| SARDS | : | South African Road Design System |

# CHAPTER ONE

# 1. INTRODUCTION

## 1.1. BACKGROUND

The road construction industry is faced with the challenge of designing and constructing high performance asphalt materials to meet the ever growing demand of increasing traffic volumes and axle loadings. EME (Enrobés à Module Elevé) or simply high modulus asphalt was developed in France in the mid-seventies. EME asphalt provides a high performance material for the use in heavy duty pavements, specifically suitable in the following situations:

- pavements that carry large volumes of heavy vehicles and require increased load spreading ability in order to protect underlying layers.
- where constraints in the allowable pavement thickness exist, normally in urban areas or motorways where geometric considerations need to be taken into account.
- areas that experience heavy traffic, such as slow lanes, climbing lanes, bus lanes and airport pavements, where an increased resistance to permanent deformation is needed.

EME asphalt is intended to have a very high resistance in terms of permanent deformation as well as a stiffness surpassing that of standard mixes used in base layers. EME mixes also have a good resistance to fatigue due to the high binder content of the mix.

## 1.2. EME BENEFITS

The layer stiffness provides a good indication of the load spreading capacity of the layer. The high shear strength and stiffness properties associated with EME improves the load spreading ability within the pavement. This shear strength and stiffness of EME is very high in relation to normal asphalt, causing the imposed stresses to also be dissipated more quickly in the EME layer. The typical stress distribution within a pavement consisting of an HMA surface or base layer, as well as pavement consisting of an EME surface or base layer is illustrated in Figure 1-1 and Figure 1-2 respectively.

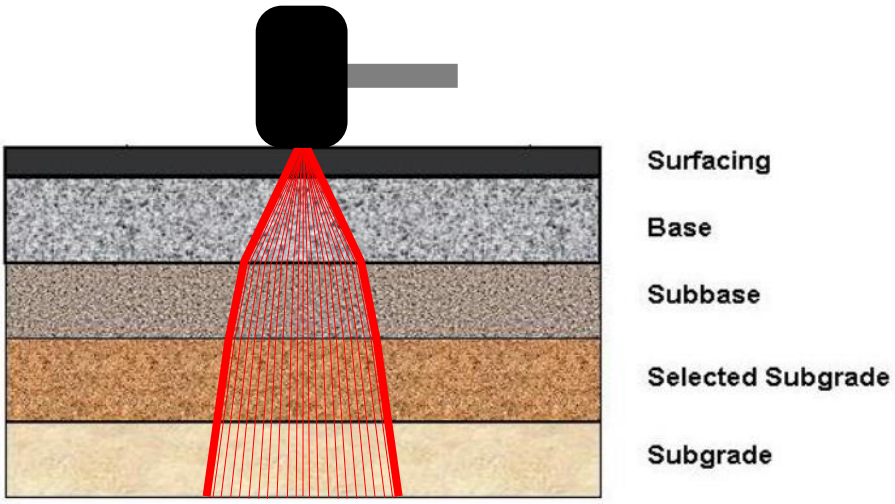


*Figure 1—1: Typical stress distribution in HMA pavement*

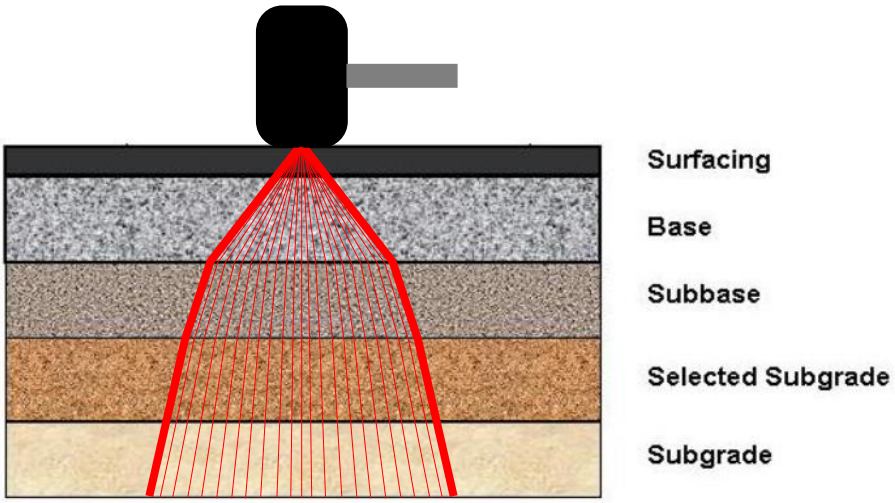


*Figure 1—2: Typical stress distribution in EME pavement*

EME asphalt can be considered as a cost-effective option when bearing in mind the following added benefits it poses:

- a reduction in layer thickness,
- a reduction in the overall life cycle costs,
- a reduction in the road user delay costs,
- improved durability,
- an increase in the sustainability of pavement structure.

## 1.3. THE IDENTIFICATION OF ENGINEERING PROPERTIES

The future success and implementation of EME technology in South Africa is greatly dependent on its performance with regards to certain engineering properties. This research study investigates the flexural stiffness (as a mix property) and fatigue cracking (as a performance criteria) of EME asphalt, as engineering properties.

**Flexural Stiffness**

The flexural stiffness of an asphalt mix is of paramount importance in predicting how well a pavement will perform and is essential for analysing pavement response to traffic loading. Flexural stiffness provides a measure of the load spreading ability of a pavement, at a given temperature and loading time. The stiffness modulus can be defined as a ratio of the stress and strain under uni-axial loading conditions. The resilient modulus is expressed as the measure of reduction in the applied stress pulses, as a result of loading, as opposed to the recoverable (resilient) strain.

**Flexural Stiffness and Master Curve development**

A Master Curve illustrates a relationship between binder stiffness and the reduced frequency over a wide range of temperatures and frequencies. A Master Curve, thus makes it possible for the viscoelastic properties of a mix to be predicted over a wide range of frequencies and temperatures, as it provide a function of temperature and frequency.

**Fatigue Cracking**

Fatigue cracking is regarded as one of the primary damage mechanisms of asphalt pavements. The occurrence of fatigue cracking can be attributed to numerous factors among which is applied load, load frequency and temperature changes or a combination of these factors. Fatigue cracking results from cyclic stresses that are lower than the ultimate tensile stress, or even the yield stress of the material. The cumulative damage concept serves as the basis for the prediction of fatigue cracking in asphalt pavements. It considers the number of allowable load repetitions related to the tensile strain at the bottom of the asphalt layer.

## 1.4. AIMS AND OBJECTIVES OF THE STUDY

The primary objective of the research study is to measure the fatigue and flexural performance behavior of EME. As a result, the research study undertakes a laboratory evaluation of EME in order to investigate the relative fatigue performance and flexural stiffness. Because of the relatively new nature of EME, especially in South Africa, there exist numerous uncertainties and challenges with regards to the technology and application of EME. This research study also aims to shed some light on these uncertainties, by giving relevant recommendations and forming educated conclusions.

The secondary objectives to achieve the main objective are as follow (see Figure 1-3):

- the determination of flexural stiffness and fatigue performance of EME in order to depict the fatigue life of EME at intermediate pavement operating temperatures.
- the development of Master Curve graphs in order to create a framework for predicting stiffness versus loading time relationship for the EME asphaltic material
- the setting up of transfer functions for EME to assist in future designs
- numerical modelling of EME beams in ABAQUS FAE and comparing results with laboratory results in order to validate the findings of the project

The laboratory evaluation of EME for fatigue and flexural stiffness was undertaken using the IPC Four Point Bending Beam Fatigue Apparatus.

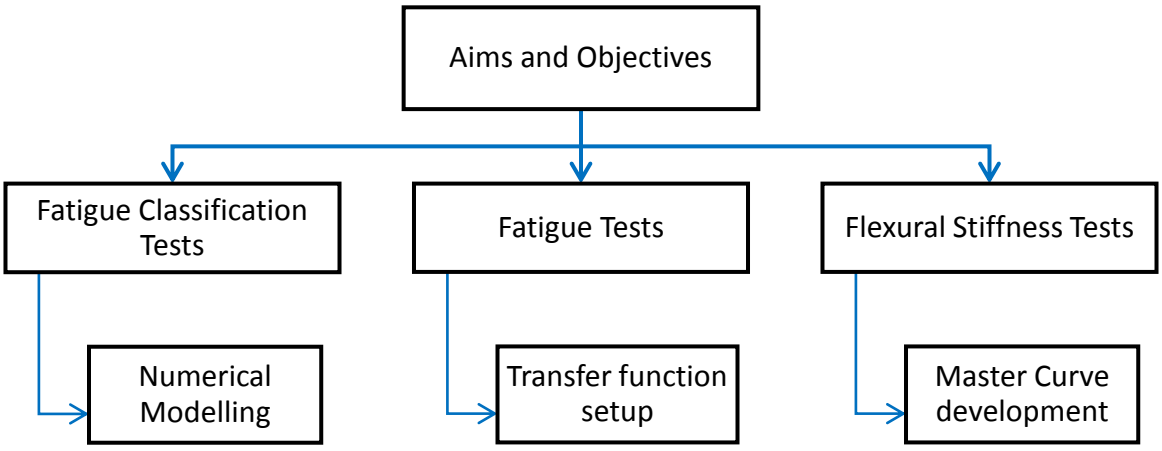


*Figure 1—3: Aims and Objectives of study*

## 1.5. LIMITATIONS OF THE STUDY

The following limitations were identified with regards to the study at hand:

- All of the EME specimens that were tested in the study were laboratory made. No reference is made to field samples.
- Limitations with regards to the Four Point Bending machine compliance were encountered, as a result of the high stiffness of EME at low temperatures (10˚C) and high frequencies (10 Hz).
- The limited amount of research and tests on EME in South Africa also proofed to be a limitation, as comparison and reference could not be made to previous work.

## 1.6. SCOPE OF THE STUDY

This research study is divided into four main parts:

- Chapter Two highlights the research principles that shed some light on EME as well as the performance related aspects as literature study regarding the subject matter.
- Chapter Three notes of the scope of work and activities undertaken including methodology used for testing and evaluation.
- Chapter Four reports on the findings, laboratory results as well as analyses of the data acquired and results attained from the laboratory evaluation.
- Chapter Five includes recommendations and conclusions of the study.

## 1.7. ENGINEERING AND ENVIRONMENTAL SIGNIFICANCE

With the ever-growing demand of increasing traffic volumes and axle loadings, the road construction industry is faced with the challenge of designing and constructing high performance asphalt materials to meet this demand. EME asphalt provides a high performance material for use in heavy duty pavements. However, because of the relative new nature of EME technology, it requires validation regarding key performance aspects such as fatigue performance and mechanical properties. In South Africa, limited research has been done on these key performance aspects of EME. This research-study aim to contribute to the initiation of

EME technology into the road construction industry by investigating the fatigue performance and mechanical properties of EME.

The engineering significance of this study can also be asserted for by the fact that it forms part of the EME N1/1 project, conducted by SANRAL, for the Master Curve Development and Fatigue Testing on Enrobés à Module Elevé (EME) asphalt that was used on the N1/1 between the Toll Plaza and the Huguenot Tunnel.

Greenhouse gas (GHG) emissions from the oil refining and petrochemical industry, contribute to a significant amount of the global GHG emissions. Reducing the layer thickness of the bituminous layer in the pavement structure the amount of bitumen is also reduced. This small saving on the amount of bitumen may have a large effect on the GHG emissions that goes along with it.

# CHAPTER TWO

# 2. LITERATURE SURVEY

## 2.1. INTRODUCTION

The evaluation of pavement materials is essential with regards to the selection and application of materials, the determination of the structural capacity and probable material performance. In order to obtain realistic field results, the evaluation should account for material performance under loading and environmental effects.

Moisture and temperature (environmental effects) are known to influence the performance of flexible pavements. Mbaraga (2011) showed that moisture predominantly influences granular materials in the base, subbase and sub-grade, while temperature influences the bituminous material in the base or surface layers. Traffic (loading effect) is another aspect which influence the performance of a pavement structure.

Read & Whiteoak (2003) indicated that the analytical design of flexible pavements involves the consideration of two aspects of material properties. The first being the load-deformation or stress-strain characteristics used to analyse critical stresses and strains within the pavement structure and secondly, the performance characteristics of the materials that indicate the mode, or modes of failure. The two principle structural distress modes can be determined to be cracking and permanent deformation. The defining research properties surrounding EME in this study can be concluded to be the prediction of flexural stiffness and fatigue life performance. These properties along with the evaluation of pavement materials are discussed in this chapter.

To better understand the concept of EME, this chapter provides a historic look at the development of asphalt pavements in France as of the 1960's. A comparison is also made between the design methodology of the South African high modulus asphalt (HiMA) and the French mix design from which it was derived.

## 2.2. EME ASPHALT

EME was originally developed and used in France over 30 years ago, but has more recently been implemented in other countries like the United Kingdom, Australia and South Africa. EME asphalt is primarily intended to reduce pavement thickness whilst still providing adequate resistance against fatigue as well as permanent deformation. This is achieved through a combination of very high modulus of elasticity and fatigue values together with a high deformation and moisture resistance (Department of Transport and Main Roads, 2015). It is difficult to design for both rut (permanent deformation) and fatigue resistance, but with an EME mix, the high binder content contribute to the fatigue resistance, while the elevated stiffness modulus assist in the resistance of permanent deformation. In France and other European countries EME is primarily used as a base course with a thick asphalt wearing course. In these cases the EME base course is primarily designed to be resistant to fatigue, while the asphalt wearing course resistant against permanent deformation.

The name EME is derived from the French *Enrobés à Module Elevé,* which translate to “asphalt with an elevated modulus,” or simply “high modulus asphalt.” The typical characteristics of high modulus asphalt, as presented by Denneman (2011), consist of the following:

- High binder content: up to 6% by mass of aggregate;
- Hard binder: Penetration 10-25;
- Low air voids content;
- High Modulus: > 14 GPa at 15°C and 10 Hz;
- High resistance against permanent deformation;
- Good fatigue resistance;
- Impermeable; and
- Increased mixing temperature.

### 2.2.1. Development of EME Asphalt in France

The first EME mixes in the mid-seventies were based on the combination of coal tar and polyvinylchloride (not used any longer). These mix combinations gave good performance, but

were replaced by the second generation high modulus asphalt in the early eighties. This second generation high modulus asphalt made use of hard grade bitumen or additives.

The minimum binder content was based on the concept of richness modulus (K), which relates to the thickness of the bitumen film surrounding the aggregate (Denneman & Petho, 2013). The richness modulus of bitumen can be calculated using the following equation:

$$K = \frac{\left(\frac{100B}{100 - B}\right)}{\alpha . \sqrt[5]{\sum}} \qquad \textbf{Equation 2-1}$$

where,

$B$ = ratio of the binder mass to the total asphalt mix mass, see Equation 2-2 (mass %)

$\alpha$ = correction coefficient relative to the density of the aggregates, see Equation 2-3 (-)

$\sum$ = the specific surface area, see Equation 2-4 ($m^2/kg$)

$$B = 100 \frac{bitumen\ mass}{dry\ aggregate\ mass + bitumen\ mass} \qquad \textbf{Equation 2-2}$$

$$\alpha = \frac{2.65}{\rho_G} \qquad \textbf{Equation 2-3}$$

where,

$\rho_G$ = the maximum density of aggregate ($g/cm^3$)

$$100 \sum = 0.25G + 2.3S + 12s + 150f \qquad \textbf{Equation 2-4}$$

where,

$G$ = the proportion of aggregate particles greater than 6.3 mm

$S$ = the proportion of aggregate particles between 6.3 mm and 0.250 mm

$s$ = the proportion of aggregate particles between 0.250 mm and 0.063 mm

$f$ = the proportion of aggregate particles less than 0.063 mm

During the early stages of development, the French practice already distinguished between two categories based on their richness modulus:

- **A richness modulus > 3.2 (rich mix):** mix exhibit not only high moduli, but also show good resistance to fatigue because of the high binder content.
- **A richness modulus between 2.5 and 3.2 (lean mix):** mix show high moduli, but its resistance to fatigue is limited.

Denneman & Petho (2013) explained that the minimum richness modulus for a rich mix was defined as 3.2 in the early development phase, but is today accepted as 3.4.

#### 2.2.1.1. Evolution of Asphalts in France

High modulus pavements in France have experienced a substantial development in the past 30 years. These pavements have been developed in order to provide a practical solution to the problem of mitigation of rutting in surfacing layers and increase the rigidity of base layers. The following section covers the history and the evolution of asphalts in France, as summarised in Figure 2-1.

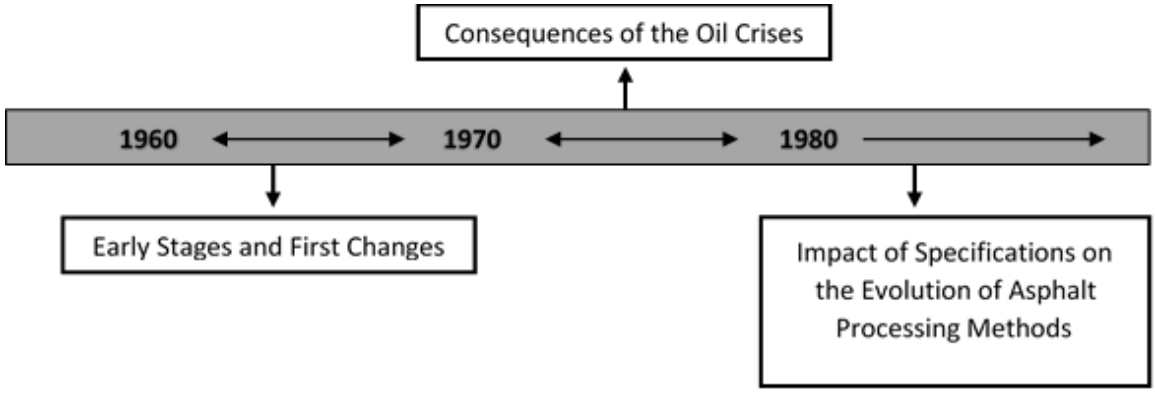


*Figure 2—1: Timeline of the evolution of Asphalts in France*

**The 1960s: Early Stages and First Changes**

Almost all paving asphalts in France, up to the beginning of the 1960s, were 80/100 and 180/220 penetration grade asphalts. These penetration grades were produced by the direct distillation from heavy crudes, which were imported from Central America. A big increase in heavy vehicle

traffic at the time demanded an asphalt mix with a higher rigidity and better resistance to plastic deformation (rutting). The production of harder asphalts, 40/50 and 60/70 penetration grade asphalts initiated in 1966, with the first 20/30 penetration grade asphalts appearing in 1968 (Corté, 2001). In September 1969, the French Road Directorate brought out a publication on the directive for construction of a surface course in asphalt mixes. This publication played a decisive role in the evolution thereof. The directive presented the choice of asphalt based on a climatic criterion, by dividing the French territory into three climatic zones, with:

- **Zone 1: Mediterranean climate -** characterised by hot summers and mild winters.
- **Zone 2: Oceanic climate -** characterised by mild summers and mild winters.
- **Zone 3: Continental climate -** characterised by hot summers and cold winters.

The recommended asphalt grade in terms of the climatic zones and altitude made at the time are summarized in Table 2-1. For the production of 40/50 penetration grade asphalts, at the end of the 1960s, the technique of air-blowing was used to increase the resistance to rutting further by reducing the thermal susceptibility of the asphalt.

*Table 2—1: Recommended choice of Asphalt Grades in terms of climatic zones and altitude (Corté, 2001)*

| | **Zone 1** | **Zone 2** | **Zone 3** |
|---|---|---|---|
| **Altitude ≤ 500m** | 40/50 | 40/50 or 60/70 | 60/70 or 80/100 |
| **Altitude > 500m** | 60/70 or 80/100* | 60/70 or 80/100 | 80/100 |

* if altitude > 1000m

**The 1970s: Consequences of the Oil Crises**

In 1973, the members of the Organization of Arab Petroleum Exporting Countries (OAPEC) announced an oil embargo. This embargo was called the “first oil shock”, which was followed by the “second oil shock” in 1979 when the United States decreased oil output in the awakening of the Iranian Revolution.

These oil crisis deeply affected the French oil market with regards to the volume of the refined oil as well as the origin of these imported crudes. The closing of a number of refineries together with the construction of new refineries with more powerful units of distillation, as a result of

these crises, forced an adaptation of industry. The development of the share of crudes imported from the Middle East, which were not as heavy as the crudes from Central America, together with the demand for 40/50 and 60/70 penetration grade asphalts, resulted in the generalization of partial air-blowing for the production of these penetration grades (Corté, 2001). This partial air-blowing process was applied to relatively soft bases which resulted in hefty chemical changes in the asphalt.

**The 1980s: Impact of Specifications on the Evolution of Asphalt Processing Methods**

The processing methods were greatly impacted by the amendment of the system of specifications for paving asphalts. This amendment was initiated early in the 1980s by the French Road Administration together with the oil industry and road contractors. The specifications used by the French in earlier years, with regards to binder selection, were primarily based on the penetration value, with the other physical characteristics serving as a supplementary element for this information.

The Ring and Ball (R&B) Softening Point was introduced in 1986 and served as a basis for the new grading system. The apprehension over the influence of aging of asphalt pavements on the field performance thereof, led to a secondary development. In order to collect relevant data from practice, an experimental program involving one hundred job sites were set up to evaluate the representativeness of the rolling thin-film oven test (RTFOT) for the simulation of ageing during the process of coating and laying of asphalt. Corté (2001) indicated that the specifications were fixed because of the field performance of 35/50 and 50/70 penetration grade asphalts used in wearing courses. These fixed specifications limited hardening of the binder after the rolling thin-film oven test (RTFOT), which resulted in a maximum increase of 9˚C for the Ring and Ball (R&B) softening point as well as a minimal value of residual penetration. These requirements were implemented in 1990 by the asphalt producers and included in the Association Française de Normalisation (AFNOR) standard for paving asphalts in 1992.

#### 2.2.1.2. French mixture design methodology

The design method as used for EME materials is similar to the design principles that are used for all asphalt layers in France. Sanders & Nunn (2005) emphasised that the philosophy of the French design methodology is to design a very stable mixture which, as a result thereof, might not be very workable. For the compaction of EME, heavy pneumatic-tyre rollers weighting up to 45 tonnes, are often used. In order to withstand rutting from traffic loading, the compaction of EME is done to a level where no further compaction is possible. The most commonly used aggregate grading in France for EME mixes are 0/10 mm, 0/14 mm and 0/20 mm. There are two main classes of EME mixtures:

- **EME Class 1**:
  - Lower binder content requirement
  - Less than 10% air voids

- **EME Class 2**:
  - Higher binder content (± 6% by mass of total aggregate)
  - Less than 6% air voids
  - Used for the most heavily trafficked roads

The French mix design methodology, in which the material is designed to satisfy mechanical criteria determined by laboratory tests, is illustrated in Figure 2-2.

A number of different aggregate gradings with the same binder content is firstly investigated in order to find a combination with acceptable workability. The workability is normally investigated with the help of a gyratory shear compactor or known in France as the PCG (Presse à Cisaillement Giratoire) test. The action of on-site compaction is simulated with the PCG test and enables the on-site void content obtained by a heavy pneumatic-tyre roller to be estimated. For an EME to be classified as a class 2 EME, it is required to achieve a void content of 6% or less in terms of the PCG test. However, if a low void content is easily achieved, the material may lack internal stability, which can be measured with the Laboratoire Central des Ponts et Chaussées (LCPC) rutting test.

When a grading that satisfy the PCG design criterion has been found, the binder richness modulus (K) is recalculated for the selected grading. This richness modulus is calculated with a

formula that takes the specific surface area together with the density of the aggregate into account (see Section 2.3.1). The Duriez test is then used to check the sensitivity of the mix to stripping, the test is performed by doing unconfined compression tests on two separate sets of cylindrical samples, with one set as is and the second after conditioning in water. The material is regarded as acceptable if the ratio of the results after and before conditioning exceed a certain fixed value. The mixture is then prepared in the LCPC pneumatic-tyre slab compaction apparatus, where after samples are cut for the performance tests as listed in Figure 2-2. The performance criteria, as listed in Table 2-2, is used to determine whether or not changes to the mix composition and design is needed.

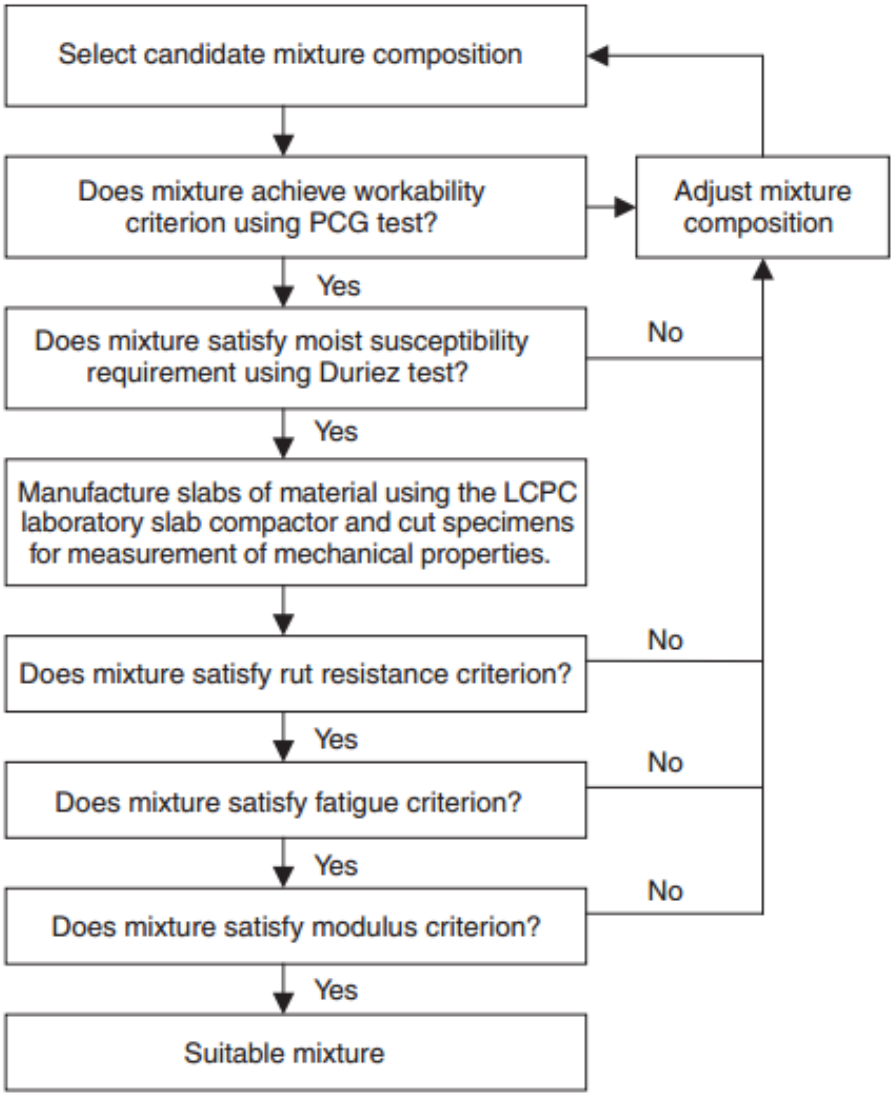


*Figure 2—2: French mixture design procedure (Sanders & Nunn, 2005)*

*Table 2—2: French design criteria using LCPC performance tests (Sanders & Nunn, 2005)*

| Test | EME Class 2 |
|---|---|
| PCG test<br>0/10 mm<br>0/14 mm<br>0/20 mm | ≤6% air voids, after<br>80 gyrations<br>100 gyrations<br>120 gyrations |
| Duriez test (after and before immersion ratio) | ≥0.75 |
| Rutting test (60°C, 30,000 cycles on 100mm slab) | ≤8% |
| Complex modulus test (15°C, 10 Hz) | ≥14 GPa |
| Fatigue test (10°C, 25 Hz - tensile micro-strain for 106 cycles) | ≥130 |
| Binder richness modulus<br>0/10 mm<br>0/14 mm<br>0/20 mm | <br>3.4<br>3.4<br>3.4 |

### 2.2.2. High Modulus Asphalt (HiMA) in South Africa

It is firstly important to note the difference between Highly Modified Asphalt (HiMA) and High Modulus Asphalt (HiMA). Highly Modified Asphalt is a new highly polymer-modified binder whereas High Modulus Asphalt is based on the French EME technology.

According to Sabita Manual 33 (2013), in 2006 they recognized the need to implement flexible pavement solutions that would meet the requirements associated with the ever growing demand of increasing traffic volumes and axle loadings. Sabita embarked on a technology transfer implementation whereby the EME technology could be introduced to South Africa as HiMA.

The design procedure for HiMA in South Africa is based on the French mix design methodology, as indicated in Figure 2-2. The performance related design process for HiMA mixes can be seen in Figure 2-3, with the steps briefly described as follows:

1. Select the appropriate mix components in terms of aggregate and binder.
2. Develop a suitable design grading for the different aggregate fractions.

3. Determine the binder content based on a minimum richness modulus, similar to the film thickness conventionally used in South Africa.
4. Using a trail mix design, compact specimens in a gyratory compactor. A maximum allowable air void content after a set number of gyrations has to be met.
5. Once workability criteria have been met specimens are subjected to a durability test.
6. When the durability is satisfactory, the following structural performance criteria are evaluated:
    a. Minimum dynamic modulus
    b. Minimum level of resistance to permanent deformation
    c. Minimum fatigue life

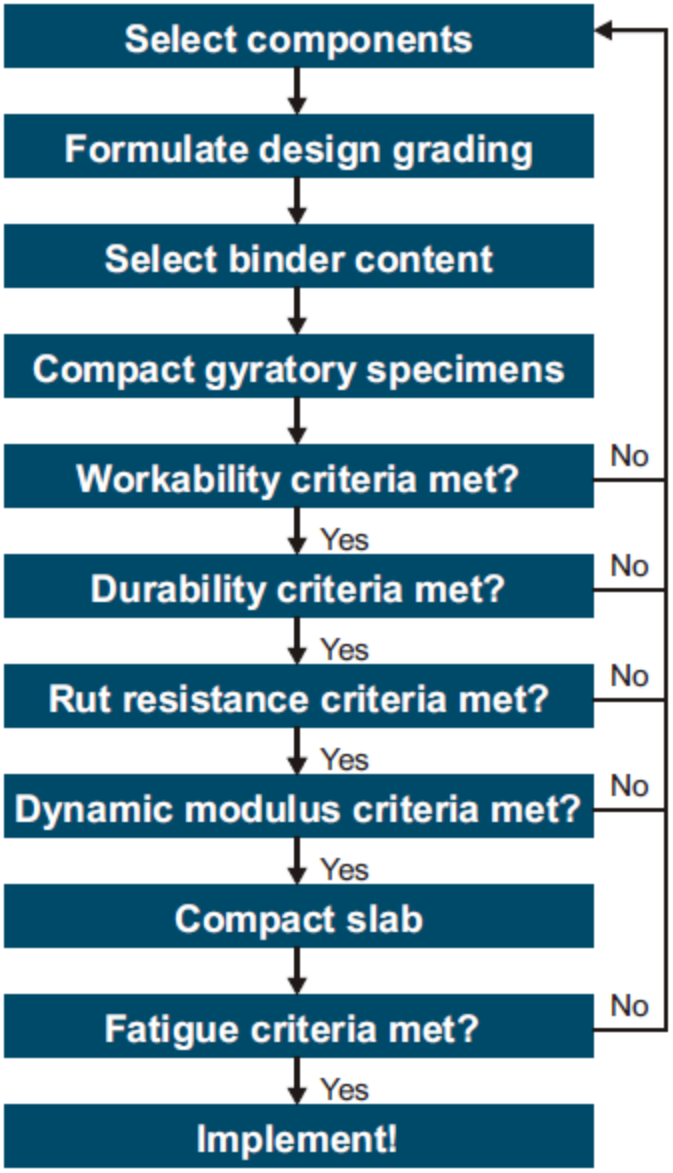


*Figure 2—3: Design procedure for HiMA in South Africa (Sabita Manual 33, 2013)*

## 2.3. BINDER GRADING SYSTEMS

Asphalt binders typically get categorized by means of one or more shorthand grading systems, in accordance to their physical characteristics. These grading systems range from simple to complex classification methods and represent an evolution in terms of the ability to characterize asphalt binder based on its properties. The grading systems include Penetration Grading,

Viscosity Grading and the latest system known as the Superpave Performance Grading (PG) System.

### 2.3.1. Penetration Grading

The penetration grading of asphalt binders are based on the depth which a standard 100g needle will penetrate an asphalt binder sample when placed under the load of the needle for 5 seconds (Figure 2-4). The basic assumption made for penetration grading's is that the less viscous the asphalt binder, the deeper the needle will penetrate the binder sample. The penetration depth correlates with the asphalt binder's performance. For this reason, asphalt binders with a high penetration number ("soft" binder) are usually used in areas with colder climates while asphalt binders with a low penetration number ("hard" binders) are used for areas with warmer climates.

*Figure 2—4: Penetration Needle (Pavement Interactive, 2008)*

The penetration depth is empirical, and due to the simple nature of the test, no fundamental engineering parameters such as viscosity can be measured. The key advantages and disadvantages of penetration grading, as listed by Roberts, et al. (1996), can be seen in Table 2-3.

*Table 2—3: Advantages and Disadvantages of Penetration Grading (Roberts, et al., 1996)*

| Advantages | Disadvantages |
|---|---|
| The test is done at 25˚C, which is reasonably in conjunction with the average temperature found in a typical pavement. | It is an empirical test in which no other fundamental engineering constraints are measured. |
| The test may serve as a better correspondence with regards to low-temperature asphalt binder properties than the viscosity test, which is performed at 60°C. | The shear rate is variable and high throughout the test. Due to the fact that asphalt binders normally behave as a non-Newtonian fluid at 25°C, the test results may be affected. |
| The change in asphalt binder rheology can be determined by performing the test at temperatures other than 25°C | The change in asphalt binder rheology cannot be determined by a single test at 25°C |
| The test can easily be used in the field, due to its inexpensive and quick nature. | No information on mixing and compaction temperatures are attained by the test. |

Penetration grades are classified as a range of penetration units, with one penetration unit equal to 0.1mm of penetration by the standard needle.

### 2.3.2. Viscosity Grading

The viscosity test was developed in the early 1960s as an upgraded asphalt grading system that includes the rational scientific viscosity of binders. The empirical penetration test was replaced by the scientific test as the main characterization test for asphalt binders. The viscosity grading test measures penetration, as in the penetration grade test, as well as binder viscosity at 60˚C and 135˚C. Viscosity grading tests can be performed on original asphalt binder samples (called AC grading) or on aged residue samples (called AR grading). Pavement Interactive (2007) explained that the AR viscosity test is based on the viscosity of aged residue from the rolling thin oven test. This grading system simulate asphalt binder properties after it has undergone a typical manufacturing process. With the AC grading, the asphalt binder is characterized by the properties it retains before undergoing the manufacturing process.

The key advantages and disadvantages of viscosity grading, as listed by Roberts, et al. (1996), can be seen in Table 2-4.

*Table 2—4: Advantages and Disadvantages of Viscosity Grading (Roberts, et al., 1996)*

| Advantages | Disadvantages |
|---|---|
| Viscosity is a fundamental engineering parameter (penetration depth is not). | The principal grading may not accurately reveal low-temperature asphalt binder rheology, as it is done at 25°C. |
| Test temperatures compare well with the following asphalt temperatures:<br>• 25°C – average pavement temperature<br>• 60°C – high pavement temperature<br>• 135°C – HMA mixing temperature | With the AC grading system, thin film oven test residue viscosities may differ significantly with the same AC grade. Hence, asphalt binders of the same AC grade may behave differently after construction. |
| The temperature susceptibility is able to be determined because viscosity measurements are taken at three different temperatures, whereas penetration is only measured at 25°C. | Tests are more expensive and time consuming than the penetration test. |
| The equipment and standards used are widely available. | |

Viscosity grades are listed in poises (cm-g-s = dyne-second/cm$^2$) which is named after Jean Louis Marie Poiseuille. The number of poises and the viscosity of the binder are directly proportional, meaning the lower the number of poises, the lower the viscosity and thus the more easily a substance flows.

### 2.3.3. Superpave Performance Grading (PG) System

Penetration grading and viscosity grading systems provide a limited ability to fully characterize asphalt binders for the use in HMA pavements. The Superpave Performance Grading (PG) system was developed as part of the Superpave research effort to more accurately and fully characterize asphalt binder for the use in HMA pavements. The PG system were designed to specifically address HMA pavement performance parameters like rutting, fatigue cracking and thermal cracking. The PG system also take into account that the HMA asphalt binder's properties is affected by the conditions under which it is used. For asphalt binders, this involves the expected climatic conditions as well as certain binder aging considerations. The PG system therefore produce a more comprehensive grading, as opposed to the penetration and viscosity grading systems, as it requires a particular asphalt binder to pass the required tests at specific

temperatures, dependent upon the specific climatic conditions in the intended area of use. Table 2-5 describes how the Superpave PG system addresses some of the general limitations which the penetration and viscosity (AC and AR) grading systems have.

*Table 2—5: Limitations of Penetration and Viscosity Grading Systems addressed by Superpave PG System (Roberts, et al., 1996)*

| Limitations of Penetration and Viscosity (AC and AR) Grading Systems | Superpave PG System features that address limitations |
|---|---|
| Due to the empirical nature of penetration and ductility tests, it's not directly related to HMA pavement performance. | The measured physical properties are directly related to field performance. |
| Tests are conducted at one standard temperature regardless of the climatic region in which the asphalt binder is intended to be used. | Test criteria remain constant, however, temperatures at which the criteria must be met changes in conjunction with the intended climatic conditions in which binder is used. |
| The range of possible pavement temperatures at a particular site are not sufficiently covered. | The entire range of possible pavement temperatures at a particular site are covered. |
| Only short-term asphalt binder aging is considered, while the long-term aging of binder plays a significant role in fatigue - and low temperature cracking. | Three critical binder ages are replicated and tested:<br>1. Original asphalt binder prior to mixing with aggregate.<br>2. Aged asphalt binder after production and construction.<br>3. Long-term aged binder. |
| Asphalt binders characteristics may differ greatly within the same grading category. | Grading is more precise with less overlap between different grades. |
| These grading systems are not suitable for modified asphalt binders. | Tests and specifications are intended for both modified and unmodified asphalt binders. |

The superpave performance grading is conveyed using two numbers, the first number lists the average seven-day maximum pavement temperature (in °C) with the second number listing the minimum pavement design temperature expected (in °C). A binder with a grading of PG 64-16 is thus intended for use in an area where the average seven-day maximum pavement temperature

is 64 °C and the expected minimum pavement temperature is -16°C. It is important to note that these temperatures describe the pavement temperatures and not the air temperature.

### 2.3.4. Typical properties associated with Penetration Grade Bitumens

Table 2-6 describes the characteristics and specifications of binders used for EME, as described by Sanders & Nunn (2005) in the TRL 636, as well as for HMA as described by ENGEN (2009).

*Table 2—6: Binder characteristics and requirements*

| | | Binders for EME | | | Binders for HMA | | | | |
|---|---|---|---|---|---|---|---|---|---|
| **Property** | Units | **10/20 pen** | **15/25 pen** | **Test Method** | **40/50 pen** | **60/70 pen** | **80/100 pen** | **150/200 pen** | **Test Method** |
| **Penetration at 25°C** | 0.1 mm | 10 - 20 | 15 - 25 | EN 1426 | 40 – 50 | 60 – 70 | 80 - 100 | 150 - 200 | ASTM D5 |
| **Softening point** | °C | 63 - 73<br>Target value 71 max | 60 - 70<br>Target value 68 max | EN 1427 | 49 -59 | 46 – 56 | 42 - 51 | 36 - 43 | ASTM D36 |
| **Dynamic viscosity @ 60°C** | Pa.s | | | | 220 – 400 | 140 - 250 | 75 - 150 | 30 - 60 | ASTM D4402 |
| **Dynamic viscosity @ 135°C** | Pa.s | 1.1 | 0.9 | EN 12595 | 0.27 - 0.65 | 0.22 - 0.45 | 0.15 - 0.4 | 0.12 - 0.3 | ASTM D4403 |
| **Binder characteristics after RTFOT** | | | | | | | | | |
| **Change of mass (max)** | % | 0.5 | 0.5 | | 0.3 | 0.3 | 0.3 | 0.3 | ASTM 2872 |
| **Retained pen 25°C (min)** | % | 65 | 65 | EN 1426 | 60 | 55 | 50 | 50 | ASTM D5 |
| **Increase in softening point (max)** | °C | 8 | 8 | EN 1427 | 7 | 7 | 7 | 7 | ASTM D36 |

## 2.4. FLEXURAL STIFFNESS

Asphalt stiffness as indicated by Read & Whiteoak (2003) can be divided into elastic and viscous stiffness, depending on the temperature or loading time. Elastic stiffness occurs under conditions of low temperatures or short loading times, and is used to calculate critical strain values in the structure in analytical design. Viscous stiffness occurs under conditions of high temperatures or long loading times, and is used to assess the resistance of a material against deformation. Read (1996) showed that at intermediate temperatures where the stiffness has both an elastic and viscous component, the stiffness is stress dependent. The assessment of the performance is made even more difficult because of the fact that high stresses result in lower stiffness and low stresses result in higher stiffness for the same material. This stress dependency however, is less important when compared to both the effects of temperature and time of loading.

The layer thickness and stiffness of a pavement is the two main factors that affect the load spreading ability within the pavement layer. The stiffness at a particular temperature and specific time of loading can be determined using a number of methods, as indicated by Read et al. (2003):

- the bending or vibration tests on a beam specimen
- the direct uni-axial or tri-axial tests on a cylindrical specimen
- the indirect tensile test on a cylindrical specimen

Raithby & Strerling (1972) explained that different types of loading cases can be used for these tests, but for the elastic stiffness relevant to moving traffic, sinusoidal or pseudo-sinusoidal repeated loading at high frequencies are highly applicable.

### 2.4.1. Prediction of Flexural Stiffness

The Indirect Tensile Stiffness Modulus (ITSM) test can be used to predict the stiffness modulus of bitumen, while the bending beam test is used to predict flexural stiffness. The bending beam test can either be in the form of the three point or the more recent four-point bending beam test. With the bending beam test, a rectangular beam is subjected to a repeated load at a constant strain under a range of loading times (frequencies) and temperatures.

### 2.4.2. Master-Curve Development

The master-curve development is made up from flexural stiffness values that have been obtained through frequency and temperature sweeps. Jenkins (2000) indicated that the stiffness of a specific asphaltic material can be defined with a master-curve, by shifting the stiffness modulus (as the ordinate) horizontally with respect to the loading time (as the abscissa) for various temperatures until the curve co-incide. The master-curve thus provide a complete stiffness versus loading time relationship for a specific asphaltic material at a selected reference temperature ($T_{ref}$).

### 2.4.3. Shift Concept and Principles

Mbaraga (2011) indicated that a mathematical relationship or model, describing the time-temperature relationship with regards to the flexural stiffness is a fundamental part in the development of the Master Curve. In this regard Jenkins (2000), also indicated that the principle of time-temperature correspondence forms the basis of master-curve development. The technique used in master-curve development uses the equivalence or correspondence between frequency and temperature for stiffness modulus of bituminous mixes as:

$$\log f_{eq} - \log f = \log \alpha_t \qquad \textbf{Equation 2-5}$$

where,

| | | |
|---|---|---|
| $f_{eq}$ | = | frequency for Master Curve converting test temperature to reference temperature (Hz) |
| $f$ | = | actual test loading frequency (Hz) |
| $\alpha_t$ | = | shift factor |

Jenkins (2000) indicated that three notable methods exist for determining the shift factor:

- graphical shifting of experimental results;
- shifting using the Arrhenius equation;
- shifting using the Williams-Landel-Ferry equation.

Jenkins (2000) indicated that, if shifting using Arrhenius equation yield satisfactory results in terms of mater curve fit, it is unnecessary for the other approaches to be utilised in a limited study. Medani & Molenaar (2003) further indicated that when the difference between the

reference temperature and the temperature to be shifted is less than 20°C, then the Arrhenius type model is applicable for the study. In this study that was the case, as a reference temperature of 20˚C was selected with the outer temperature in the study being 40˚C. The Arrhenius type model was thus applied in the study.

The shifting using Arrhenius approach uses the following equation:

$$\log \alpha_t = C\left(\frac{1}{T} - \frac{1}{T_{ref}}\right) = \log e.\frac{\Delta H}{R}\left(\frac{1}{T} - \frac{1}{T_{ref}}\right) \qquad \textbf{Equation 2-6}$$

where,

| | | |
|---|---|---|
| $T$ | = | experimental or test temperature (K) |
| $T_{ref}$ | = | reference temperature selected (K) |
| $C$ | = | constant (K) |
| $\Delta H$ | = | activation energy (J/mol) |
| $R$ | = | ideal gas constant = 8.314 (J/(mol.K)) |

In literature, different values were reported for the constant C, as used in Arrhenius equation:

- Francken: C = 10920 K (Francken & Clauwaert, 1988)
- Lytton : C = 13060 K (Lytton, et al., 1993)
- Jacobs: C = 7680 K (Jacobs, 1995)

A typical example of the shifting of experimental stiffness data, with a reference temperature of 10˚C, can be seen below in Figure 2-5.

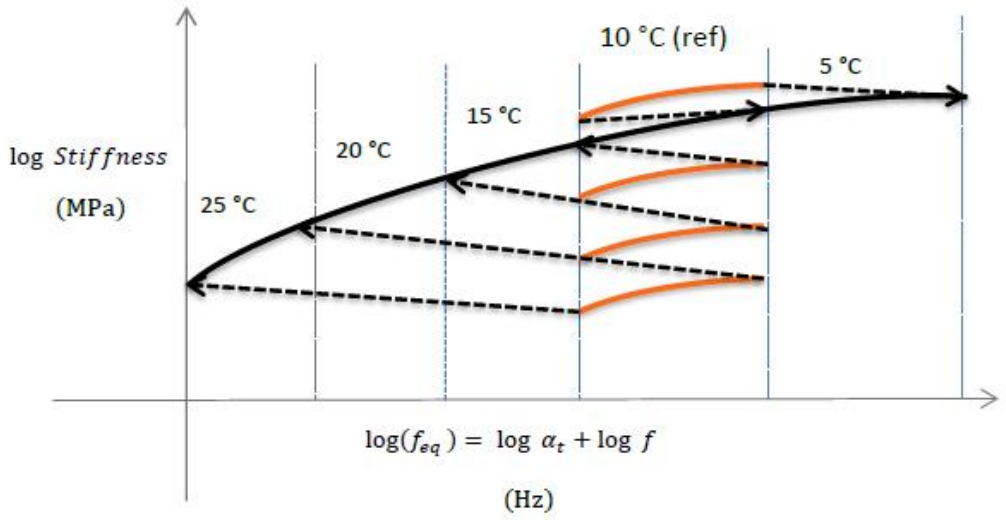


*Figure 2—5: Example of typical shift using Arrhenius type model (Cloete, 2015)*

### 2.4.4. Fundamental Calculations relating to flexural tests

The following equations are a list of all the relevant calculations that forms part of the flexural test protocols as described by ASTM International (2010) and Mbaraga (2011):

**a) maximum tensile stress (Pa):**

$$\sigma_t = \frac{0.357P}{bh^2} \qquad \textbf{Equation 2-7}$$

where,

$P$ = load applied by actuator (N)
$b$ = average beam specimen width (m)
$h$ = average beam specimen height (m)

**b) maximum tensile strain (m/m):**

$$\varepsilon_t = \frac{12\delta h}{3L^3 - 4a^2} \qquad \textbf{Equation 2-8}$$

where,

$\delta$ = maximum deflection at centre of beam specimen (m)
$a$ = space between inside clamps [0.119m]
$L$ = length of beam specimen between outside clamps [0.357m]

**c) flexural stiffness (Pa):**

$$S = \frac{\sigma_t}{\varepsilon_t} \qquad \textbf{Equation 2-9}$$

**d) phase angle (degrees):**

$$\varphi = 360fs \qquad \textbf{Equation 2-10}$$

where,

$f$ = load frequency (Hz)
$s$ = time lag between $P_{max}$ and $\delta_{max}$

**e) dissipated energy (J/m$^3$) per cycle:**

$$D = \pi \sigma_t \varepsilon_t \sin(\varphi) \qquad \textbf{Equation 2-11}$$

**f) cumulative dissipated energy (J/m$^3$):**

$$\sum_{i=1}^{i=n} D_i \qquad \textbf{Equation 2-12}$$

where,

$D_i$ = D for the i$^{th}$ load cycle

**g) initial stiffness (Pa):**

$$S = Ae^{bn} \qquad \textbf{Equation 2-13}$$

where,

$e$ = natural logarithm to the base e
$A, b$ = constants

**h) load cycles to failure:**

$$n_{f,50} = \left[\ln\left(\frac{S_{f,50}}{A}\right)\right]/b \qquad \textbf{Equation 2-14}$$

where,

$S_{f,50}$ = stiffness 50% of the initial stiffness (Pa)

## 2.5. FATIGUE CRACKING

Fatigue cracking is regarded as one of the primary damage mechanisms of asphalt pavements. The occurrence of fatigue cracking can be attributed to numerous factors among which is applied load, load frequency and temperature changes or a combination of these factors.

Fatigue cracking results from cyclic stresses that are lower than the ultimate tensile stress, or even the yield stress of the material (Read & Whiteoak, 2003). The fact that these stresses are below the ultimate tensile stress makes fatigue damage especially dangerous as the only warning sign of an impending fracture is often a small crack. Fatigue cracking in asphalt pavements can be attributed to the repeated loading of traffic.

Read et al. (2003) indicates that the continuous flexural and relaxation over a period of time produces the possibility of fatigue cracks propagating in pavement layers. Fatigue cracks can initiate either at the bottom of the bituminous layer and propagate to the surface under repeated load applications ('bottom-up' or 'classical' fatigue cracking) or from the top and propagate downwards through the bitumen concrete layer over time ('top-down' cracking).

Bottom-up cracking first shows as small longitudinal cracks in the wheel path, but can quickly spread and become interconnected to form alligator cracking. Bottom-up cracking is a result of tensile strains and stresses forming at the bottom of the bituminous layer because of repeated bending under wheel loads. Bottom-up cracking tends to occur in relatively thin and weak bituminous layers.

Top-down cracking appear as short longitudinal cracks just outside the wheel path developing into longer longitudinal cracks that are connected by short transverse cracks. Top-down cracking tends to occur in thicker bituminous layers.

Figure 2-6 shows an exaggerated illustration of the two types of crack propagation as described above.

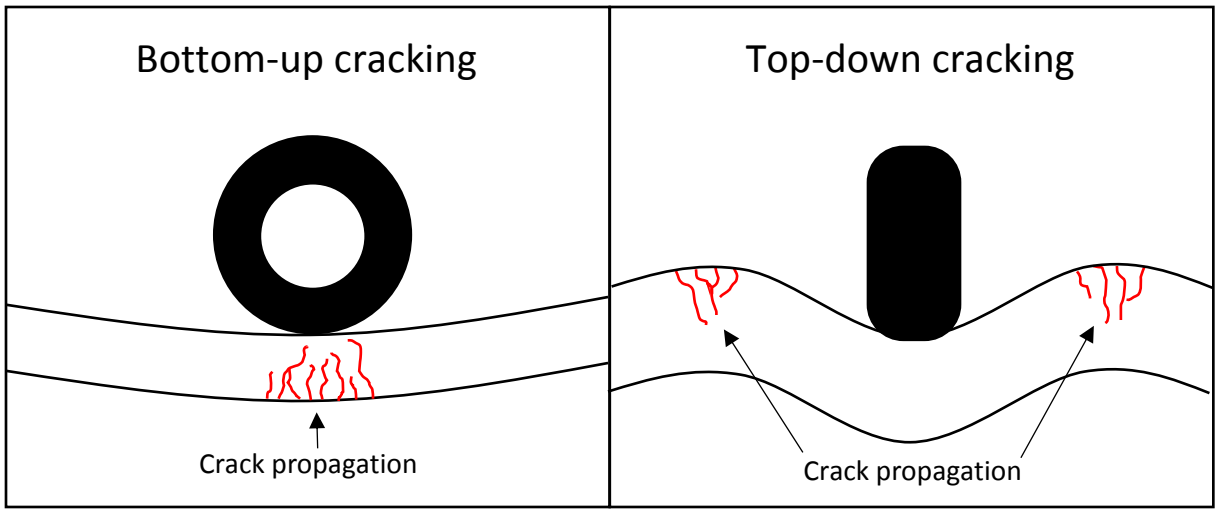


*Figure 2—6: Bottom-up and Top-down cracking*

Thin asphalt pavements are preferred over thick pavements in South Africa, because bottom-up cracking is of most concern. EME asphalt is, among other aspects, intended to reduce the thickness of pavements even more. Bottom-up cracking is thus a big consideration in the design and placement of EME pavements.

### 2.5.1. Prediction of Fatigue Performance

Molenaar (2007) indicate that the fatigue performance of asphalt concrete pavements is difficult to predict because many of the input parameters needed for the analyses are difficult to obtain. Most analysis strategies take the tensile strain at the bottom of the asphalt layer as the factor that explains fatigue, although top-down cracking has nothing to do with the tensile strain at the bottom of the asphalt layer.

The prediction of the fatigue life of asphalt involves the establishment of a fatigue relation line for a specific asphalt mixture. Molenaar (2007) indicates that the slope of this fatigue relation line is the only aspect that can be established with confidence from laboratory fatigue testing. The Four Point Beam fatigue apparatus is one of the devices used to conduct fatigue testing.

Large shift factors are needed to apply laboratory fatigue relations to field predictions. In this regard, Molenaar (2007) states that the magnitude of these shift factors depends on the type of fatigue test and mode of loading.

### 2.5.2. Factors Affecting Fatigue Life of Asphalt Pavements

Road pavements are subjected to repeated wheel loads of varying magnitude and intensity, and as explained previously, this fluctuating stresses and strains within the pavement may induce fatigue failure through cracking and deformation. These cracks weaken the ability of the pavement structure to adequately support the load. Mashaan et al. (2014) indicated that the fatigue behaviour of bituminous materials are affected by the mode of testing, loading variables and mixture variables.

#### 2.5.2.1. Mode of Testing

The mode of testing can be described as the variation of the stress and strain levels during a fatigue loading test. The fatigue tests on bituminous specimens can be performed under the

controlled condition of either stress (load) or strain (displacement). The evaluated laboratory fatigue life of a pavement is greatly dependent on the mode of the controlled condition used during the test. In the case where the stress (load) is the controlled condition during the fatigue test, the stress (load) applied is kept constant while the strain (displacement) gradually increase as the specimen weaken. The accumulation of strain in this case, culminate into rapid failure of the specimen almost immediately after crack initiation (see Figure 2-7). For the case where the applied strain (displacement) is kept constant, the specimen becomes weaker as testing progresses due to accumulated damage. The stress (load) required to maintain the initial strain (displacement) gradually decreases as the specimen weaken (see Figure 2-7). Roberts et al. (1991) showed the stress (load) controlled condition to be applicable when investigating thick bituminous pavement layers, exceeding 130mm. In the case where thin pavement layers are investigated, the strain (displacement) controlled condition is recommended. Barksdale (1978), showed that the application of a constant strain (displacement) during testing displays better fatigue life, as opposed to a constant stress (load), if all other variables are kept constant.

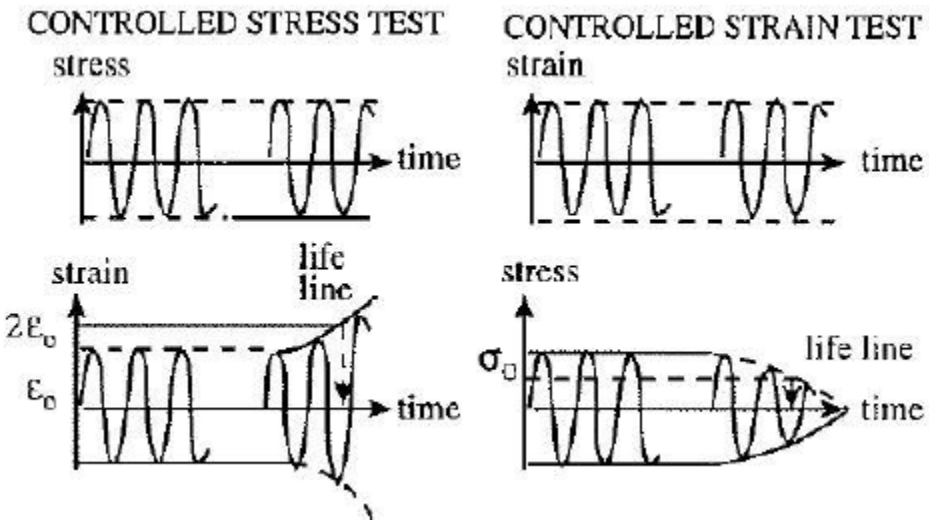


*Figure 2—7: Principles of stress and strain controlled configurations (Bonnaure, et al., 1980)*

#### 2.5.2.2. Loading Variables

The loading variables that affect fatigue life are loading waveform, rate of loading (frequency) and rest period. Raithby & Ramshaw (1972) was of the opinion that the influence of the loading waveform had very small effect on the laboratory fatigue testing of bituminous specimens. This may be the case for softer bitumen's, when considering hard grade bitumen samples, the loading waveform can affect the fatigue life of a pavement through the initial damage caused by certain waveforms. The loading frequency and duration significantly affects the fatigue life of a specimen. The loading frequency mainly influence the fatigue life of asphalt pavements by influencing the stiffness of the material. Higher load frequencies result in higher mix stiffness, resulting in an increase in fatigue life. Read & Collop (1997) showed that decreasing the duration of the load pulse (increasing the rest period) the stiffness of the mix is increased and so too the fatigue life. Raithby & Sterling (1972) found that an increase in load repetition from 30 to 100 cycles per minute, reduce the fatigue life by 20%. The application of a continuous loading mode resembles the most extreme in field loading situation. In practice, a pavement is mostly loaded discontinuously, with a rest period between successive wheel loads of a vehicle or between successive vehicles.

#### 2.5.2.3. Mixture Variables

The fatigue response of a bituminous mixture is directly influenced by the composition thereof. Pell & Cooper (1975) explained that the most important mixture variables include mix stiffness, bitumen content and properties, porosity and degree of compaction and aggregate characteristics.

**Mix Stiffness**

The stresses and strains within a pavement layer are affected by both the temperature and loading time. The stresses and strains which arise as a result of traffic loading moving at different speeds and at different pavement temperatures are dependent on the stiffness of the pavement. When the stress (load) is controlled, a mixture with a high stiffness will experience an increase in fatigue life, conversely for the controlled strain (displacement) case, there will be a decrease in fatigue life. Read & Collop (1997) showed that pavements with lower stiffness's exert longer service lives than high stiffness pavements due to crack propagation relationships.

**Bitumen Content and Properties**

The bitumen content affects the fatigue response of the mix, by increasing or decreasing the bitumen content the fatigue resistance is also increased and decreased, respectively. Goddard et al. (1978) showed that a reduction of one-percent in bitumen content can reduce the fatigue life by up to 70%. To achieve the longest fatigue life, the bitumen content should be as high as possible, but keeping in mind that an increase in bitumen content can promote permanent deformation. The hardness and type of bitumen mainly influence the fatigue life of asphalt pavements by influencing the stiffness of the bituminous mix.

**Air Voids and Compaction**

The compaction level influences the fatigue life through the volume of air voids, the lower the volume of air voids the higher the expected fatigue life will be. Barksdale (1978) showed that, for a decrease in porosity from 8% to 6% increases the fatigue life by a factor of nine. He further showed that a decrease in porosity of 6% to 3% increases the fatigue life by a factor of 200. Epps & Monismith (1971) also reported that, for each 1% increase in air voids the fatigue life of asphalt is reduced by 10% to 30%. There however subsists a compromise between fatigue life and permanent deformation; when the air voids are reduced by too much, it will become congested with bitumen, pushing the aggregates apart, leading to major rutting (Read & Collop, 1997).

**Aggregate Characteristics**

Goddard et al. (1978) indicated that the type and gradation of aggregates, filler content and compaction level have minimal influence on the fatigue life of laboratory bituminous specimens. The effect of these properties are mainly accounted for by the influence they have on the dynamic stiffness of a mix. Baladi (1989) concluded that angular aggregate increases the fatigue life of a mix by a factor of 1.14 relatively to rounded aggregates. Read & Collop (1997) illustrated that aggregate shape plays an important role in the propagation of cracks, flaky aggregates tend to orientate themselves normally to the applied load, slowing down the rate of crack propagation as opposed to spherical aggregates. The strength and toughness of coarse aggregates play a major role in the fatigue failure of a mixture with rough textured aggregates.

### 2.5.3. Fatigue Models

Adhikari et al. (2009) explained that numerous fatigue models can be used to determine fatigue life, with the simplest being the models that consider fatigue prediction on the basis of either strain-controlled or stress-controlled. These models don't consider temperature, modulus or loading frequencies. The strain- and stress-controlled models are illustrated in Equation 2-15 and Equation 2-16, respectively:

- Strain-controlled model:

$$N_f = k_1 \left(\frac{1}{\varepsilon_t}\right)^{k_2} \qquad \textbf{Equation 2-15}$$

- Stress-controlled model:

$$N_f = k_1 \left(\frac{1}{\sigma_t}\right)^{k_2} \qquad \textbf{Equation 2-16}$$

where,

| | | |
|---|---|---|
| $N_f$ | = | fatigue life (cycles) |
| $\varepsilon_t$ | = | tensile strain at bottom of specimen (in/in) |
| $\sigma_t$ | = | applied tensile stress (psi) |
| $k_1, k_2$ | = | experimentally determined coefficients |

The coefficients $k_1$ and $k_2$ are determined by fitting a power law regression function to the testing data on a log scale.

Brown et al. (1996) and Taute et al. (2001) makes a distinction between the strain-controlled and stress-controlled mode of loading. With the strain-controlled mode, a preselected strain value at the bottom of the beam is selected and remain constant throughout the test period. With the stress-controlled mode, the load remains constant while the stress fluctuates until the beam cracks. Materials that are more flexible perform better in the strain-controlled test, while materials with higher stiffness values perform better in the stress-controlled test.

The main purpose of fatigue models are to provide a relationship between the number of load repetitions to failure and certain properties like mixture properties and pavement response

(strain). Adhikari et al. (2009) indicated that the parameters used in many of the fatigue models are based on a continuous-loading sequence, while the coefficients are determined from empirical data regression. These fatigue models are unable to predict the fatigue life for all the possible situations that develop within an actual pavement, such as temperature, loading frequency and rest periods between loads. Some of these fatigue models can be shown by the Finn fatigue model, the Asphalt Institute model and the Shell model.

- Finn fatigue model:

$$\log(N_f) = 15.947 - 3.291 \log\left(\frac{\varepsilon_t}{10^{-6}}\right) - 0.854 \log\left(\frac{E_1}{10^3}\right) \quad \textbf{Equation 2-17}$$

- Asphalt Institute model:

$$N_f = 0.0796(\varepsilon_t)^{-3.291} (E_1)^{-0.841} \quad \textbf{Equation 2-18}$$

- Shell model:

$$N_f = 0.0685(\varepsilon_t)^{-5.671} (E_1)^{-2.363} \quad \textbf{Equation 2-19}$$

where,

$E_1$ = initial flexural modulus (psi)

Monismith et al. (1985) presented a fatigue life prediction model from the initial modulus and tensile strain of asphalt mixtures. Before Monismith's contribution, Pell & Cooper (1975) introduced a fatigue model that was based on the effect of the volumetric asphalt content and air void content of an asphalt mixture. Equation 2-20 and Equation 2-21 shows the fatigue life prediction models from Monismith et al. (1985) and Pell & Cooper (1975), respectively:

- Monismith et al. (1985) model:

$$N_f = k_1 \left(\frac{1}{\varepsilon_t}\right)^{k_2} \left(\frac{1}{E}\right)^{k_3} \quad \textbf{Equation 2-20}$$

- Pell & Cooper (1975) model:

$$N_f = k_1 \left(\frac{1}{\varepsilon_t}\right)^{k_2} \left(\frac{1}{E}\right)^{k_3} \left(\frac{V_b}{V_b + AV}\right)^{k_4} \quad \textbf{Equation 2-21}$$

where,

| | | |
|---|---|---|
| $E$ | = | asphalt initial modulus (psi) |
| $V_b$ | = | volumetric binder content (%) |
| $AV$ | = | air void content (%) |
| $k_{1,2,3,4}$ | = | experimentally determined coefficients |

In the Pell and Cooper fatigue model, the impact of the volumetric composition of a specimen on the fatigue life is noted. When all factors are held constant while changing the binder content, the fatigue life of the mix will change accordingly.

Different fatigue lives have been observed for a diverse variation in the test parameters. Pell & Cooper (1975) found that the line indicating the fatigue life (see Figure 2-8) for certain materials at different testing temperatures lies almost parallel with that of longer fatigue lives at a higher testing temperature. This trend was reaffirmed when tests were conducted at different speed (different rate of loading). When plotting the results in terms of tensile strain ($\varepsilon_t$), it was found that the results from various stiffness's coincide, showing that strain is indeed the criterion of failure. The strain criterion in fatigue performance therefore takes the temperature and rate of loading (speed) into account.

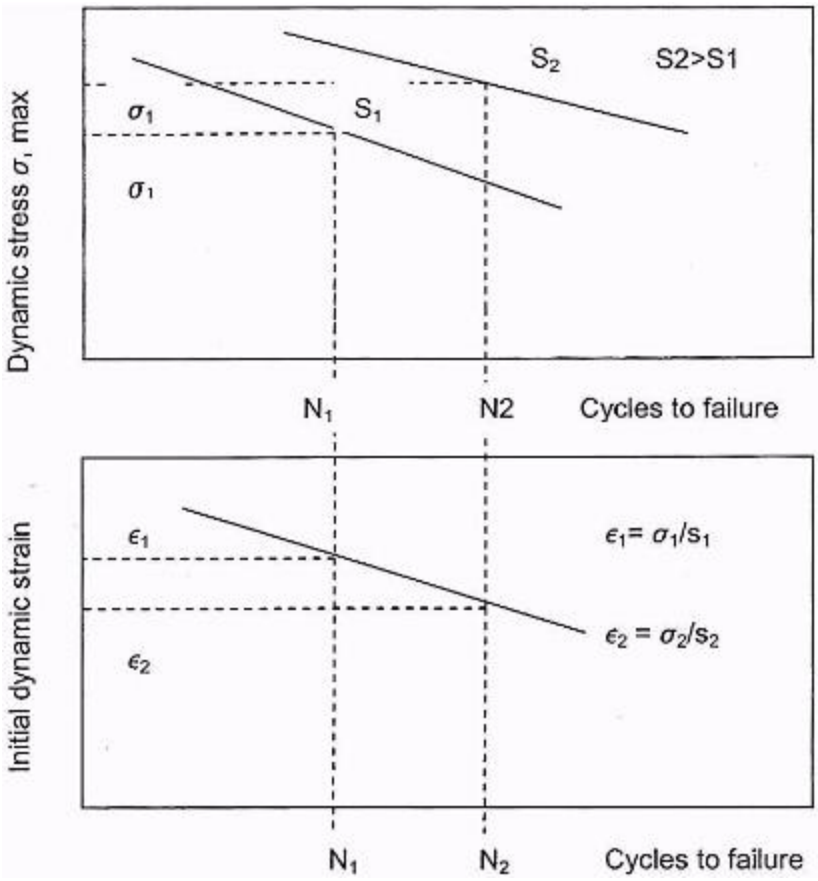


*Figure 2—8: The Strain Criteria (Pell & Cooper, 1975)*

### 2.5.4. Overview of the Dissipated Energy Approach

Dissipated Energy can be defined as the energy that is put into a material from outside work, and can physically be defined as the area under the stress-strain curve. SHRP (1994) indicated that the energy dissipated during each load cycle captures the effects not only of the imposed strain but also of the dynamic mixture properties.

Carpenter et al. (2003), Shen & Carpenter (2005) and Shen & Carpenter (2007), found that the fatigue life of asphalt mixtures under various loading conditions can be uniquely related to an energy parameter. This energy parameter is called the plateau value (PV) and can be defined as the constant value of the ratio of dissipated energy change (RDEC) during a flexural beam fatigue test. As a fundamental energy parameter, the PV can be determined from the material properties and loading levels. Shen & Carpenter (2007) found that the PV is a function of tensile

strain, flexural stiffness, a volumetric parameter as a function of asphalt content and air void of the mixture, and a gradation parameter. The PV can be used to calculate the fatigue life ($N_f$), with the following equations:

$$PV = 44.422\,\varepsilon^{5.14}\;S^{2.993}\;VP^{1.85}\;GP^{-0.4063} \qquad \textbf{Equation 2-22}$$

$$N_f = 0.4801\,PV^{-0.9007} \qquad \textbf{Equation 2-23}$$

where,

| | | |
|---|---|---|
| $\varepsilon$ | = | tensile strain (in/in) |
| $S$ | = | flexural stiffness mix from the laboratory fatigue test (MPa) |
| $VP$ | = | volumetric parameter |
| $GP$ | = | aggregate gradation parameter |

The VP and GP parameter can be calculated using Equation 2-24 and Equation 2-25, as presented below:

$$VP = \frac{AV}{AV + V_b} \qquad \textbf{Equation 2-24}$$

$$GP = \frac{P_{NMS} + P_{PCS}}{P_{200}} \qquad \textbf{Equation 2-25}$$

with,

$$V_b = 100 \times \frac{G_{mb} \times P_{ac}}{G_b} \qquad \textbf{Equation 2-26}$$

where,

| | | |
|---|---|---|
| $AV$ | = | air voids of mixture (%) |
| $V_b$ | = | asphalt content by volume (%) |
| $G_{mb}$ | = | bulk density of mixture |
| $P_{ac}$ | = | asphalt content by total weight of mix (%) |
| $G_b$ | = | bulk specific gravity of asphalt binder |
| $P_{NMS}$ | = | aggregate passing nominal maximum size sieve (%) |
| $P_{PCS}$ | = | aggregate passing primary control sieve (%) |
| $PCS$ | = | NMS × 0.22 |
| $P_{200}$ | = | aggregate passing No. 200 (0.075-mm) sieve (%) |

Shen & Carpenter (2007) explained that the fatigue prediction model can be extended to take various field conditions such as temperature, loading rates (frequency), and rest periods into account. The reason for this is the model is based on fundamental energy principles. The model developed by Shen & Carpenter (2007), although laboratory based, has the capability of portraying real field conditions when variables like the daily and annual temperature fluctuations or the relationship between rest period and vehicle speed are considered.

### 2.5.5. Crack Propagation and The Paris law

The Paris law is the most popular fatigue crack growth model used in fracture mechanics and material sciences. The Paris law relates the stress intensity factor range to sub-critical crack growth under a fatigue stress regime, see Figure 2-9.

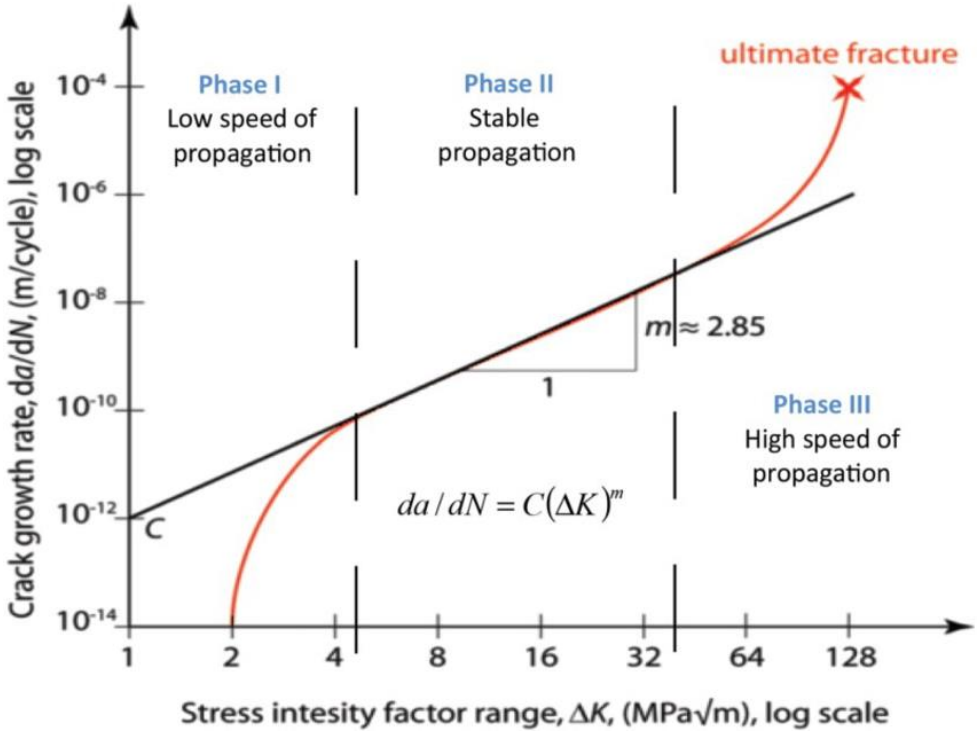


*Figure 2—9: The three phases of crack growth, Paris law (Jaoude, 2015)*

The Paris law is calibrated to model the linear interval around the centre (Phase II), as shown in Figure 2-9. The basic formula reads:

$$\frac{da}{dN} = C\Delta K^m \qquad \textbf{Equation 2-27}$$

where,

| | | |
|---|---|---|
| $\frac{da}{dN}$ | = | crack growth rate |
| $\Delta K$ | = | range of the stress intensity factor, $[K_{max} - K_{min}]$ |
| $C, m$ | = | material constants |

Crack propagation can be related to fatigue life with the following equation:

$$N_f = \int_{a_i}^{a_c} \frac{da}{C\left(\Delta\sigma Y\sqrt{\pi a}\right)^m} \qquad \textbf{Equation 2-28}$$

### 2.5.6. Endurance limit for asphalt concrete

The principle of the endurance limit is that there is a certain strain limit below which no fatigue will occur. Molenaar (2007) explained that this principal is similar to what is common practice in the concrete pavement design, in which it is stated that no fatigue will occur when the ratio of applied stress over stress at failure is below 0.5. Ayers (2006) showed that the endurance limit of asphalt concrete is a strain value of around 70 µm/m.

Molenaar (2007) also indicated that the existence of an endurance limit for asphalt concrete can be deliberated for the following reasons:

1. If fatigue failure in asphalt mixes is because of accumulating plastic strain, then fatigue will occur only if the tensile strain applied exceeds the elastic limit.
2. The elastic limit is dependent on temperature and loading time.

When considering points 1 and 2 above, it can be concluded that no single value for the endurance limit exists. Figure 2-10 illustrates the theoretical concept of the endurance limit, as it would be applied to asphaltic materials.

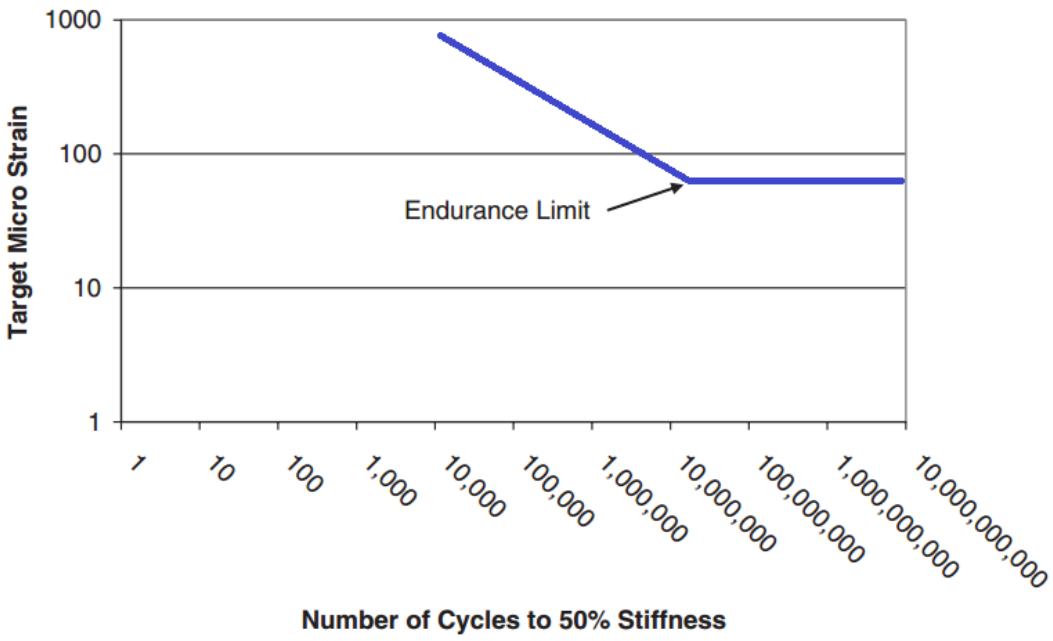


*Figure 2—10: Idealized concept of the endurance limit (NCHRP Report 646, 2010)*

### 2.5.7. Fatigue Testing Principles

Fatigue prediction can be done using several procedures and methodologies, however it is desirable that the tests be as closely simulated to real in-field properties as possible. Adhikari et al. (2009), Shen & Carpenter (2005) and Shen & Carpenter (2007) indicated that the test used should incorporate a logical relationship of test data acquired to field performance criterion.

Tangella et al. (1990), Airey (1995) and Twagira (2006) established that the following tests can be regarded when considering fatigue testing:

- flexural test (supported as well as simple flexural tests)
- wheel tracking test
- fracture mechanics test
- triaxial test
- diametral test
- direct triaxial

In this regard, Castelo et al. (2008) indicate that the fatigue life depends on numerous factors amongst other is the mode of loading, geometry of specimen, loading configuration and frequency. Different failure criteria is used in different methods to define material failure, which include:

- 50% reduction in initial stiffness
- 90% reduction in complex modulus
- 100% increase in the initial strain value (controlled stress test)
- achievement of maximum phase angle
- complete failure of specimen

Airey (1995) and Adhikari et al. (2009) emphasised the importance of understanding the basic principles under which a test is done, before selecting a test method. The AASHTO T321 make reference to the flexural stiffness beam test and specifies application of constant sinusoidal loading on the beam specimen. With regards to this model, a fatigue failure criterion of 50% reduction in initial stiffness of the beam specimen is noted.

## 2.6. SUMMARY

This chapter provides a historic look at the development of EME asphalt in France as well as the evolution and design methodology thereof. The link between EME in France and the development of High Modulus Asphalt (HiMA) in South Africa are also discussed. The most important aspect of EME asphalt is the high stiffness properties, as a result of the low penetration grade bitumen, it holds. The chapter also focusses on the different binder grading systems, in order to better understand the properties of low penetration grade bitumen.

The principle guidelines with regards to EME asphalt mixtures, fatigue and flexural stiffness evaluation is discussed in detail. The principles, findings and recommendations from notable research papers and literature in relation to flexural stiffness and fatigue evaluation is considered. This chapter pronounces the literature on fatigue cracking and numerous fatigue models as well as their approaches.

The following chapter builds from principles highlighted in this chapter, clear references are made in these cases.

# CHAPTER THREE

# 3. RESEARCH METHODOLOGY

## 3.1. INTRODUCTION

In October 2014, SANRAL appointed Royal HaskoningDHV (Pty) Ltd as the service provider for the special maintenance of the truck crawler lane on the National Route 1 Section 1. This research study forms part of the EME N1/1 project, conducted by SANRAL, for the Master Curve Development and Fatigue Testing on Enrobés à Module Elevé (EME) asphalt that was used on the N1/1 between the Toll Plaza and the Huguenot Tunnel.

The activities involved in the manufacturing process of the samples and the testing of the specimens can be divided into three phases:

- Production phase (Much Asphalt)
- Laboratory Testing phase (Stellenbosch University)
- Numerical Modelling Phase

The production phase was undertaken at and by Much Asphalt, situated in Eerste River in Cape Town. The production phase activities included:

- the production and preparation of the EME mix
- the manufacturing and compaction of slabs
- securing slab support for transportation
- delivering compacted slabs

The laboratory phase was undertaken at the University of Stellenbosch, and included the following activities:

- visual inspection of slabs
- saw cutting of slabs into required beam specimen dimensions
- labelling beam specimens
- conducting BRD tests on beams specimens
- loading beam specimens into the fatigue beam apparatus for testing
- harvesting and processing of results

The Numerical Modelling phase was done to investigate the effect that the loading waveform, sinusoidal compared to haversine, has on the tensile stress developed in the beam. This modelling will aim to explain the premature failure in certain haversine loaded beams.

This chapter covers the tests and test procedures followed in order to investigate all aspects surrounding the fatigue life and flexural tests on the EME asphalt. The chronological project plan followed during the duration of this study is illustrated in Figure 3-1.

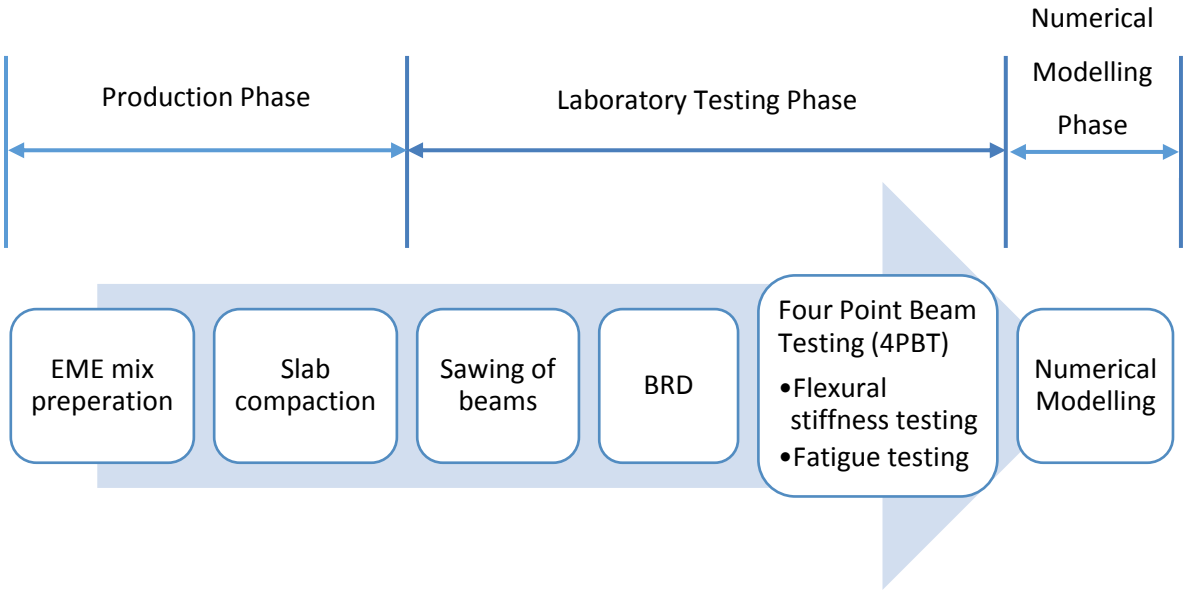


*Figure 3—1: Chronological project plan followed in the study*

The laboratory tests done on the EME asphalt consists of Flexural Stiffness – and Fatigue testing using the Four Point Beam Testing (4PBT). Upon completion of the first Flexural Stiffness test it was evident that the initial suggested temperatures (10˚C, 20˚C, 40˚C) did not yield overlapping results for the Master Curve, because of the high flexural stiffness of EME asphalt. It was therefore decided to increase the temperature range with 5˚C increments, i.e. (10˚C, 15˚C, 20˚C, 25˚C, 30˚C, 35˚C, 40˚C). The expanded testing matrix for the study can be seen in Table 3-1. It is important to note that the ten initial Fatigue classification tests and the Flexural Stiffness tests were performed on a lab mix design, whereas the Fatigue tests were performed on a plant mix. It is suspected that the lab mix were done with imported 10/20 unmodified penetration grade bitumen from, while the plant mix is suspected to be done using local 10/20 unmodified penetration grade bitumen from Shell (Sapref) in Kwa-Zulu Natal.

*Table 3—1: Testing matrix for project*

| | Quantity |
|---|---|
| **1) Flexural Stiffness (Lab mix Design)** | |
| Frequency and temperature sweep (0.5Hz, 1Hz, 2Hz, 5Hz, 10Hz at 10˚C, 15˚C, 20˚C, 25˚C, 30˚C, 35˚C, 40˚C) | 2 |
| **2) Fatigue Testing (Plant mix)** | |
| Fatigue Testing at 250με at 10˚C | 3 |
| Fatigue Testing at 175με at 10˚C | 2 |
| Fatigue Testing at 100με at 10˚C | 1 |
| Fatigue Testing at 50με at 10˚C | 2 |
| Fatigue Testing at 250με at 40˚C | 1 |
| Fatigue Testing at 175με at 40˚C | 2 |
| Fatigue Testing at 100με at 40˚C | 2 |
| Fatigue Testing at 50με at 40˚C | 2 |
| **3) Fatigue Classification Testing (Lab mix Design)** | |
| Fatigue Testing at 250με at 10˚C | 10 |

## 3.2. PREPARATION OF MIX

The mix design was developed beforehand by Much Asphalt. The primary components of the mix can be seen in Table 3-2.

*Table 3—2: EME mix design*

| Mix Mass Proportions: 5.7% Bitumen | |
|---|---|
| **Mix Type:** | **EME with 10/20 Bitumen** |
| Aggregate Type: | % in Mix |
| 13.2mm Stone | 36% |
| 9.5mm Stone | 14% |
| Crusher Dust | 49% |
| Lime | 1% |

The preparation of the mix was done at and by Much Asphalt. Raw materials were heated up and mixed in a drum mixer at 180˚C. During every production, the mix produced was assessed for mix quality and viability of use. Each mix was used to manufacture one slab of around 20kg. All mixes used contained a target binder content of 5.7% and were mixed until all the aggregate

was completely coated with asphalt binder. An illustration of the mixing drum before, during and after the addition of binder can be seen in Figure 3-2.

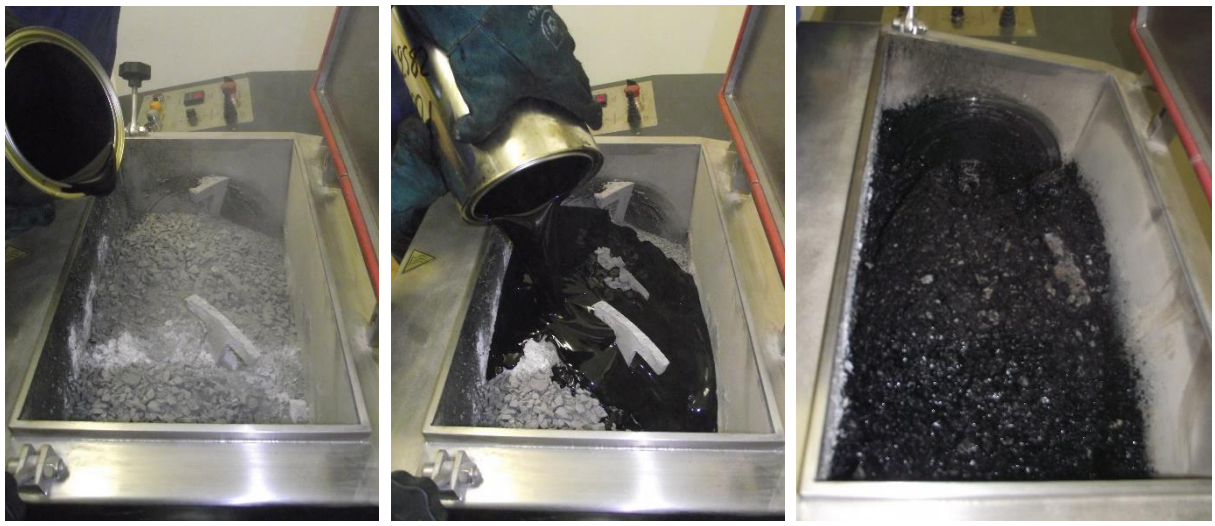

*Figure 3—2: Much Asphalt - mixing drum*

## 3.3. COMPACTION OF SLABS

The compaction of slabs was also performed by Much Asphalt using an advanced asphalt slab roller compactor as illustrated in Figure 3-3. The steel mould used in the slab compaction process has internal dimensions of 400x300x63mm. The desired void ratio of the slabs were achieved through trial and error together with certain input variables requested by the software of the compactor. A fixed amount of asphalt was placed inside the mould, where after the height and density requirements of the slab was entered.

The slab compactor uses a heated roller to ensure overall consistent compaction under preferred temperatures. This roller is heated to a temperature of 150°C before the compaction process starts. The roller presses down on the mix and measures the height of the mix with each pass. As the density of the slab increases the force of the roller pressing down by the slab is increased. Once the desired height and/or density of the slab has been achieved the slab compactor applies a smooth finish before the roller is lifted up.

*Figure 3—3: Much Asphalt - slab compactor*

After the slabs reach the desired compaction densities, they are removed from the compact roller, while still secured within the mould (see Figure 3-4). In order to prevent any damage to the slabs, they are left in the mould to cool down before removal. The cooled down slabs are carefully removed and placed on wooden planks to support the slab as a whole during transportation to the University of Stellenbosch. The supported slab can be seen in Figure 3-5.


*Figure 3—4: Slab left to cool down within mould*

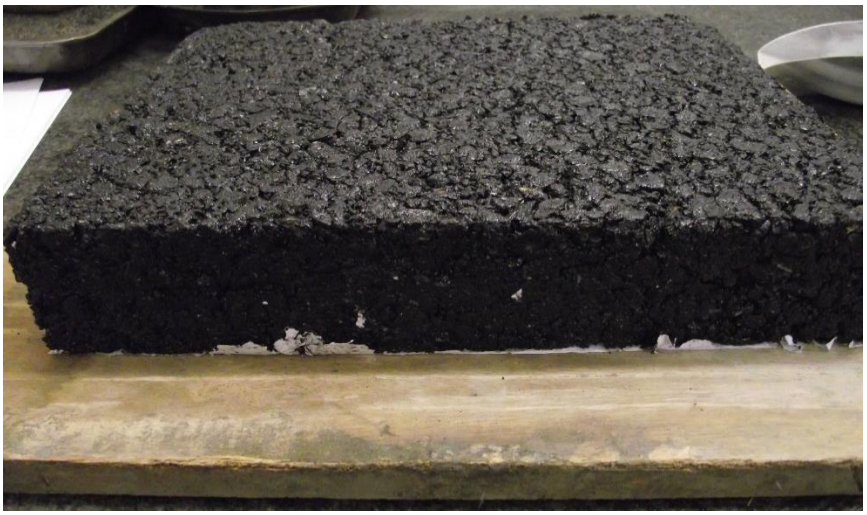

*Figure 3—5: Slab secured on wooden plank for transport*

Some challenges were experienced in the preparation of these slabs. These challenges related to inconsistent void percentages found in different slabs, with identical preparation processes. The compaction process were improved, through trial and error as well as experienced gained as the study progressed. However, queries still remain for improvement on uniform compaction results over a range of specimens. Additional challenges and troubleshooting are referred to in Section 3.8.

## 3.4. SAWING AND NUMBERING OF BEAMS

The slabs received by Much Asphalt were sawed at the University of Stellenbosch, using a diamond blade saw. Wet sawing was preferred over dry sawing to minimise possible damage to the asphalt beams. Each slab yielded three beams with predefined dimensions of 400x63x50mm as shown in Figure 3-6. When considering Figure 3-6 (a) and (b), the dotted lines represent the sawing of the beams from the supplied slabs, with the grey areas representing the asphalt that were cut off and disposed of. Figure 3-6 (c) shows a three dimensional view of the slab with the beams indicated by the three grey objects. A total variation of 3mm was accepted in both the width and height of beam specimens, the width measurements were thus allowed to range from 61.5mm – 64.5mm, with the height measurements allowed to range from 48.5 mm – 51.5 mm. Because of the great effect that these variation could have on the response results, close

attention was payed to perfecting the sawed beam dimensions to a width of 63 mm and a height of 50 mm.

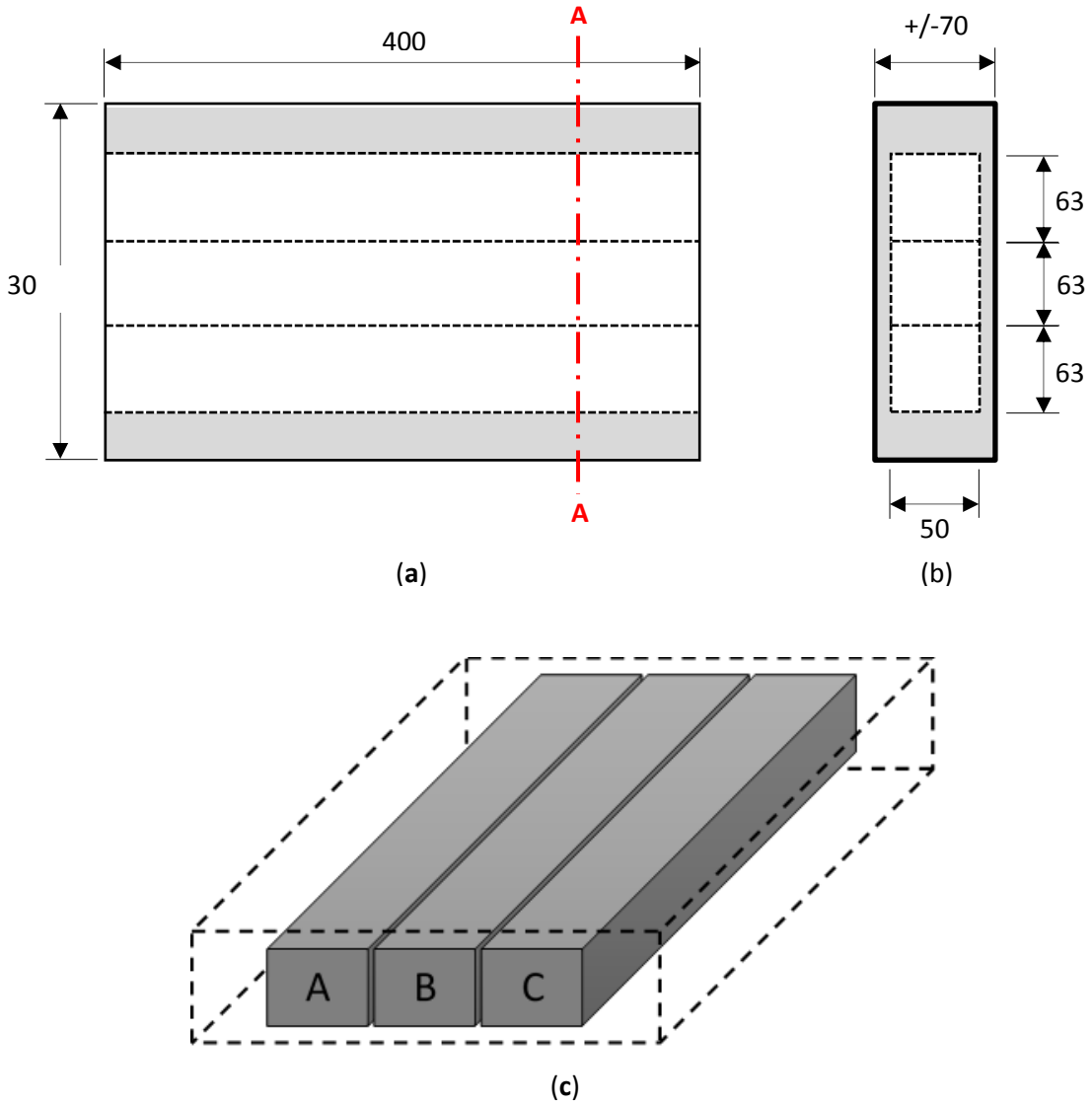


*Figure 3—6: Sawing process with (a) Top view of slab (b) Section A-A and (c) 3D final view*

The sawing process was initiated by sawing off one longitudinal edge from the slab (+/- 50 mm), this piece was discarded. Three beams, each with a width of 63mm, were then sawed in the longitudinal direction. The three beams went through the last process by sawing them to a height of 50mm. As indicated in Figure 3-6, sawing to both the top and bottom of the beams was preferred in order to prevent possible surface effects to influence test results.

The numbering of beams were done in the form of the slab number followed by A, B or C depending on the position of the beam in the slab, i.e. S1-BA, meaning SLAB 1 – BEAM A. Figure 3-7 illustrates the numbering process for Slab number 1.

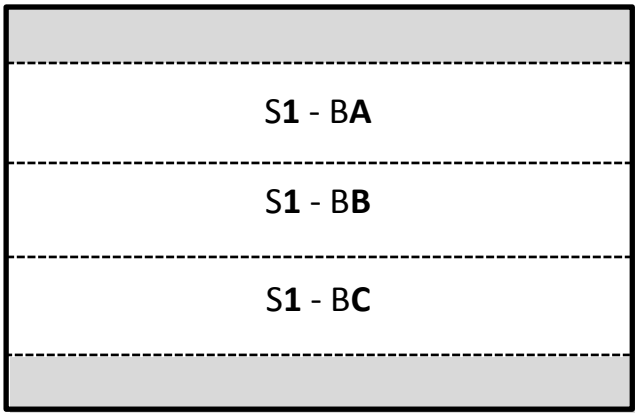


*Figure 3—7: Numbering of beams*

## 3.5. BULK RELATIVE DENSITY TEST (BRD)

The Bulk Relative Density (BRD) test is done in order to determine the void content of a compacted material. The BRD is determined by weighing the specimen (beam) under three different conditions:

1. Dry (no water in sample)
2. Submerged in water (underwater)
3. Saturated surface dry (water fills the air voids)

This proses includes firstly weighing the specimen when it is dry. It is then placed in water with a constant temperature of 25°C for no less than 5 minutes. This specimen is then weighed under water, removed and surface dried before weighing it again. With the three different weights known, the BRD of a specimen can be calculated using Equation 3-1.

$$BRD = \frac{Dry\ weight}{Surface\ dry\ weight - Weight\ in\ water} \qquad \textbf{Equation 3-1}$$

Before the void content of the specimen can be determined, the theoretical maximum specific gravity (Rice Density) of the mix need to be known. The test for the determination of the Rice Density is done based on '*AASHTO T 209 and ASTM D 2041: Theoretical Maximum Specific Gravity and Density of Bituminous Paving Mixtures'*. The basic principle to determine the maximum specific gravity is to divide the mass of the sample by the volume of the sample with the air voids excluded. The mass of the sample is determined by weighing the dry sample, either at the beginning of the test or at the end of the test, when it had time to dry. The volume of the sample, with the air voids excluded, is calculated by measuring the mass of the water that is displaced by the sample and dividing this measurement by the unit weight of water.

With the BRD and Rice density known the percentage voids of the specimen can be calculated with Equation 3-2. The percentage voids could be used to explain certain fatigue and stiffness attributes of the specimen. This is an important factor for EME asphalt as it can become brittle at low temperatures when over-compacted.

$$Voids\ (\%) = (1 - \frac{BRD}{Rice})/100 \qquad \textbf{Equation 3-2}$$

## 3.6. FLEXURAL FATIGUE TEST

The Flexural Fatigue Test, as described by Pavement Interactive (Flexural Fatigue – 2011), is used to properly characterize the fatigue life of asphalt at intermediate pavement operating temperatures. The characterization of the fatigue life is useful as it provide estimates of asphalt pavement layer fatigue life under repeated traffic loading. This repeated traffic loading cause deflections in the pavement which creates tensile stresses and strains in the pavement layers, as shown in Figure 3-8. The strains in a well-designed pavement are low enough for fatigue not to cause excessive damage. In an under-designed pavement strains are sufficiently higher, in this case fatigue failures can be a problem under repeated load. These failures will lead to fatigue cracking (Figure 3-9) which, if not maintained in time, will result in disintegration of the pavement.

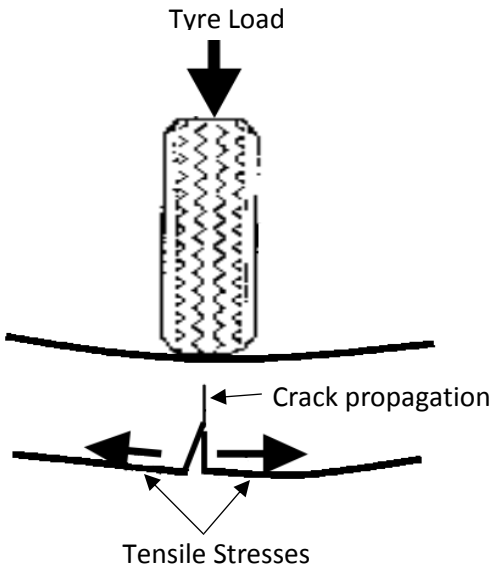


*Figure 3—8: Crack development under wheel load (Walubita & Ven, 2000)*

*Figure 3—9: Extensive fatigue cracking (Pavement Interactive, 2011)*

To simulate these deflections and strains in the asphalt layer, the Four Point Beam Testing (4PBT) apparatus is used (see Figure 3-10), in conjunction with the test procedure as described in *AASHTO T321: Determining the Fatigue Life of Compacted Hot-Mix Asphalt (HMA) Subjected to Repeated Flexural Bending*. In order to simulate field conditions, the 4PBT can control, strain (displacement), frequency and temperature at which tests are done.

All tests were carried out using strain (displacement) controlled testing. The procedure followed in setting up the 4PBT is:

- Open the clamps and slide the beam specimen into place, ensuring that no damage occur to either the specimen or the apparatus parts.
- Centre the beam by ensuring the offset on each end to be identical.
- When the beam is in place, begin by closing the side clamps followed by the vertical clamps on the outside and inside. The clamps will ensure that the specimen is held in place during testing.
- Attach and clamp the Linear Variable Differential Transducer (LVDT) into position, so that the LDVT reading is as close to zero as possible.
- Close the environmental chamber and select the desired input variables on the operating software.

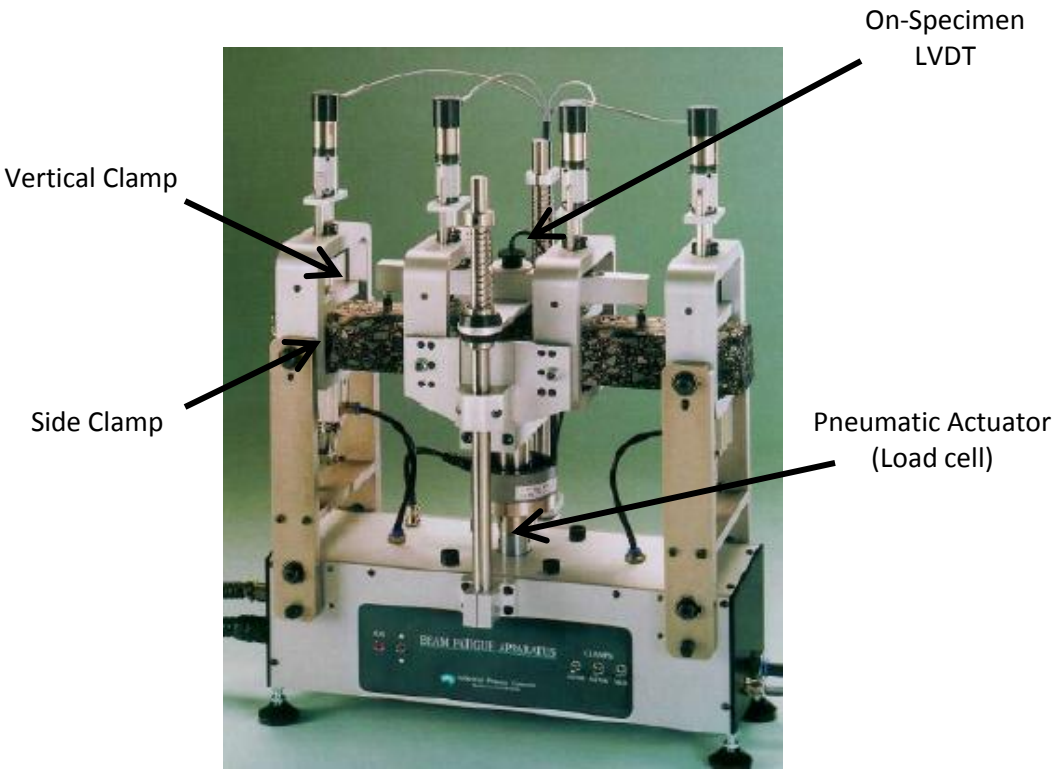


*Figure 3—10: Four Point Beam Testing apparatus (IPC, 1998)*

The flexural fatigue test matrix, as used in the study at hand, can be seen in Figure 3-11.

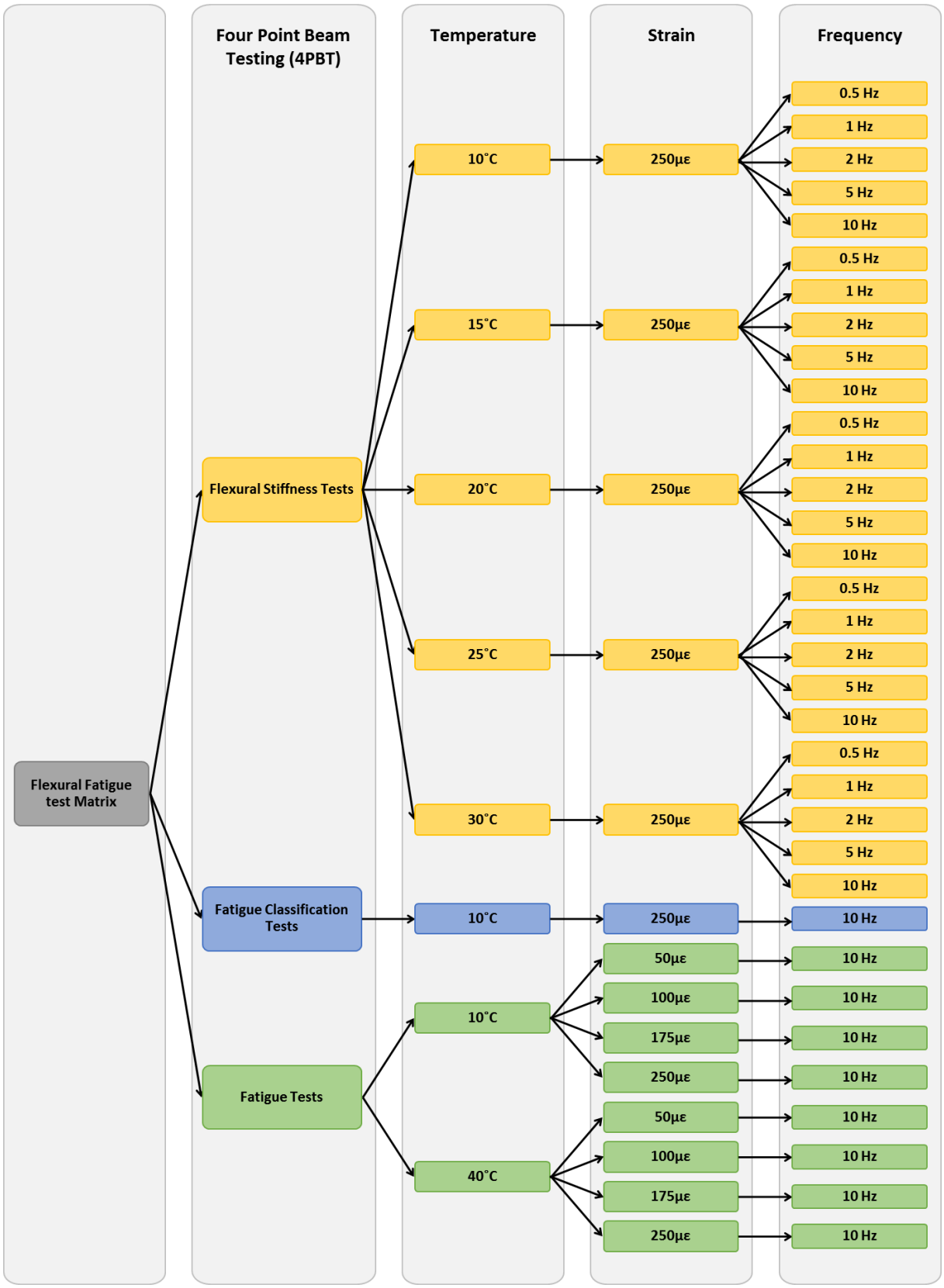


*Figure 3—11: Flexural Fatigue test matrix*

### 3.6.1. Flexural stiffness test procedure

The flexural stiffness tests were done in order to develop a Master Curve for the investigated mix. With regards to flexural stiffness testing, the following parameters were set:

- sinusoidal strain as loading mode
- pulse frequencies of 0.5, 1, 2, 5 and 10 Hz
- conditioning temperatures of 10, 15, 20, 25, 30, 35 and 40°C
- 300 cycles for a complete mix stiffness analysis
- initial flexural stiffness measured at the 50$^{th}$ cycle

The flexural stiffness tests were started at 40˚C and worked downwards to 10˚C to minimize damage caused to the beam during testing. The beams were tested at all pulse frequencies, starting at 0.5 Hz and moving up to 10 Hz, before lowering the temperature. After each temperature array were completed for all the pulse frequencies, the temperature was adjusted and the beam left to condition for four hours at the new temperature.

### 3.6.2. Fatigue test procedure

Sabita is in the process of updating *Manual 33 – Interim Procedure for the Design of High Modulus Asphalt (EME).* The current fatigue criteria as stipulated in the manual were based on limited data at the time, this yielded unduly conservative results. Further work carried out by the CSIR has since resulted in the adjustment of the classification strain value from 330 με to 260 με for a class 2 mix. The current fatigue classification criteria can be seen below in Table 3-3.

*Table 3—3: Sabita EME fatigue criteria*

| Test | Method | Number of specimens | Class 1 | Class 2 |
|---|---|---|---|---|
| Four point bending at 10Hz, 10˚C to 50% stiffness reduction | AASHTO T321 | 9 | ≥ $10^6$ repetitions @ 210με | ≥ $10^6$ repetitions @ 260με |

With regards to fatigue classification testing, the following parameters were set:

- haversine and sinusoidal strain as loading mode (investigative purposes)
- pulse frequency of 10 Hz
- temperature of 10˚C
- 50 conditioning cycles
- 250 με as peak to peak strain
- initial flexural stiffness measured at 50 cycles
- 1 000 000 target cycles

The beam samples were placed in the environmental chamber at 10˚C and left for at least 4 hours, in order to undergo sufficient conditioning prior to testing.

With regards to fatigue testing, the following parameters were set:

- sinusoidal strain as loading mode
- pulse frequency of 10 Hz
- temperature of 10˚C and 40˚C
- 50 conditioning cycles
- peak to peak strain range of 50, 100, 175 and 250 με
- test run until 50% stiffness reduction or 2 000 000 cycles (later changed to 4 000 000 cycles to get a better understanding with regards to fatigue results)

The beam samples were placed in the environmental chamber at the investigated temperature (10˚C and 40˚C respectively) and left for at least 4 hours, in order to undergo sufficient conditioning prior to testing.

On selecting the temperatures for the fatigue tests, the pavement design method was selected to be the South African Road Design System (SARDS). The reason for this being the inclusion of recursive analysis of daily temperature cycles that range between 10°C and 40°C – see Figure 3-12.

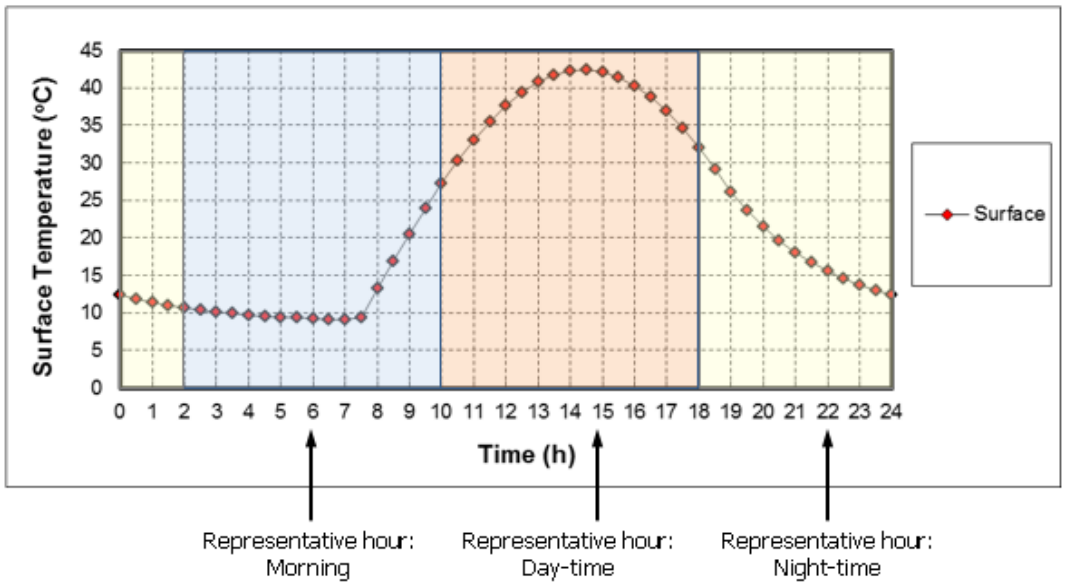


*Figure 3—12: Surface temperature vs Time of day* (Theyse, 2015)

### 3.6.3. Sinusoidal versus Haversine wavefronts

The Four Point Beam apparatus can be set to apply either a sinusoidal or haversine loading wave to the beam specimen. This implies that for a sine wave loading pattern the beam will bend to a strain of 0.5 strain value fraction, return to the original position and bend to a strain of 0.5 strain value fraction in the other direction. For the haversine wave loading pattern, the beam will bend to a strain of 1 strain value fraction in one direction and return to the original position. The peak to peak strain value for both loading cases are thus the same. Figure 3-13 shows the strain over one loading cycle for the (a) sine and (b) haversine loading waves respectively. The strain value fractions for both cases, as discussed above, can also be seen in Figure 3-13.

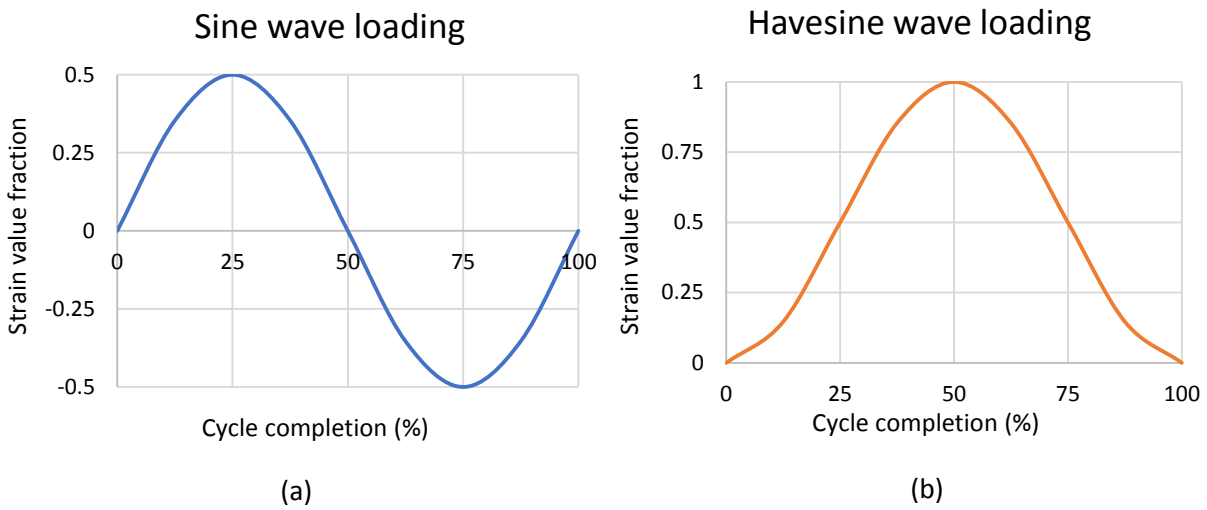


*Figure 3—13: Representation of (a) sine vs (b) haversine wave loading*

Displacement controlled haversine and sinusoidal fatigue test protocols are defined in ASTM D7460 and AASHTO T321, respectively. Figure 3-16 illustrates the position of the neutral axis and the extreme positions of a beam specimen during the sinusoidal deflection-controlled test and the haversine deflection-controlled test. Witczak, et al. (2013) indicated that during the sinusoidal test (Figure 3-14 (a)), the deflection pattern is sinusoidal, bending the beam in both directions. The neutral axis of the beam stays unchanged during the test and remains in the original position halfway between the two extreme positions. During the haversine test (Figure 3-14 (b)), the deflection pattern is haversine, bending the beam with the same peak-to-peak magnitude as the sinusoidal test but only in one direction. Because of the static force component in the load signal and the viscous character of the material, creep (permanent deformation) will occur in the beam, causing the neutral axis of the beam to shift downwards after a few loading cycles. After the shift of the neutral axis the original haversine loading pattern will become a sine loading pattern with respect to the new neutral axis, as shown in Figure 3-14 (b).

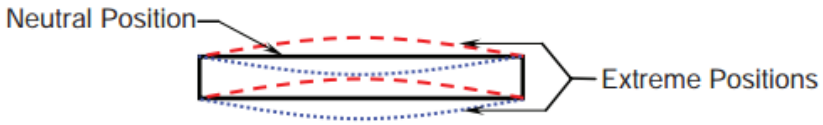


(a) Sinusoidal (AASHTO T321)

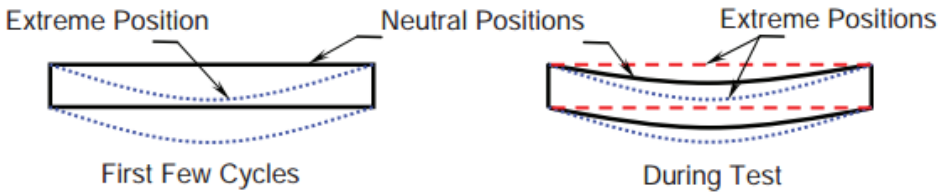


(b) Haversine (ASTM D7460)

*Figure 3—14: Neutral axis and extreme positions using sinusoidal and haversine loading* (Witczak, et al., 2013)

Figure 3-15 illustrates the deflection input together with the stress and strain outputs that is created in the beam during the fatigue test. During the sinusoidal test, the developed strains and stresses are also sinusoidal, causing alternating tension and compression in the beam as shown in Figure 3-15 (a). Witczak, et al. (2013) indicated that for the haversine test, the deflection input remains haversine throughout the test, with the developed strain and stress pulses starting as haversine waveforms causing strain and stress in one direction. Because of the shifted position of the neutral axis, the developed strain and stress pulses change to sinusoidal after a few cycles. This change cause alternating tension and compression in the beam, with half of the magnitude of the stress applied at the beginning of the test as shown in Figure 3-15 (b).

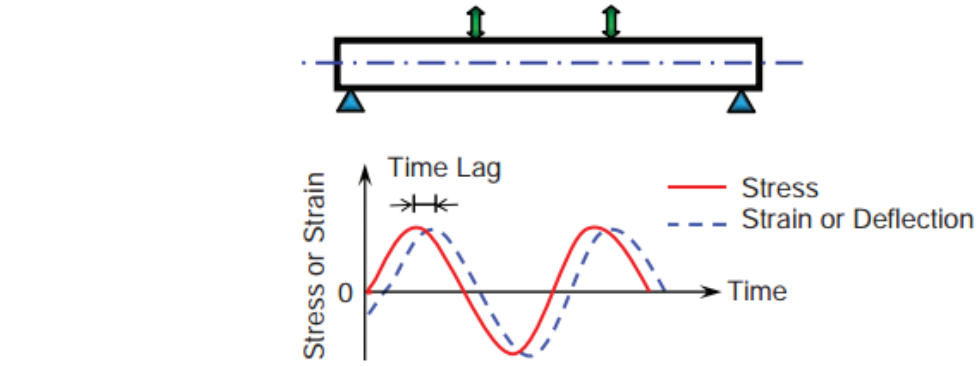


(a) Sinusoidal (AASHTO T321)

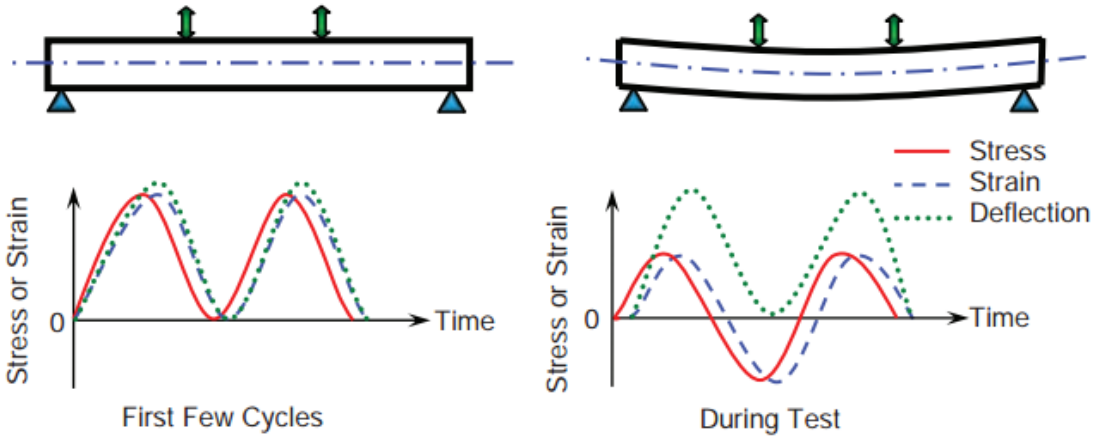


(b) Haversine (ASTM D7460)

*Figure 3—15: Stress, strain and deflection vs time for sinusoidal and haversine loading (Witczak, et al., 2013)*

Evidence of this shifted neutral axis phenomenon was found in the test results and can be seen in Chapter Four.

### 3.6.4. Conclusion

When considering EME asphalt with a flexural stiffness four times higher than that of a typical asphalt, the process of haversine wave loading to sine wave loading will take much longer. The longer exposure to the high strain level caused by the haversine wave loading will cause more damage to EME than a typical asphalt. EME asphalt is therefore very sensitive to the loading condition, and for that reason it was concluded that the deflection-controlled sinusoidal test

(AASHTO T321) is more consistent than the deflection-controlled haversine test (ASTM D7460), since it produces the intended stress and strain waveform.

## 3.7. NUMERICAL MODELLING

The numerical modelling for the EME beams, based on simulation using the finite element method, were done with the help of ABAQUS FAE Software. The simulation was done in order to investigate the initial tensile stresses created in the beams when loaded with a sinusoidal as well as a haversine waveform in the Four Point Beam Test (4PBT). This investigation was brought forth after premature failure to beam specimens, loaded with a haversine waveform, were observed during the fatigue classification tests.

In order to yield comparative results, it was aimed to simulate the 4PBT and all of its dimensions accurately in the modelling process. The dimensions of the beam setup and clamp positions can be seen as a plan view in Figure 3-16. The beam width is 63 mm.

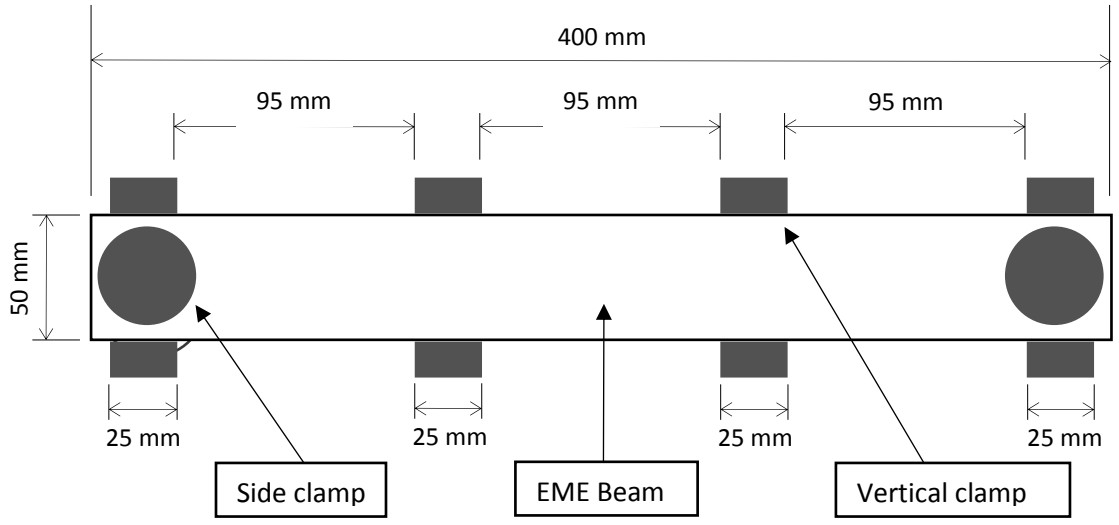


*Figure 3—16: Simulated beam setup and dimensions*

Figure 3-17 illustrates the completed beam setup prior to testing, the beam properties as used in ABAQUS FAE Software will be discussed in Chapter Four.

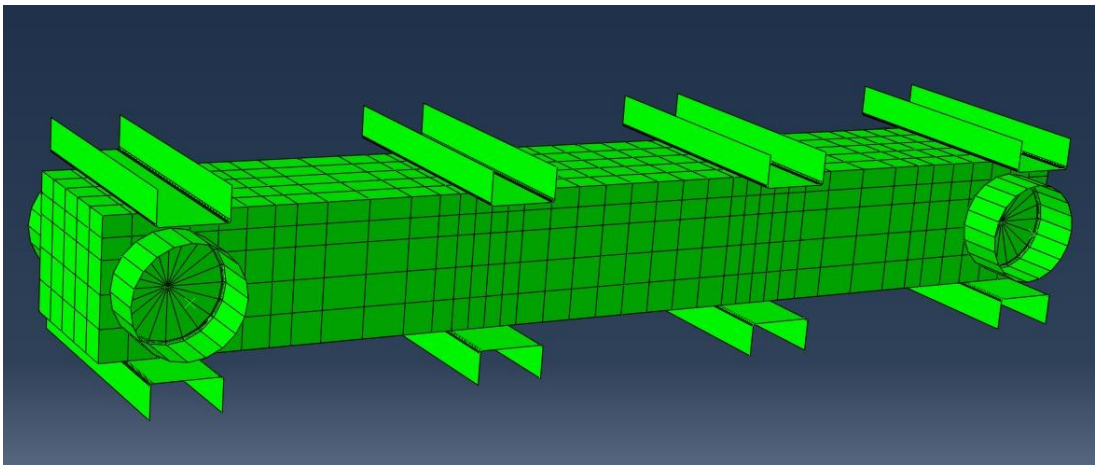

*Figure 3—17: Completed beam setup in ABAQUS FAE*

## 3.8. CHALLENGES FACED AND TROUBLESHOOTING

During the duration of the project, the following challenges were encountered and addressed:

1. Some challenges were found in the preparation of the slab specimens. The slabs for this research project, were compacted with a brand new slab compactor, at Much Asphalt. Because of the inexperience regarding the slab compactor, challenges relating to the repeatability of the percentage air voids were found.

   ✓ To some degree the consistency of results were improved through calibration of the slab compactor as well as numerous repetition of compaction samples. However, some queries remain for improvement.

2. During the initial stages of testing, it was decided to load the beam with a haversine loading pattern. Because of the high stiffness of EME, this loading pattern caused immediate brittle failure to the beams.

   ✓ This was solved by converting to sinusoidal loading.

3. Fatigue tests done at a load frequency of 10 Hz take 4 days and 15 hours to complete the maximum of 4 000 000 load cycles. The tests were done in 2015 when South Africa

experienced regular load shedding, and as a result thereof a number of tests were interrupted prematurely.

- ✓ Planning was done so that the running time of the test did not overlap with the predicted load shedding schedule.

# CHAPTER FOUR

# 4. LABORATORY TEST RESULTS AND DISCUSSION

## 4.1. INTRODUCTION

This chapter provides, beam properties, laboratory test results and the evaluation of test results and findings. The beam properties provide information on the BRD and air void percentages of the various beams, as used during testing.

## 4.2. BEAM PROPERTIES

During the initial stages of testing, various options were investigated for load signals on the Four Point Beam test, namely haversine wave (ASTM D7460) and sinusoidal wave (AASHTO T321). After testing both loading profiles it was obvious that the sine loading signal was the only viable option. Because of the high stiffness properties of EME asphalt, the beams failed in a brittle way by snapping prematurely when loaded with a haversine loading signal. The fatigue results for both loading cases will be shown and discussed later on in the chapter.

Table 4-1 illustrates beam details as used in the testing regime. These details consist of slab number, beam number, BRD calculation and void content (%). The different colour schemes are an indication of the test in which the respective beams were used. Because the fatigue tests on S13-BA, S13-BB and S15-BB was done at the same test details, 10 Hz, 10˚C and sine wave signal with a peak to peak strain value of 250με, as used for the fatigue classification, these three beams were also added to the fatigue classification results.

The target air void percentage was 4%, with the initial acceptance ranging between 3% and 5%. Because of the challenges related to compaction in the early stages, as described in Section 1.2.2, some exceptions had to be made for the study. Numerous beams outside this range was used for the fatigue classification tests as well as the flexural stiffness tests. For the fatigue performance the acceptance range was strictly abided by – see Table 4-1.

The individually measured beam dimensions are presented in Table 4-2. These measurements were taken at three points, the start, middle and end point.

*Table 4—1: Beam properties and details*

| Slab Number | Beam Number | BRD Results | | | | |
|---|---|---|---|---|---|---|
| | | Mass of Briquette (g) | | | BRD a/(b-c) | Voids (%) (1-BRD/Rice)x100 **Rice = 2.495** |
| | | Dry (a) | Surface Dry (b) | In Water (c) | | |
| 1 | A | 2943.54 | 2947.7 | 1722.58 | 2.403 | 3.70 |
| 1 | B | 2973.46 | 2977.22 | 1742.36 | 2.408 | 3.49 |
| 1 | C | 3021.22 | 3026.71 | 1768.18 | 2.401 | 3.78 |
| 2 | A | 1874.5 | 1875.47 | 1107.35 | 2.440 | 2.19 |
| 2 | B | 1928.33 | 1930.65 | 1141.5 | 2.444 | 2.06 |
| 2 | C | 1808.59 | 1809.53 | 1067.98 | 2.439 | 2.25 |
| 3 | A | 2985.84 | 2987.02 | 1754.29 | 2.422 | 2.92 |
| 3 | B | 1737.37 | 1738.3 | 1024.18 | 2.433 | 2.49 |
| 3 | C | 2987.68 | 2989.66 | 1757.62 | 2.425 | 2.81 |
| 4 | A | 2901.97 | 2911.35 | 1669.85 | 2.337 | 6.31 |
| 4 | B | 1586.32 | 1592.48 | 913.01 | 2.335 | 6.43 |
| 5 | A | 3007.37 | 3010.45 | 1757.18 | 2.400 | 3.82 |
| 5 | B | 2993.11 | 2995.67 | 1750.54 | 2.404 | 3.65 |
| 5 | C | 3013.58 | 3016.93 | 1762.78 | 2.403 | 3.69 |
| 6 | A | 3010.92 | 3014.16 | 1744.2 | 2.371 | 4.97 |
| 6 | B | 2973.62 | 2976.09 | 1727.71 | 2.382 | 4.53 |
| 6 | C | 2892.26 | 2894.61 | 1680.95 | 2.383 | 4.49 |
| 7 | A | 2984.13 | 2986.04 | 1754.04 | 2.422 | 2.92 |
| 10 | C | 3094.16 | 3095.29 | 1821.48 | 2.429 | 2.64 |
| 11 | B | 3076.69 | 3077.86 | 1812.24 | 2.431 | 2.57 |
| 12 | B | 2865.74 | 2869.6 | 1667.32 | 2.384 | 4.47 |
| 13 | A | 2936.23 | 2938.62 | 1701 | 2.372 | 4.91 |
| 13 | B | 2962.32 | 2964.71 | 1723.08 | 2.386 | 4.38 |
| 13 | C | 3088.39 | 3090.47 | 1796.94 | 2.388 | 4.31 |
| 14 | A | 2926.53 | 2929.88 | 1693.61 | 2.367 | 5.12 |
| 14 | B | 2990.57 | 2993.47 | 1740.22 | 2.386 | 4.36 |
| 15 | B | 2929.6 | 2932.9 | 1701.5 | 2.379 | 4.65 |
| 17 | A | 2939.3 | 2942.3 | 1720.3 | 2.405 | 3.59 |
| 17 | B | 2964 | 2966.2 | 1738.1 | 2.413 | 3.27 |
| 18 | A | 2911.8 | 2914.2 | 1701.9 | 2.402 | 3.73 |
| 18 | B | 2935.6 | 2938.9 | 1711.4 | 2.392 | 4.15 |
| 19 | A | 2991 | 2992.8 | 1742.5 | 2.392 | 4.12 |
| 19 | C | 2929.6 | 2931.7 | 1709.6 | 2.397 | 3.92 |
| 20 | C | 2987.6 | 2990.1 | 1751.7 | 2.412 | 3.31 |
| 21 | C | 3057.3 | 3059.8 | 1793.1 | 2.414 | 3.26 |

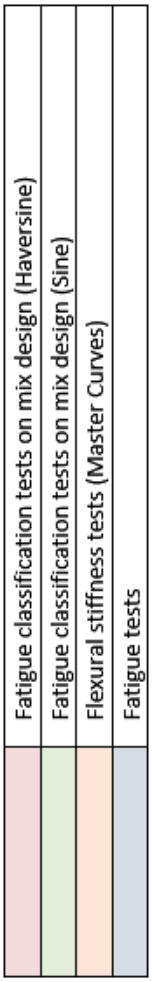

*Table 4—2: Beam measurements*

| Slab Number | Beam Number | Dimensions | | | | | | | | |
|---|---|---|---|---|---|---|---|---|---|---|
| | | Height (mm) | | | | Width (mm) | | | | Length (mm) |
| | | 1 | 2 | 3 | Average | 1 | 2 | 3 | Average | |
| 1 | A | 50 | 50 | 50 | 50.0 | 62 | 62 | 63 | 62.3 | 400 |
| 1 | B | 51 | 50.5 | 50 | 50.5 | 61.5 | 62 | 62.5 | 62.0 | 400 |
| 1 | C | 51 | 50 | 49.5 | 50.2 | 64.5 | 63.5 | 62.5 | 63.5 | 400 |
| 2 | A | 49.5 | 50.5 | 51 | 50.3 | 63 | 63 | 63.5 | 63.2 | 400 |
| 2 | B | 50.5 | 50.5 | 50 | 50.3 | 64 | 64 | 64 | 64.0 | 400 |
| 2 | C | 50 | 50.5 | 49.5 | 50.0 | 62 | 62 | 62 | 62.0 | 400 |
| 3 | A | 50.5 | 50 | 50 | 50.2 | 62.5 | 62 | 62 | 62.2 | 400 |
| 3 | B | 51 | 49 | 48 | 49.3 | 62.5 | 62 | 62 | 62.2 | 400 |
| 3 | C | 50.5 | 50 | 49.5 | 50.0 | 63.5 | 63 | 62 | 62.8 | 400 |
| 4 | A | 48 | 48.5 | 50.5 | 49.0 | 62 | 64 | 65 | 63.7 | 400 |
| 4 | B | 50 | 49.5 | 49 | 49.5 | 62.5 | 62.5 | 62.5 | 62.5 | 400 |
| 4 | C | 51.5 | 50 | 49 | 50.2 | 62.5 | 62.5 | 62 | 62.3 | 400 |
| 5 | A | 51 | 50 | 50 | 50.3 | 63.5 | 62.5 | 62.5 | 62.8 | 400 |
| 5 | B | 51.5 | 50.5 | 50 | 50.7 | 62.5 | 62.5 | 62 | 62.3 | 400 |
| 5 | C | 49.5 | 50 | 51 | 50.2 | 62.5 | 62.5 | 63 | 62.7 | 400 |
| 6 | A | 50 | 50 | 51 | 50.3 | 63 | 62.5 | 63 | 62.8 | 400 |
| 6 | B | 50.5 | 50.5 | 50.5 | 50.5 | 61.5 | 62 | 64 | 62.5 | 400 |
| 6 | C | 49 | 49 | 49 | 49.0 | 63.5 | 63 | 62.5 | 63.0 | 400 |
| 7 | A | 50 | 49.5 | 49 | 49.5 | 62.5 | 62 | 62 | 62.2 | 400 |
| 10 | C | 49.5 | 50 | 50.5 | 50.0 | 62.5 | 63.5 | 64 | 63.3 | 400 |
| 11 | B | 49.5 | 50 | 51 | 50.2 | 64 | 63 | 62.5 | 63.2 | 400 |
| 12 | B | 47.5 | 48 | 49.5 | 48.3 | 62.5 | 62.5 | 63 | 62.7 | 400 |
| 13 | A | 48.5 | 49 | 49.5 | 49.0 | 63 | 63.5 | 63.5 | 63.3 | 400 |
| 13 | B | 49 | 49 | 49 | 49.0 | 63.5 | 63 | 63 | 63.2 | 400 |
| 13 | C | 51 | 50.5 | 50 | 50.5 | 62.5 | 63.5 | 64.5 | 63.5 | 400 |
| 14 | A | 49.5 | 49.5 | 50 | 49.7 | 63.5 | 63.5 | 63 | 63.3 | 400 |
| 14 | B | 50 | 50 | 49.5 | 49.8 | 62 | 62.5 | 63 | 62.5 | 400 |
| 15 | B | 51 | 50 | 49.5 | 50.2 | 63 | 64 | 64 | 63.7 | 400 |
| 17 | A | 50 | 49 | 49.5 | 49.5 | 62 | 62.5 | 62.5 | 62.3 | 400 |
| 17 | B | 50 | 49 | 49 | 49.3 | 62.5 | 63 | 63.5 | 63.0 | 400 |
| 18 | A | 49.5 | 49.5 | 50 | 49.7 | 61.5 | 62 | 62 | 61.8 | 400 |
| 18 | B | 48.5 | 49 | 50 | 49.2 | 62 | 62 | 63 | 62.3 | 400 |
| 19 | A | 51.5 | 50.5 | 50 | 50.7 | 62 | 63 | 64 | 63.0 | 400 |
| 19 | C | 47 | 49 | 50 | 48.7 | 62 | 63 | 63 | 62.7 | 400 |
| 20 | C | 50 | 49.5 | 49 | 49.5 | 63 | 63.5 | 63.5 | 63.3 | 400 |
| 21 | C | 49 | 50 | 49.5 | 49.5 | 63 | 63 | 62 | 62.7 | 400 |

From the measured dimensions as presented in Table 4-2, the average, standard deviation, median as well as the minimum and maximum of all the measured data was calculated – see Table 4-3.

*Table 4—3: Statistical analysis of beam dimension data*

| | Number of beams | Average | Standard deviation | Median | Minimum | Maximum |
|---|---|---|---|---|---|---|
| **Height** | 36 | 49.8 | 0.6 | 50.0 | 48.3 | 50.7 |
| **Width** | 36 | 62.8 | 0.5 | 62.8 | 61.8 | 64.0 |
| **Length** | 36 | 400.0 | 0.0 | 400.0 | 400.0 | 400.0 |

## 4.3. FLEXURAL STIFFNESS RESULTS

The flexural stiffness test procedure is described in Section 3.6.1.

The vertical force required to reach the desired displacement is measured during the pulsing action. Variation in the initial readings during a test is substantial and reduces considerably within the first fifty to one hundred pulses. For this reason, Jenkins (2000) suggested that the initial Flexural Stiffness ($S_i$) be defined as being measured from a linear regression line, fitted to the first 300 cycles, at the 50$^{th}$ pulse, see Graph 4-1.

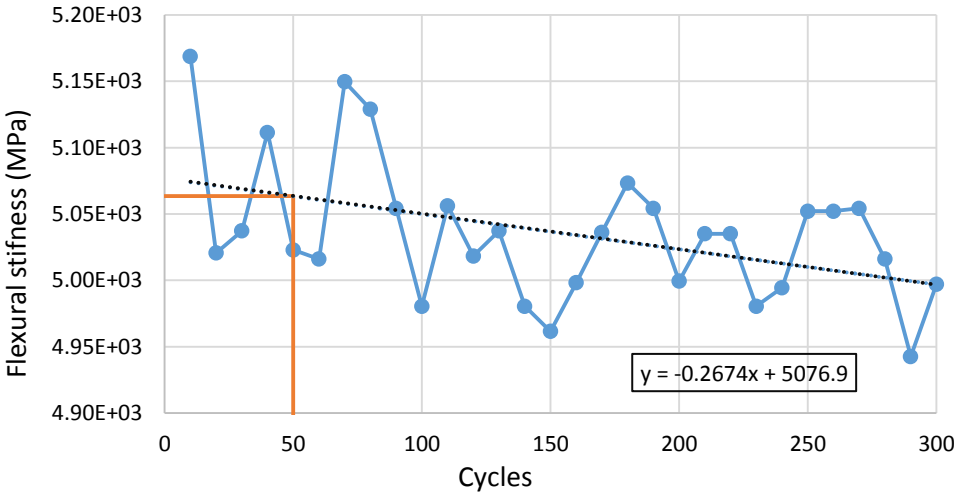


*Graph 4—1: Flexural Stiffness as a function of load cycles in a displacement controlled 4PBT*

Due to the visco-elastic nature of bitumen binder in asphalt mixes, they generally exhibit an increase in flexural stiffness with a decrease in temperature and higher frequency of loading cycles. The flexural stiffness can be defined by a unique curve or "Master Curve" for a given asphalt material by shifting the stiffness modulus horizontally with respect to loading time for various temperatures until the curves overlap. The shift is done by including an adjustment factor, in this case a coefficient of C = 15580, in Arrhenius's equation. The concept of Arrhenius's Equation is described in Section 2.6.3.

Flexural frequency sweeps were carried out on two beam specimens in order to develop the Master Curves. The range of temperatures selected for testing spanned 10˚C to 40˚C in intervals of 5˚C, inclusive. The range of loading frequency in these displacement-controlled tests consists of 0.5, 1, 2, 5 and 10 Hz. To minimise potential damage to the beam specimens during testing, it was decided to commence testing at the lower temperatures and higher frequencies. Moving forward all Master Curve development was carried out using a sine wave signal with a peak to peak strain value of 250 με.

The flexural stiffness results from the two beam specimens for the different load frequencies at the respective temperatures can be seen in Table 4-4.

*Table 4—4: Flexural Stiffness results*

| **Flexural Stiffness Results for S10-BC (MPa)** | | | | | | | |
|---|---|---|---|---|---|---|---|
| Frequency (Hz) | 10˚C | 15˚C | 20˚C | 25˚C | 30˚C | 35˚C | 40˚C |
| 0.5 | 20203 | 14972 | 10149 | 6189 | 3307 | 1964 | 1292 |
| 1 | 21390 | 16134 | 11222 | 7163 | 3952 | 2316 | 1300 |
| 2 | 24080 | 17253 | 12758 | 8480 | 5064 | 2968 | 1541 |
| 5 | 26176 | 19267 | 14948 | 10608 | 6930 | 4334 | 2207 |
| 10 | 24927 | 21133 | 16705 | 12481 | 8531 | 5650 | 2974 |
| **Flexural Stiffness Results for S11-BB (MPa)** | | | | | | | |
| Frequency (Hz) | 10˚C | 15˚C | 20˚C | 25˚C | 30˚C | 35˚C | 40˚C |
| 0.5 | 18070 | 13270 | 8605 | 5240 | 2691 | 1618 | 1389 |
| 1 | 18916 | 14347 | 10076 | 6155 | 3257 | 1884 | 1362 |
| 2 | 19955 | 15761 | 11551 | 7549 | 4301 | 2409 | 1508 |
| 5 | 22604 | 17390 | 13611 | 9619 | 5978 | 3679 | 2128 |
| 10 | 22204 | 18903 | 15266 | 11669 | 7515 | 4832 | 3002 |

The flexural stiffness's determined on the principle described above provides uniform results for the load frequency sweeps at the different temperatures, see Graph 4-2 and Graph 4-3. The EME, as in the case of asphalt pavements, shows a stiffness modules increase with decreasing temperature and increasing loading frequency.

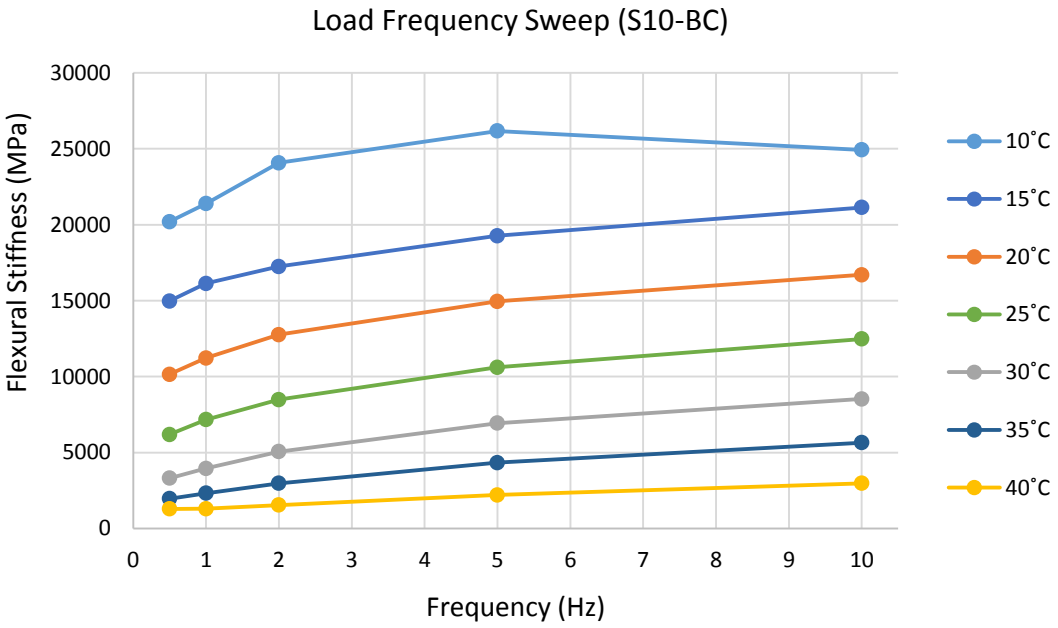


*Graph 4—2: Flexural Stiffness determined for frequency-temperature sweeps (S10-BC)*

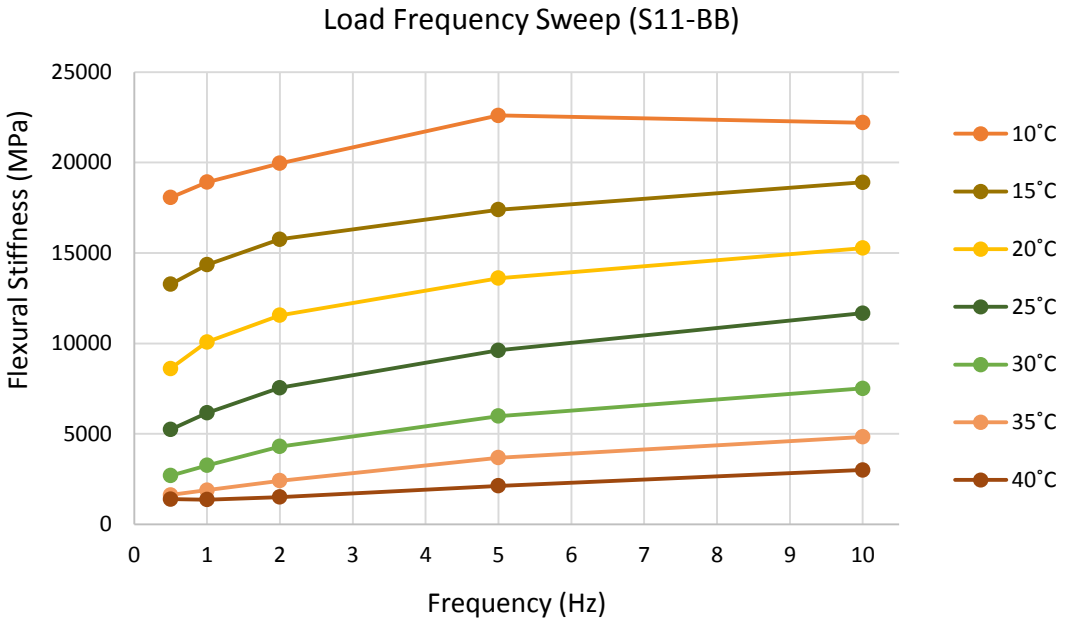


*Graph 4—3: Flexural Stiffness determined for frequency-temperature sweeps (S11-BB)*

It is important to note the Flexural Stiffness reduction in both cases from a frequency of 5 Hz to 10 Hz at a temperature of 10˚C (see Table 4-2 as well as Graph 4-2 and Graph 4-3). Because of the high stiffness result of EME asphalt at a frequency of 10 Hz and 10˚C, the Four Point Beam apparatus was unable to reach the desired strain amplitude of 250 με within the first 300 load cycles.

The principle of Master Curve development is discussed in Section 2.6.2. The employment of Lytton constant for the Arrhenius Equation was used as a starting value, in order to produce a constant (C) that give the best fitting of the shifted frequencies. A reference temperature of 20˚C was selected for the master curve. The two investigated samples were evaluated based on their measured dimensions as well as their void percentage in order to select the ideal beam sample to represent the master curve for the investigated mix (see Table 4-5). The beam properties of the investigated two beams were more or less the same, it was however decided to use the data from S10-BC.

*Table 4—5: Comparison between beam properties*

| | Height (mm) | Width (mm) | Length (mm) | Void % |
|---|---|---|---|---|
| S10-BC | 50.0 | 63.3 | 400 | 2.64 |
| S11-BB | 50.2 | 63.2 | 400 | 2.57 |

The flexural stiffness data from S10-BC were linearly shifted using Arrhenius shift function. This produced a good fit, as the coefficient of determination ($R^2$) yield a very good result – see Graph 4-4. The coefficient The coefficient of determination serves as a statistical measure of how close the data are to the fitted regression line. A value of 0 indicates that the model explains none of the variability of the response data around its mean, while a value of 1 indicates that the model explains all the variability of the response data around its mean.

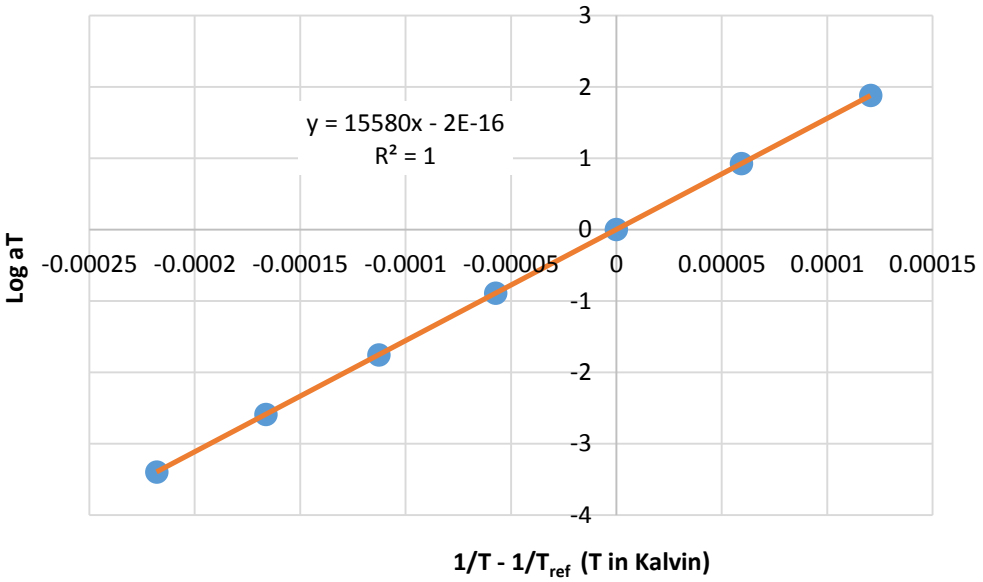


*Graph 4—4: Arrhenius shift factor applied at $T_{ref}$ = 20C & C = 15580*

The Master Curve for the beam specimen can be seen in Graph 4-5. The proposed Master Curve provide a reasonable estimate for the mix stiffness at a large number loading frequencies. The Master Curve equation was calculated by solving a logistic function for the data obtained. This function can also be seen, as the black line, in Graph 4-5.

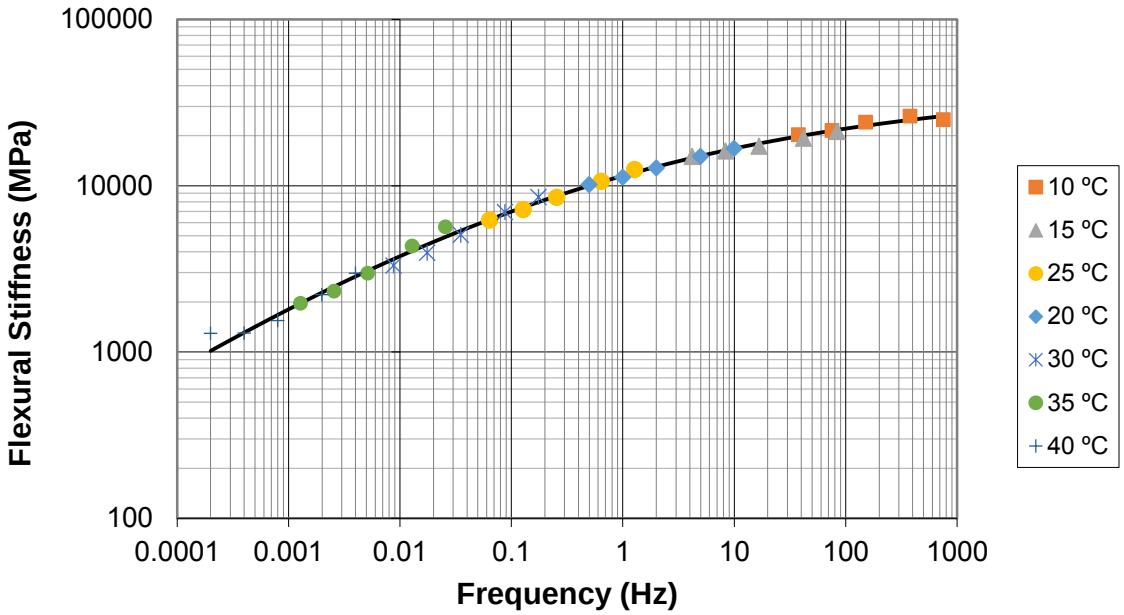


*Graph 4—5: Master Curve for S10-BC (Reference temperature = 20°C)*

The Master Curve equation can be seen to be:

$$\text{Flexural stiffness} = 5.31 + \frac{39334}{[1+(\frac{0.1}{f})^{0.194}]^{2.495}}$$

In the Master Curves a flattening of the data is observed at the 40˚C and 10˚C testing temperature points. This behaviour is expected, the fitted function however doesn't show this behaviour at the low frequency values. The flattening out of the data represented by the curve function, will happen at a much lower frequency value. It will thus be necessary to conduct additional tests at lower frequency values or at higher temperatures, in order to explain the behaviour at the lower point.

## 4.4. FATIGUE BEHAVIOUR RESULTS

The fatigue test procedure is described in Section 3.6.2. This section will include firstly the fatigue classification results, subsequently these results will be measured against one another on the basis of the loading waveform used. The influence of the void percentage as well as the initial flexural stiffness will also be investigated for both loading cases. Evidence of the shifted

neutral axis for the haversine loading condition is presented. This section will lastly cover the fatigue performance of the EME mix.

### 4.4.1. Fatigue Classification Testing

As mentioned in Section 3.6.2. Sabita is in the process of updating *Manual 33 – Interim Procedure for the Design of High Modulus Asphalt (EME)*. The updated fatigue classification criteria can also be seen in the above mentioned section in Table 3-3.

The fatigue classification tests on the mix design was firstly done by using a haversine loading pattern, as standardised in ASTM D7460. After observing the results, it was decided to repeat the tests, by loading the specimens with a sinusoidal loading pattern, as standardised in AASHTO T321. In the case of haversine loading, the beam was bend to a strain of 250 με in one direction and returned to the original position, this action represented one load cycle. In the case of sinusoidal loading one load cycle was achieved by bending the beam to a strain of 125 με in one direction, returning it to the original position and bending it to a strain of 125 με in the opposite direction. Hence the peak to peak strain remained constant at 250 με.

The results obtained following the Sabita EME fatigue criteria for the mix design investigated in this project, using haversine and sinusoidal loading respectively can be seen below in Table 4-6 and Table 4-7. These tables show the slab and beam numbers, the percentage voids, the initial Flexural Stiffness ($S_i$), the Termination Flexural Stiffness ($S_f$), the number of load cycles to reach 50% stiffness reduction and whether or not the test was affected by load shedding (indicated by an *).

*Table 4—6: Fatigue classification results for mix design with haversine loading*

| Slab Number | Beam Number | % Voids | $S_i$ (MPa) | $S_f$ (MPa) | Number of load cycles |
|---|---|---|---|---|---|
| 1 | A | 3.70 | 16862 | 8200 | 131700 |
| 1 | B | 3.49 | 14260 | 8000 | 517260 |
| 1 | C | 3.78 | 14260 | 8139 | 797000 |
| 2 | A | 2.19 | 21569 | 10784 | 90 |
| 2 | B | 2.06 | 21642 | 10821 | 70 |
| 2 | C | 2.25 | 22035 | 11018 | 70 |
| 3 | A | 2.92 | 16402 | 8201 | 1787530 |
| 3 | B | 2.49 | 17817 | 8909 | 70 |
| 3 | C | 2.81 | 16758 | 8379 | 345670 |
| 4 | A | 6.31 | 15911 | 7500 | 1271870 |
| 4 | B | 6.43 | 14846 | 6200 | 323170 |

*Table 4—7: Fatigue classification results for mix design with sine loading*

| Slab Number | Beam Number | % Voids | $S_i$ (MPa) | $S_f$ (MPa) | Number of load cycles |
|---|---|---|---|---|---|
| 5 | A | 3.82 | 19313 | 9000 | 475990 |
| 5 | B | 3.65 | 19542 | 7000 | 861950 |
| 5 | C | 3.69 | 17553 | 7369 | 931040 |
| 6 | A | 4.97 | 18363 | 9231 | 691000 |
| 6 | B | 4.53 | 18418 | 12664 | 856000* |
| 6 | C | 4.49 | 17535 | 8645 | 718630 |
| 7 | A | 2.92 | 19521 | 11295 | 1070000* |
| 13 | A | 4.91 | 16610 | 8200 | 657110 |
| 13 | B | 4.38 | 16617 | 8258 | 735250 |
| 15 | B | 4.65 | 18106 | 8913 | 742070 |

**Note: Two cases of influence from load shedding (S6-BB & S7-BA)

Considering the results from Table 4-6 and 4-7 it was decided to only proceed with sinusoidal loading (AASHTO T321) in further fatigue tests. The high initial stiffness value of EME asphalt together with the high one directional strain value because of the haversine wave pattern, caused large amounts of initial fatigue damage and in some cases immediate failure to beams. Further seconding of this decision will follow in the chapter.

Graph 4-6 illustrates the effect of the two loading cases as discussed above. The scattered blue bars represent the haversine loading cases, whereas the more constant orange bars represent the sinusoidal loading cases. The fatigue criteria of 1 000 000 load cycles, as specified in Sabita Manual 33, is also indicated on the graph.

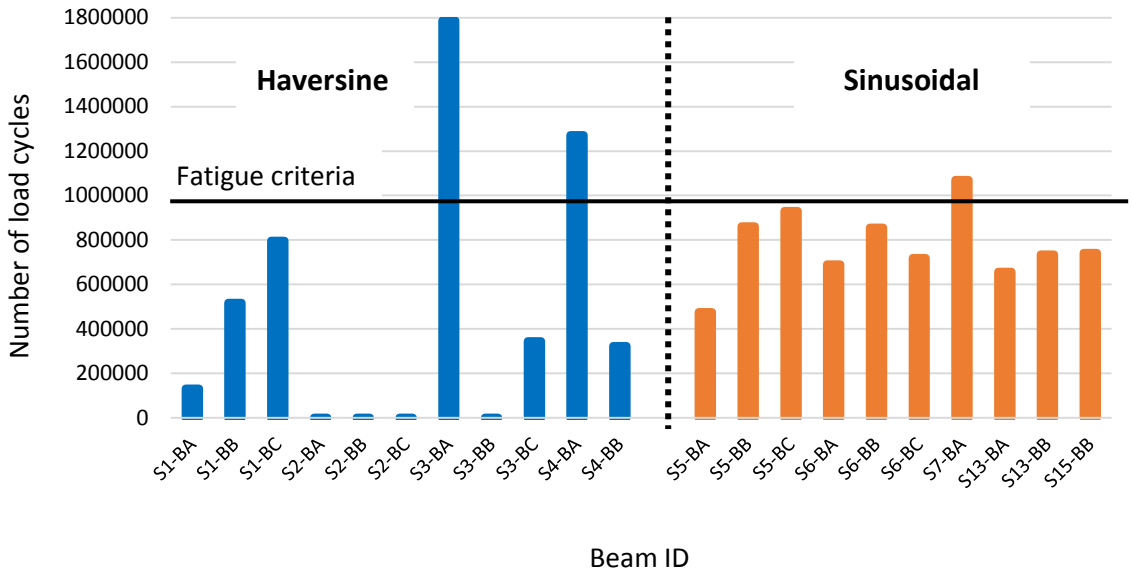


*Graph 4—6: Effect of loading model on fatigue life*

A numerical modelling on the beam specimens, relating to both loading profiles will follow in Section 4.5. The aim of the numerical modelling will be to explain the premature failure in some of the haversine loaded beams, by investigating the tensile stresses in the beam for both loading cases.

Because of the number of variables present when testing a diverse sample of beams, it was decided to investigate the possible effect of the void percentage and beam stiffness in particular. Keeping the results from the haversine and sinusoidal loading cases apart, the variables were investigated based on the number of load cycles from the fatigue classification tests, as shown in Graph 4-6.

#### 4.4.1.1. Influence of Percentage Voids

The influence of the void percentage on the number of load cycles were investigated by ranking the beams from lowest to highest percentage voids, for the two loading cases. The result can be seen in Graph 4-7, with the void percentages indicated by the green line and measured on the right hand vertical axis.

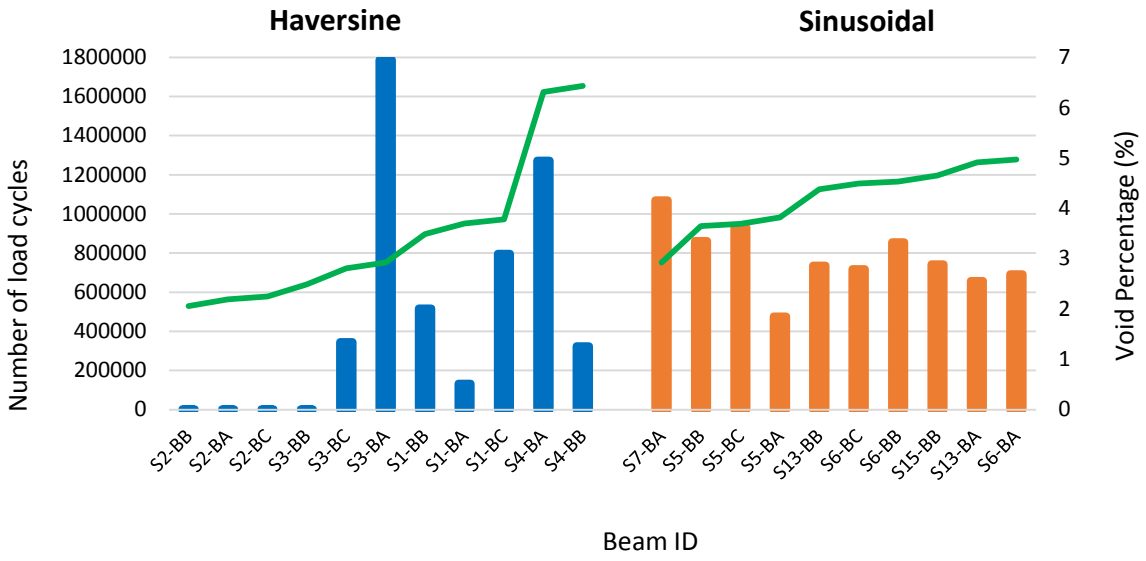


*Graph 4—7: Influence of void percentage on the number of load cycles*

The most notable aspect is that in the case of haversine loading, the four beams which failed prematurely has the lowest void percentages. This may be as a result of stress concentration that is created in the beam specimen due to the low void percentages. These void percentages ranged from 2.06% to 2.49%. It is also observed that for the same loading case, the highest number of load cycles were encountered at a void percentage of 2.92%. For the haversine loading case, no further obvious conclusions can be made with regards to the void percentages.

The results from the sinusoidal loading case shows no apparent trend with regards to void percentage. However, the highest number of load cycles were encountered at the low void percentages, ranging from 2.92% to 3.69%.

#### 4.4.1.2. Influence of Initial Flexural Stiffness

The influence of the initial flexural stiffness on the number of load cycles were investigated by ranking the beams from lowest to highest initial flexural stiffness, for the two loading cases. The result can be seen in Graph 4-8, with the initial flexural stiffness indicated by the red line and measured on the right hand vertical axis.

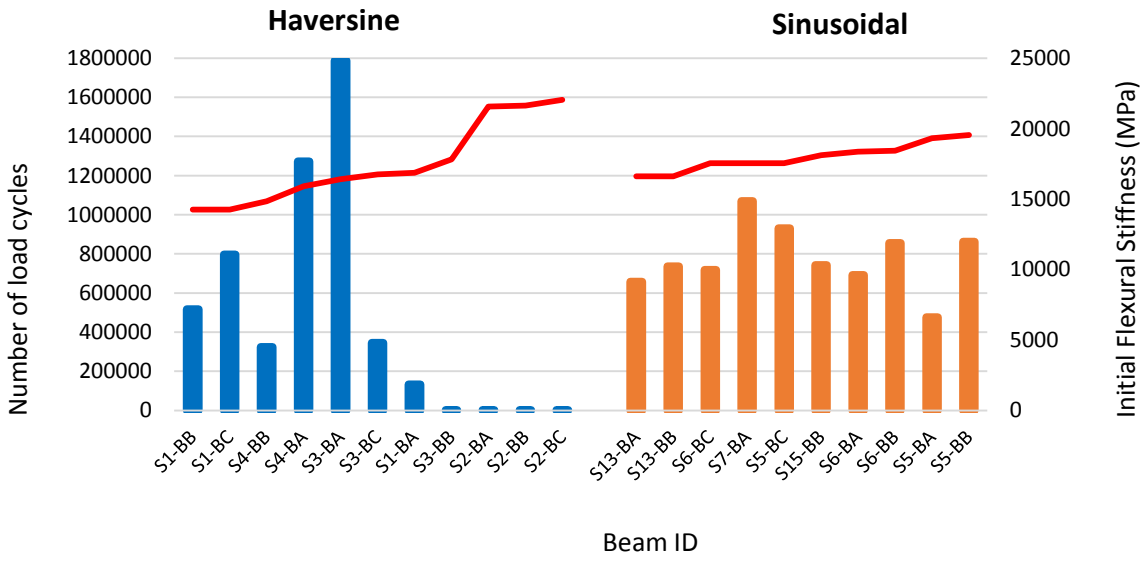


*Graph 4—8: Influence of the initial flexural stiffness on the number of load cycles*

Again, the most notable aspect is that in the case of haversine loading, the four beams which failed prematurely has the highest initial stiffness. These beams showed brittle performance as a result of the high stiffness values. For the haversine loading case, no further obvious conclusions can be made with regards to the initial flexural stiffness.

The results from the sinusoidal loading case shows no apparent trend with regards to the initial flexural stiffness.

#### 4.4.1.3. Shift of the Neutral Axis

With regards to the shift of the neutral axis, as described in Section 3.6.3, evidence was found in the 4PBT software output that verifies this phenomenon. Witczak, et al. (2013) indicated that for the haversine test, the deflection input remains haversine throughout the test, with the

developed strain and stress pulses starting as haversine waveforms causing strain and stress in one direction. Because of the shifted position of the neutral axis, the developed strain and stress pulses change to sinusoidal after a few cycles. Graph 4-9 illustrates the minimum and maximum applied load over the first 2000 cycles in a 4PBT that is loaded with a sinusoidal waveform, with Graph 4-10 illustrating the same case when loaded with a haversine waveform. The minimum applied load represents the downward pulsing load to achieve the desired amplitude (125 με for the sinusoidal case and 250 με for the haversine case at the start of the test). The maximum applied load represents the upward pulsing load to achieve the desired amplitude (125 με for the sinusoidal case and 0 με for the haversine case at the start of the test). The indicated neutral axis was found by taking the points between the maximum and minimum load, as this point serve as the pivot point around which the loads are applied.

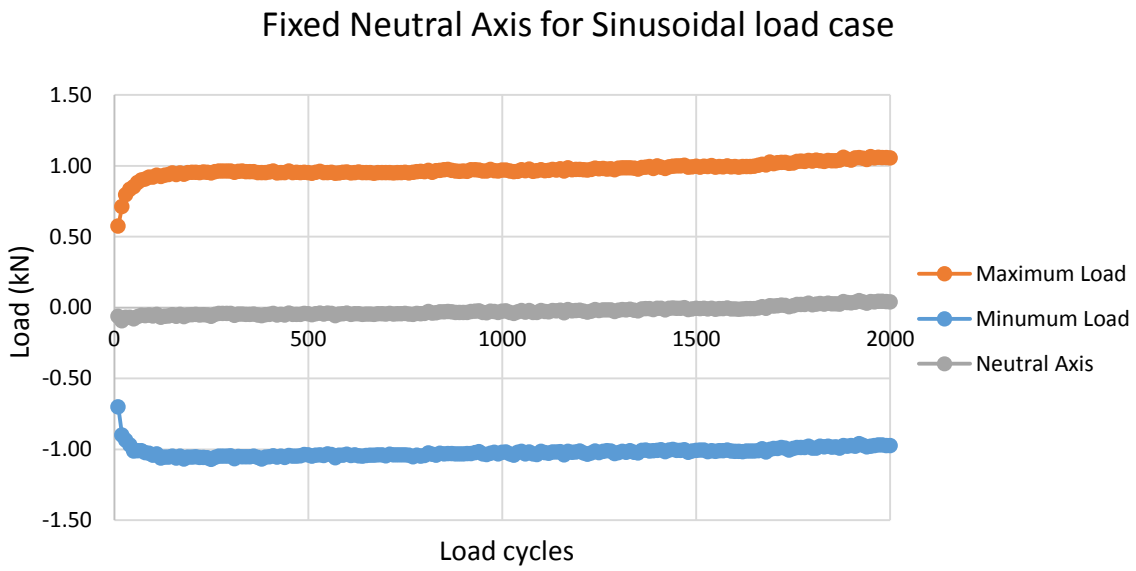


*Graph 4—9: Fixed neutral axis for sinusoidal load case*

When considering Graph 4-9, it is evident that the maximum and minimum loads are the same but in different directions, as to achieve the 125 με amplitude for the sinusoidal waveform. As expected, the neutral axis is situated at the center point of the beam.

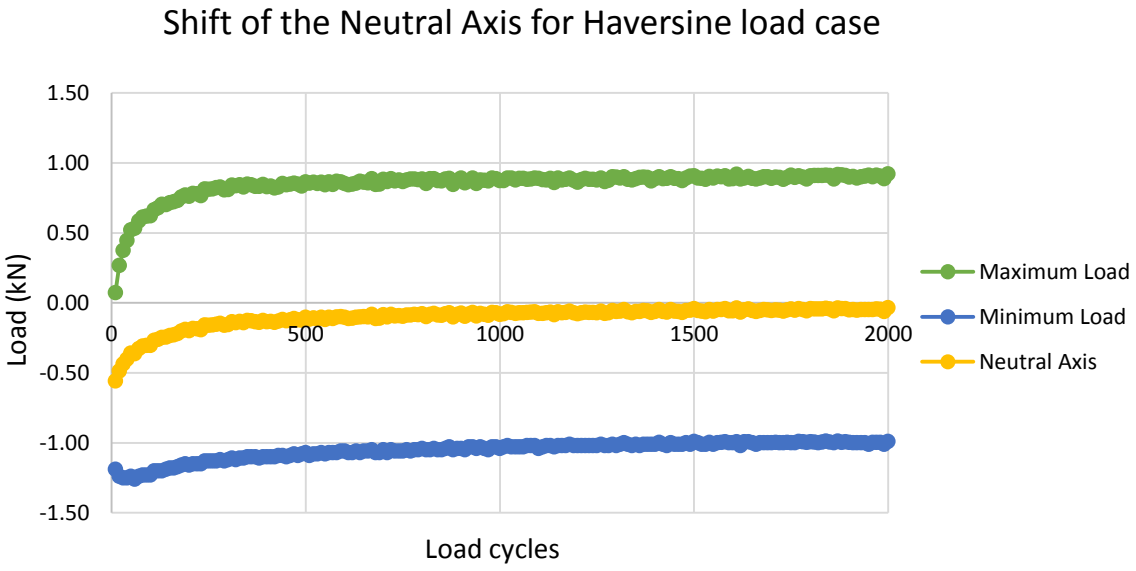


*Graph 4—10: Shift of the Neutral Axis for Haversine load case*

When considering Graph 4-10, it can be seen that after a small amount of load cycles the maximum load increases from zero, while the minimum load decreases until they correspond, as in the case of the sinusoidal waveform. At this point the neutral axis has shifted towards the center point and the loading profile acts around it, comparable to an equivalent sinusoidal load. Evidently, this shift is initiated within the first 50 load cycles and the neutral axis is completely shifted after 1500 load cycles. Figure 4-1 illustrates the shifted neutral axis, as it would appear in a haversine loaded beam specimen when tested in the 4PBT.

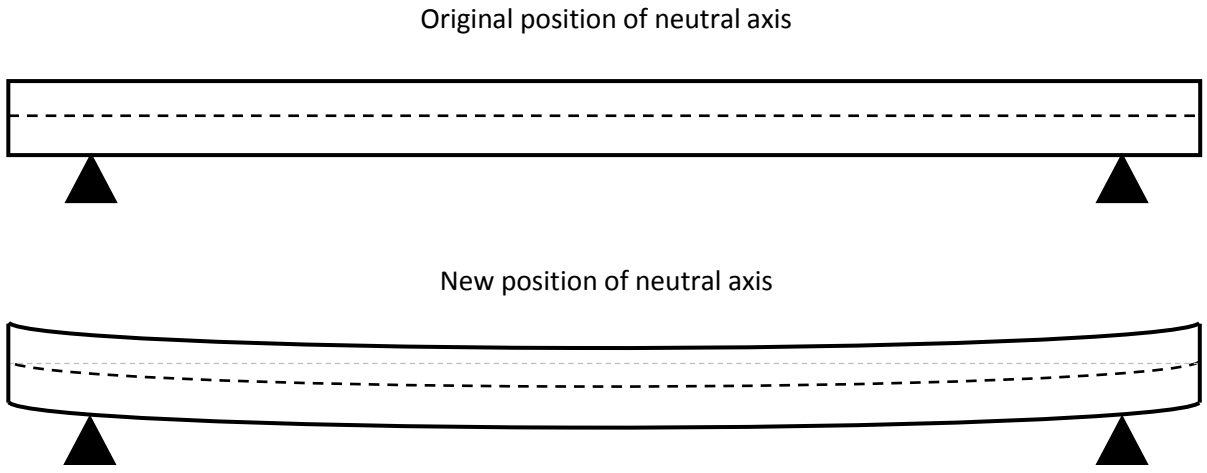


*Figure 4—1: Illustration of shifted neutral axis in loaded beam*

#### 4.4.1.4. Investigation into premature failure with haversine loading

Further investigation into the premature failure of beams loaded with a haversine loading profile was done by examining the tensile strength of the investigated EME mix. The investigation was started by evaluating the stiffness modulus of the bitumen ($S_{bit}$) as well as the stiffness modulus of the mix ($S_{mix}$), based on the Shell method as obtained in Read & Whiteoak (2003). This method utilises the nomograph for penetration index, Van der Poel nomograph for determining the stiffness modulus of bitumen and the nomograph for predicting the stiffness modulus of asphalt. The tensile strength of the investigated mix was then determined with the help of Heukelom (1996). The following steps were followed in the investigation:

**Step 1: Determining the Penetration Index**

The penetration index (PI) was determined by plotting the softening point and the penetration at 25˚C for the 10/20 binder, used in the manufacturing of the EME slab specimens, on the nomograph for penetration index (see red line in Figure 4-2). The result can be seen in Table 4-8.

*Table 4—8: PI as determined from the nomograph for penetration index*

| **Characteristics** | | |
|---|---|---|
| Penetration @ 25˚C | 18 | 0.1mm |
| Softening Point | 62 | ˚C |
| **Result** | | |
| PI | -1 | - |

The exercise was done with regards to virgin bitumen. A short term ageing (STA) sensitivity analysis was done, and can be seen in Figure 4-2 with the green line. The analysis was done by assuming that the PI stays constant with the penetration at 25˚C reducing with 20%, as a result of ageing. Figure 4-2 shows that short term ageing will not have a significant influence, as the softening point is increased with only one degree.

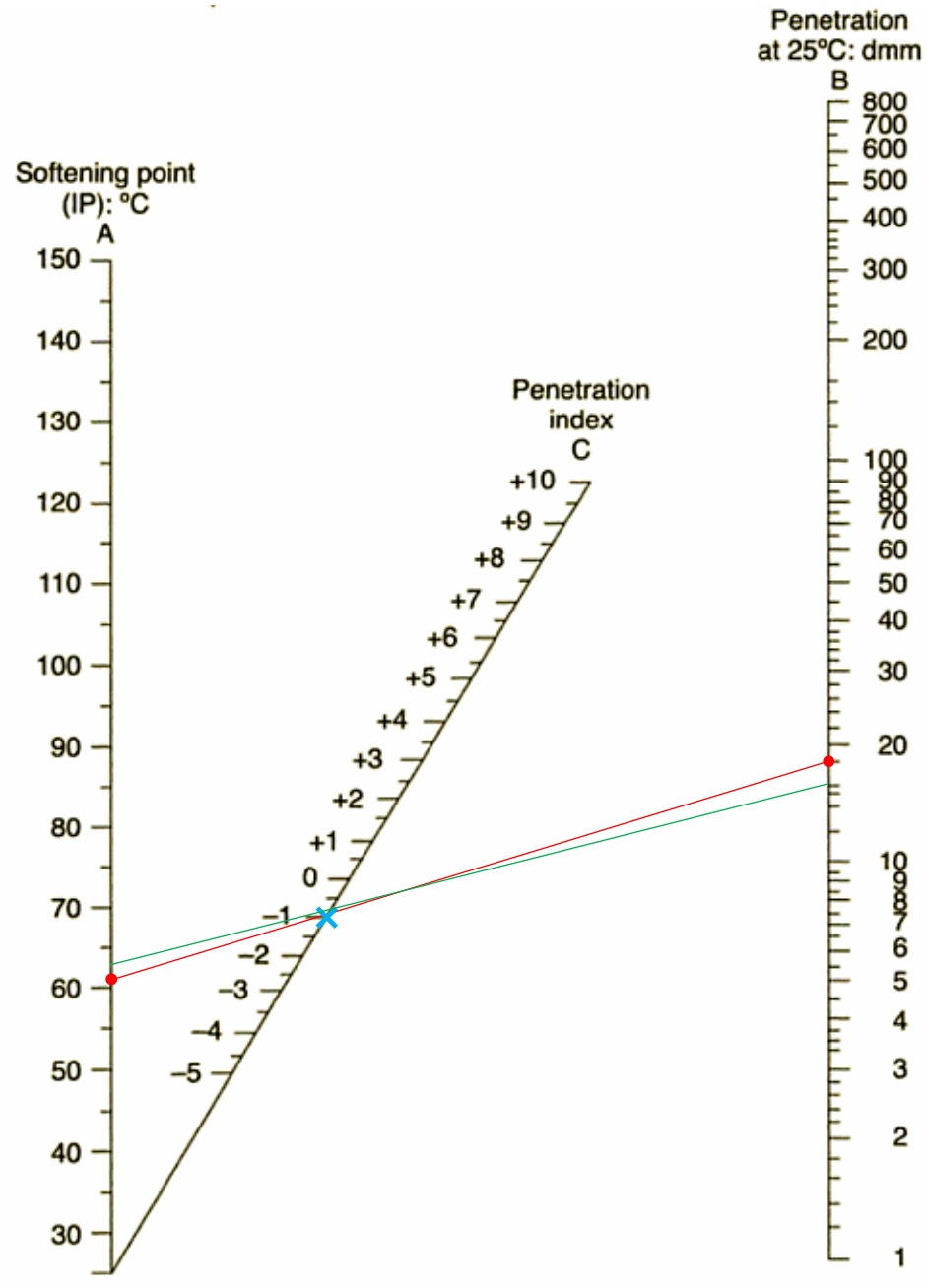


*Figure 4—2: Nomograph for penetration index (Read & Whiteoak, 2003)*

**Step 2: Determining stiffness modulus of the bitumen ($S_{bit}$)**

The stiffness modulus of the bitumen ($S_{bit}$) was determined by using Van der Poel nomograph (see Figure 4-3), in conjunction with the test frequency, the temperature difference and the PI (as calculated in step 1). The temperature difference is determined by subtracting the operating temperature from the softening point temperature. The result can be seen in Table 4-9.

*Table 4—9: $S_{bit}$ as determined from Van der Poel nomograph*

| **Operating conditions** | | |
|---|---|---|
| Temperature | 10 | ˚C |
| Frequency | 10 | Hz |
| **Characteristics** | | |
| PI | -1 | - |
| Temperature Difference | 52 | ˚C |
| **Result** | | |
| $S_{bit}$ | $6x10^8$ | $N/m^2$ |

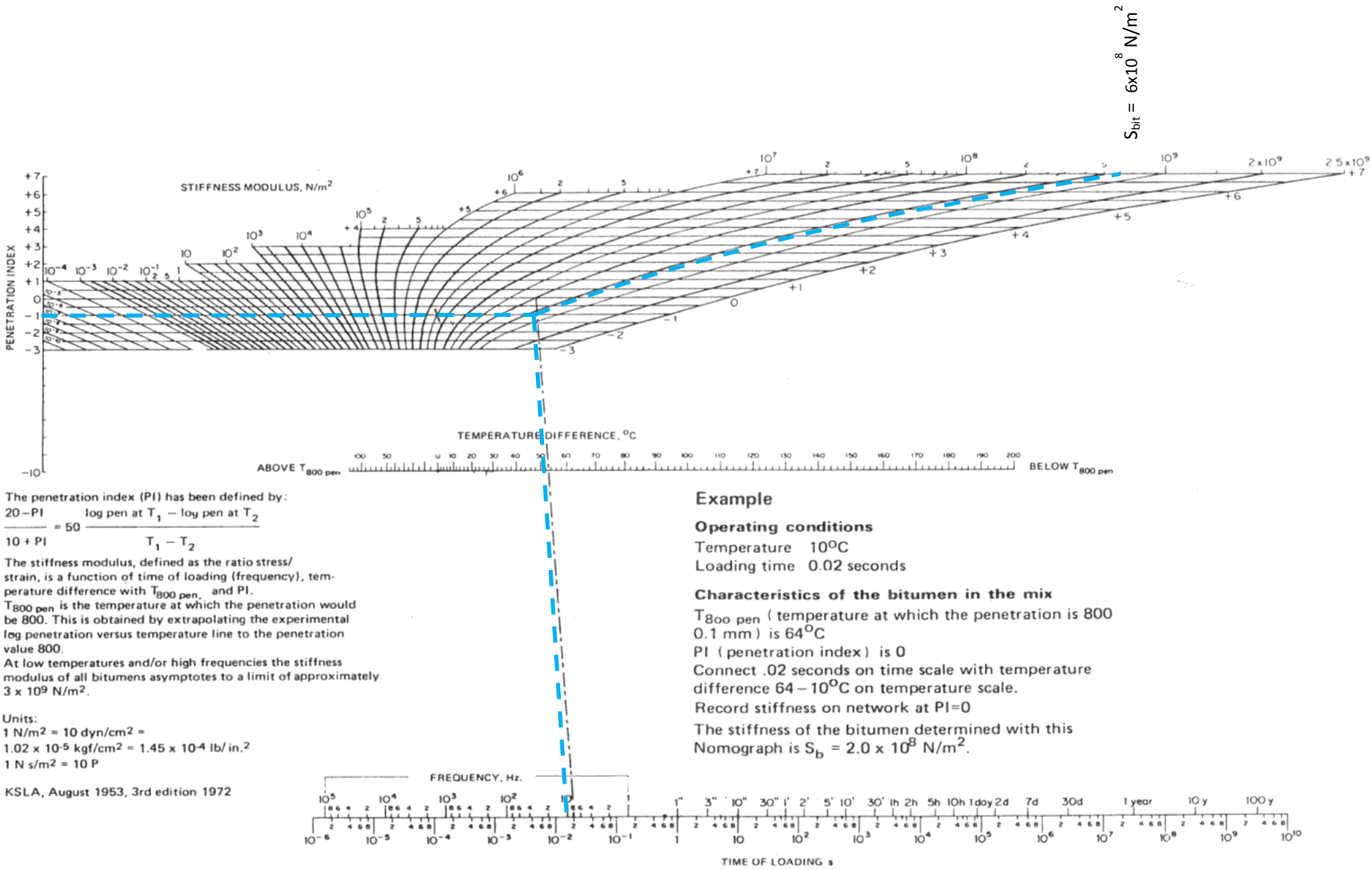


*Figure 4—3: Nomograph for determining the stiffness modulus of bitumens (Read & Whiteoak, 2003)*

**Step 3: Determining stiffness modulus of the asphalt mix ($S_{mix}$)**

The stiffness modulus of the asphalt mix ($S_{mix}$) was determined by using the nomograph for predicting the stiffness modulus of asphalt (see Figure 4-4), in conjunction with the stiffness modulus of the bitumen (as calculated in step 2), the bituminous binder volume and the mineral aggregate volume. The bituminous binder volume is calculated by multiplying the binder percentage of 5.7% with the specific gravity (SG) of 2.495. The mineral aggregate volume is determined by subtracting the bituminous binder volume together with the percentage voids in the mix from 100%. The result can be seen in Table 4-10.

*Table 4—10: $S_{mix}$ as determined from nomograph for predicting the stiffness modulus of asphalt*

| **Characteristics** | | |
|---|---|---|
| $S_{bit}$ | $6x10^8$ | $N/m^2$ |
| Bituminous Binder volume | 14.2 | % |
| Voids in mix | 4 | % |
| Mineral Aggregate volume | 81.8 | % |
| **Result** | | |
| $S_{mix}$ | $2.3x10^{10}$ | $N/m^2$ |

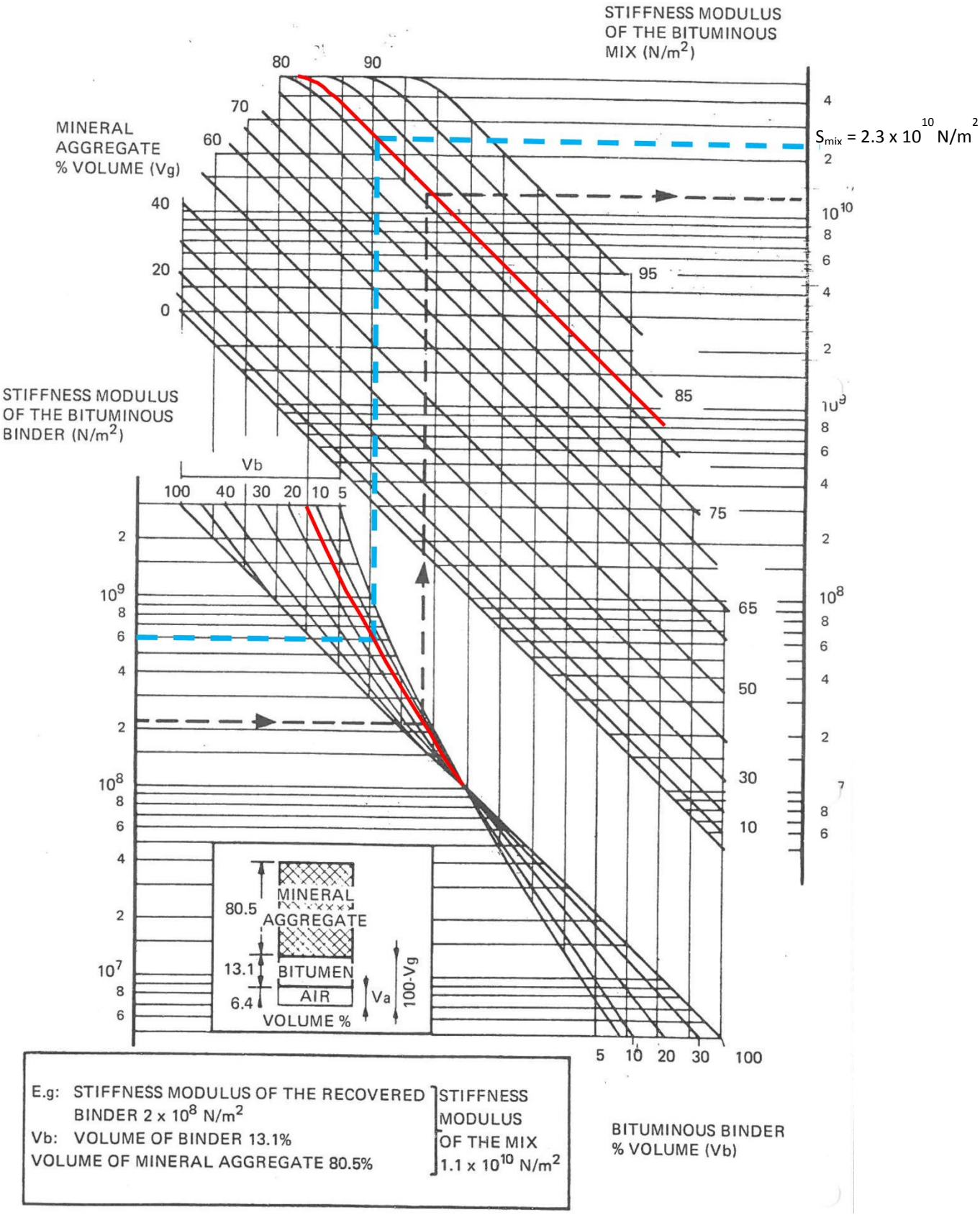


*Figure 4—4: Nomograph for predicting the stiffness modulus of asphalt (Read & Whiteoak, 2003)*

**Step 4: Determining tensile strength of mix**

The tensile strength of the investigated mix was then determined with the help of Heukelom (1996) together with the stiffness modulus of the bitumen (as calculated in step 2). The Heukelom graph, as shown in Figure 4-5, enables the user to determine the tensile strength of the bitumen and two different asphaltic mixes. These two mixes represent the following:

- Mix I: A normal mix with variability in terms of binder content and compaction.
- Mix II: A perfect mix with a void content of 4% and an optimal grading and compaction.

Mix I can be considered to be a mix which represents a worst case scenario, while mix II represents a more realistic case. The tensile strength result for both mixes can be seen in Table 4-11.

*Table 4—11: Tensile strength as determined from Heukelom graph*

| **Characteristics** | | |
|---|---|---|
| $S_{bit}$ | $6x10^8$ | $N/m^2$ |
| **Result** | | |
| Tensile Strength of mix I | 32 | $kg/cm^2$ |
| | 3.14 | MPa |
| Tensile Strength of mix II | 62 | $kg/cm^2$ |
| | 6.08 | MPa |

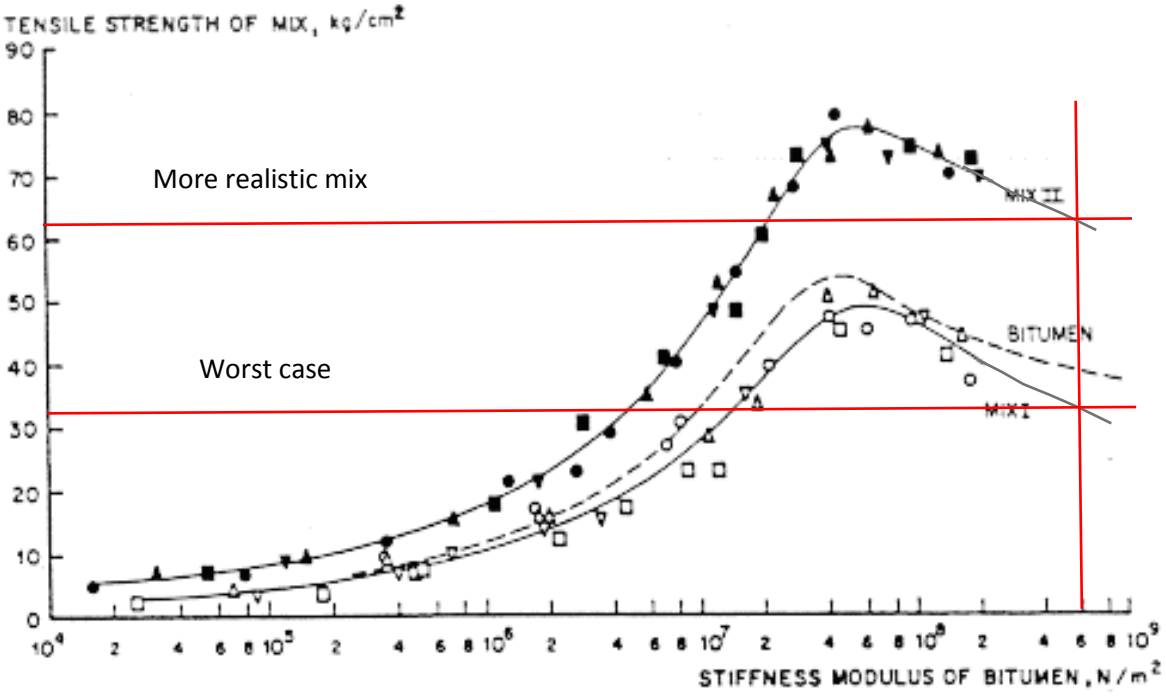


*Figure 4—5: Tensile strength of bitumen and mixes as a function of the $S_{bit}$ (Heukelom, 1966)*

**Step 5: Comparison between tensile strength, maximum tensile stress and stress based on strain in haversine loading**

The maximum tensile stress, with regards to haversine loading, can be determined for the beam specimens by using the following known variables:

- idealised beam width of 63mm
- idealised beam height of 50mm
- applied load of 1460 N

The applied load was taken from Table 4-12, as the lowest applied load at which premature failure occurred. The data in Table 4-12 was obtained from the 4PBT software with regards to the fatigue classification tests. The maximum tensile stress can be calculated as follows:

$$\sigma_t = \frac{0.357P}{bh^2}$$

$$\sigma_t = \frac{0.357(1460)}{(0.063).(0.05)^2}$$

$$\sigma_t = 3.3 \text{ MPa}$$

*Table 4—12: Haversine tests data as obtained during 4PBT*

| **Haversine** | | |
|---|---|---|
| Number | Number of load cycles | Initial applied load (N) |
| S1-BA | 131700 | 1190 |
| S1-BB | 517260 | 1060 |
| S1-BC | 797000 | 1160 |
| S2-BA | 90 | 1500 |
| S2-BB | 70 | 1520 |
| S2-BC | 70 | 1480 |
| S3-BA | 1787530 | 688 |
| S3-BB | 70 | 1460 |
| S3-BC | 345670 | 1360 |
| S4-BA | 1271870 | 1450 |
| S4-BB | 323170 | 1490 |

The stress based on strain in haversine loading was calculated by multiplying the stiffness modulus of the asphalt mix ($S_{mix}$) with the applied strain, as presented below.

$$\sigma = E.\varepsilon$$

$$\sigma = 23000 \text{ MPa} \times 250\ \mu\varepsilon$$

$$\sigma = 5.75\ MPa$$

Comparing the maximum tensile stress as well as the stress generated during the haversine loading test to the calculated tensile strength of the mixture, it is evident that these stresses exceed the tensile strength of mix I. This can possibly explain the damage and premature failure to some beams, as the beams bearing capacity is surpassed. Another possible assumption that can be made is that the mixes may have underperformed.

### 4.4.2. Fatigue Testing

Fatigue testing on the plant mix was performed at the two most extreme temperatures (10˚C and 40˚C). All tests were performed at a Frequency of 10 Hz, with four strain cases as shown below:

- 3 tests at 10˚C with a peak to peak strain value of 250 με
- 2 tests at 10˚C with a peak to peak strain value of 175 με
- 1 test at 10˚C with a peak to peak strain value of 100 με
- 2 tests at 10˚C with a peak to peak strain value of 50 με

- 1 test at 40˚C with a peak to peak strain value of 250 με
- 2 tests at 40˚C with a peak to peak strain value of 175 με
- 2 tests at 40˚C with a peak to peak strain value of 100 με
- 2 tests at 40˚C with a peak to peak strain value of 50 με

Each test was performed until fatigue caused the beam stiffness to decrease to a value of 50% of the Initial Flexural Stiffness or until a specified number of load cycles were reached. The specified number of load cycles were initially set to 2 million, it was later increased to 4 million. In the cases where the specified number of load cycles were achieved before the 50% fatigue decrease were reached, a percentage fatigue at termination were calculated. The percentage fatigue experienced were calculated as shown below:

$$\%\ Fatigue\ @\ Termination = \frac{End\ flexural\ stiffness}{Initial\ flexural\ stiffness} \times 100 \qquad \textbf{Equation 4-1}$$

This percentage fatigue at termination had to be calculated as a mean to express the results of the beams that did not reach the 50% stiffness reduction within the designated number of load cycles.

Table 4-13 illustrates the fatigue behaviour in terms of the number of load cycles together with the percentage fatigue experienced for the cases described above. The table shows the slab and beam numbers, the initial Flexural Stiffness ($S_i$), the Termination Flexural Stiffness ($S_f$), the number of load cycles together with the percentage fatigue at termination and whether or not the test was affected by load shedding (indicated by an *).

*Table 4—13: Fatigue behaviour results*

| Slab | Beam | Voids (%) | $S_i$ (MPa) | $S_f$ (MPa) | Strain (με) | Temperature (˚C) | Number of load cycles | % Fatigue @ Termination |
|---|---|---|---|---|---|---|---|---|
| 13 | A | 4.91 | 16610 | 8200 | 250 | 10 | 657110 | 50% |
| 13 | B | 4.38 | 16617 | 8258 | | | 735250 | 50% |
| 15 | B | 4.64 | 18106 | 8913 | | | 742070 | 50% |
| 14 | B | 4.36 | 4368 | 2159 | | 40 | 128590 | 50% |
| 12 | B | 4.47 | 17494 | 13242 | 175 | 10 | 2000000 | 24% |
| 14 | A | 5.12 | 17116 | 16379 | | | 2000000 | 4% |
| 19 | A | 4.12 | 3156 | 2003 | | 40 | 4000000 | 37% |
| 17 | B | 3.27 | 3749 | 2398 | | | 4000000 | 36% |
| 17 | A | 3.59 | 18157 | 19502 | 100 | 10 | 4000000 | 0% |
| 18 | B | 4.15 | 3884 | 3156 | | 40 | 4000000 | 19% |
| 19 | C | 3.92 | 3308 | 2694 | | | 4000000 | 19% |
| 13 | C | 4.31 | 17494 | 16733 | 50 | 10 | 2000000 | 4% |
| 20 | C | 3.31 | 18231 | 18599 | | | 4000000 | 0% |
| 18 | A* | 3.73 | 3983 | 3407 | | 40 | 3348430* | 14% |
| 21 | C | 3.26 | 3787 | 2946 | | | 4000000 | 22% |

**Note: S18-BA was interrupted by load shedding before completing the desired number of cycles.

The Flexural Stiffness vs the number of load cycles graphs for all the tests listed in Table 4-13 can be seen in Appendix A. These graphs illustrate the percentage fatigue at termination (green line) as well as the position at which the 50% stiffness reduction is located, as illustrated in the example on Graph 4-11.

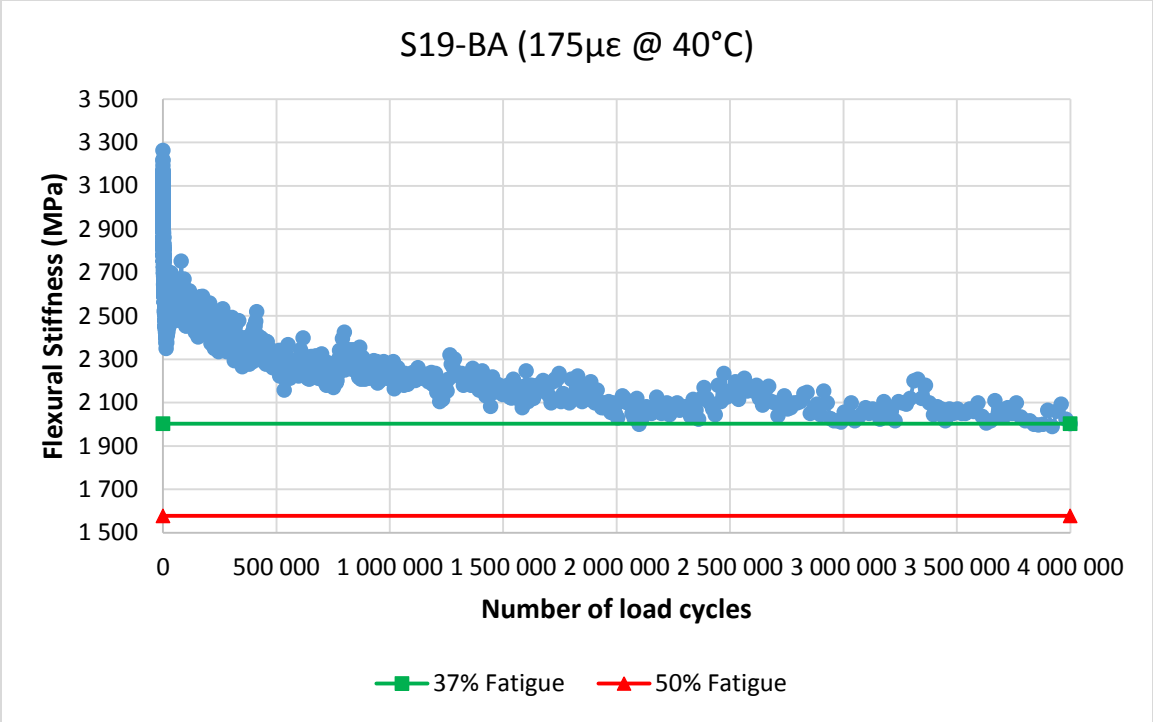


*Graph 4—11: Example of flexural stiffness vs the number of load cycles graphs*

Due to the nature of EME asphalt and the minimum amount of fatigue that was experienced by a number of specimens, it was not possible to determine the Endurance Limit of the material by plotting the logarithmic number of load repetitions to achieve a certain fatigue experienced vs the logarithmic strain. This will be illustrated in the next section.

### 4.4.3. Endurance limit and Transfer functions

The principle of an endurance limit is discussed in Section 2.5.6. and can be concluded to be a certain strain limit below which no fatigue will occur. When considering the percentage fatigue experienced at termination for the mixes tested at 10˚C (Table 4-10), it can be expected that the endurance limit of the investigated mix falls within the tested strain values, as some specimens experienced no fatigue after the limiting amount of load cycles. The 40˚C case will have to be investigated further, in order to predict a possible endurance limit.

It was initially decided to predict the number of load cycles each beam would have to experience in order to reach the 50% stiffness reduction point, by linearly extrapolating the generated results to this point. As most of the tests did not nearly reached the 50% stiffness

reduction point, the extrapolated points yielded inaccurate and inconsistent results. It was decided to rather use the data at the points where the percentage fatigue experienced was 30% and 20% at 10˚C and 30% at 40˚C, as to some degree most of the generated data could be used without extrapolating. The reason for only investigating a fatigue of 30% at 40˚C can be attributed to the fact that at lower fatigue values the flexural stiffness against the number of load cycle graphs display a sudden drop in flexural stiffness before settling into a linear regression, as indicated in Graph 4-11 (see all graphs in Appendix A). This sudden drop may display an inaccurate representation of the data, and for that reason it were left out.

The cases where these percentage fatigue experienced were insufficient in reaching the above mentioned fatigue points, linear extrapolation of data were applied. The linear extrapolation was done as follows:

- linear equation fitted over the last 500 000 load cycles where the limiting number of load cycles were set at 2 000 000 (see Graph 4-12)
- linear equation fitted over the last 1 000 000 load cycles where the limiting number of load cycles were set at 4 000 000.

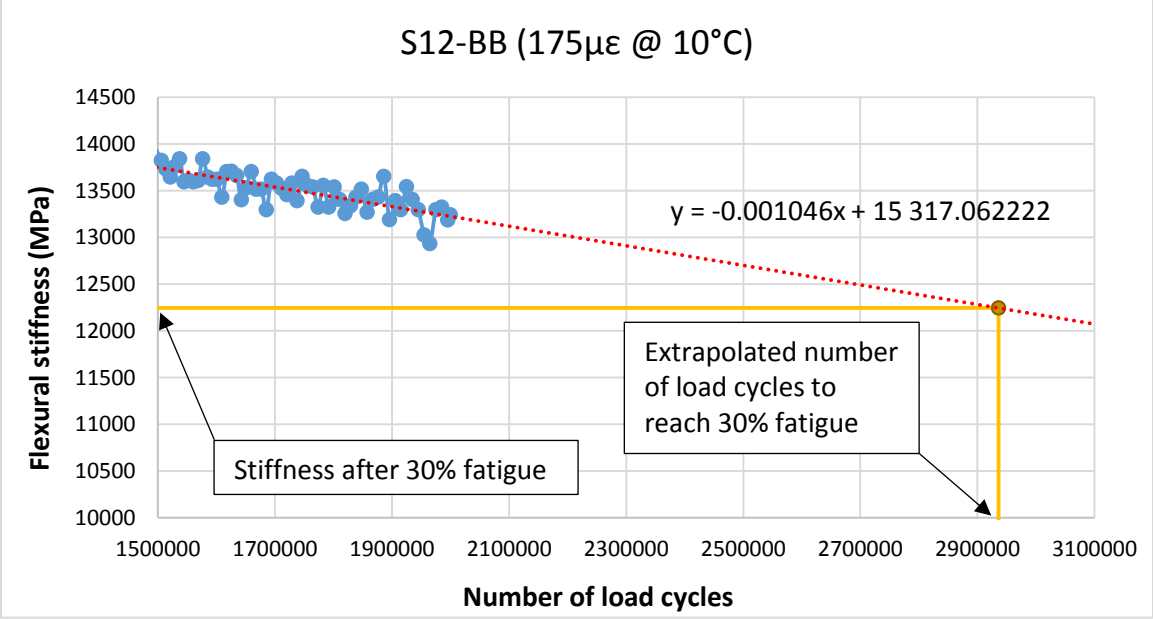


*Graph 4—12: Linear extrapolation of number of load cycles from flexural stiffness*

The results for the beam stiffness and number of load cycles after the respective percentage fatigue experienced, for the 10˚C and 40˚C cases can be seen in Table 4-14 and Table 4-15.

*Table 4—14: Stiffness and number of load cycle results at 10˚C*

| Slab | Beam | Strain (με) | $S_i$ (MPa) | Stiffness after respective % Fatigue experienced | | Number of load cycles after respective % Fatigue experienced | |
|---|---|---|---|---|---|---|---|
| | | | | 20% | 30% | 20% | 30% |
| 13 | A | 250 | 16610 | 13288 | 11627 | 346730 | 471330 |
| 13 | B | | 16617 | 13294 | 11632 | 237130 | 360300 |
| 15 | B | | 18106 | 14485 | 12674 | 243590 | 360300 |
| 12 | B | 175 | 17494 | 13995 | 12246 | 1252500 | 2936197 |
| 14 | A | | 17116 | 13693 | 11981 | 6142165 | 8961934 |
| 17 | A | 100 | 18157 | 14526 | 12710 | ∞ | ∞ |
| 13 | C | 50 | 17494 | 13995 | 12246 | ∞ | ∞ |
| 20 | C | | 18231 | 14585 | 12762 | ∞ | ∞ |

*Table 4—15: Stiffness and number of load cycle results at 40˚C*

| Slab | Beam | Strain (με) | $S_i$ (MPa) | Stiffness after respective % Fatigue experienced | Number of load cycles after respective % Fatigue experienced |
|---|---|---|---|---|---|
| | | | | 30% | 30% |
| 14 | B | 250 | 4368 | 3058 | 6080 |
| 19 | A | 175 | 3156 | 2209 | 534970 |
| 17 | B | | 3749 | 2624 | 528850 |
| 18 | B | 100 | 3884 | 2719 | ∞ |
| 19 | C | | 3308 | 2316 | ∞ |
| 18 | A | 50 | 3983 | 2788 | ∞ |
| 21 | C | | 3787 | 2651 | ∞ |

The transfer function graphs for the two temperature cases were set up using the stiffness and number of load cycle results, as presented in Table 4-14 and Table 4-15. The graphs illustrate the logarithmic value of the number of load cycles [log (N)] plotted against the logarithmic value of the stiffness [log (ε)] for the respective fatigue intervals, see Graph 4-13 and Graph 4-14.

When considering the % Fatigue @ Termination in Table 4-13, it can be seen that for S17-BA @ 100 με and S20-BC @ 50 με at 10˚C no fatigue was experienced. This can be interpreted as the probable endurance limit, as illustrated in Graph 4-13. For the 40˚C case, at strain values of 50 με and 100 με, fatigue was experienced to some degree however when considering the flexural stiffness versus number of load cycle graphs in Appendix A, it is evident that the fatigue experienced after the limiting number of load cycles can be as a result of the initial drop in stiffness. The graphs in Appendix A show that minimum to none fatigue was experienced after the initial drop for the strain values of 50 με and 100 με. It was thus interpreted as a probable endurance limit, as illustrated in Graph 4-14.

The transfer functions aim to supply an equation that is able to predict the fatigue experienced by the investigated mix after a particular number of wheel loads as well as be used for design purposes. The fact that two out of the four strain value cases showed an endurance limit at 10˚C, only two strain cases were used in setting up the transfer functions. It is noted that this yield controversial transfer functions, and it would be recommended to test at supplementary intermediate strain values in future tests. The same apply to the 40˚C case, as again, only two strain values yielded useable results. When considering the fatigue experience percentages in Table 4-13 and the probable endurance limit results for both temperature cases.

The transfer functions for both temperature cases, were set up by fitting a linear function to the data points. In both cases the transfer function equation is questionable due to the high gradient values.

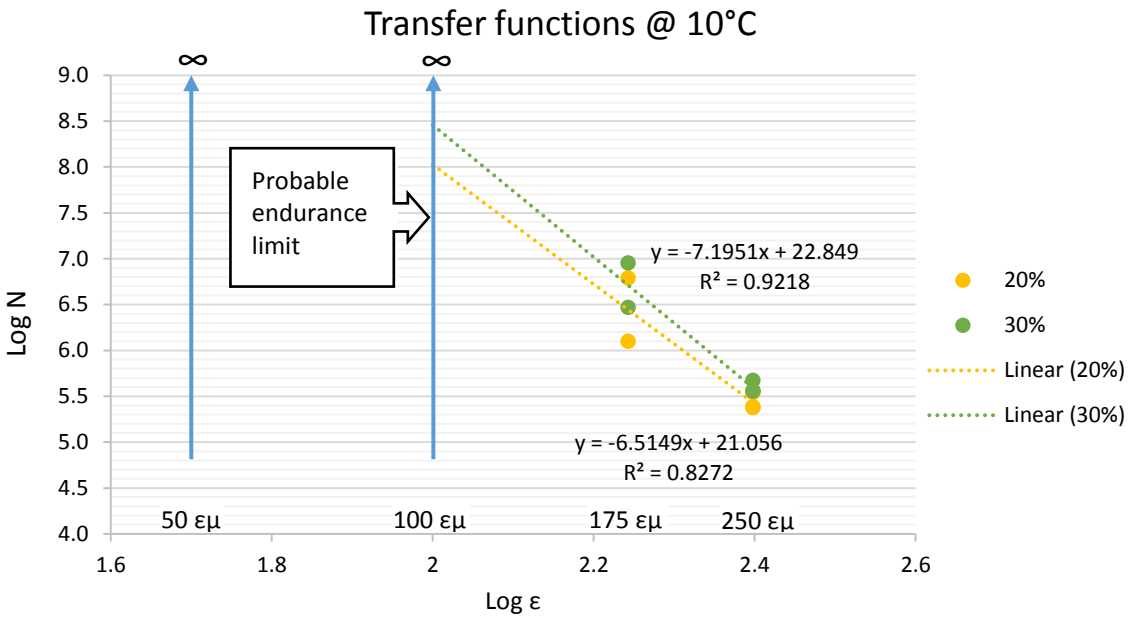


*Graph 4—13: Transfer function @ 10˚C*

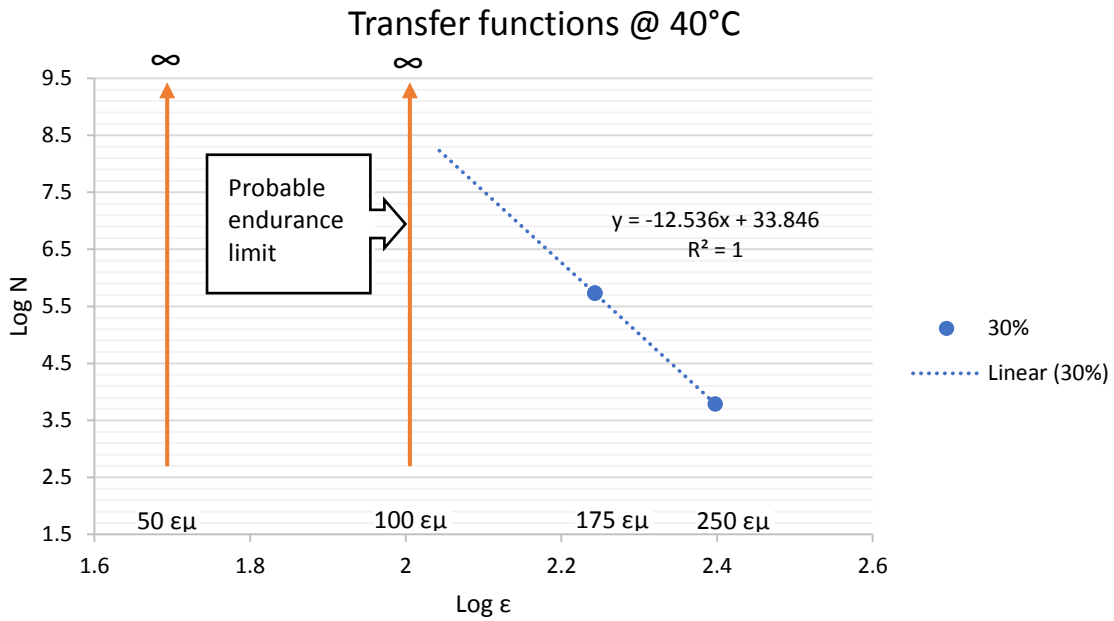


*Graph 4—14: Transfer function @ 40˚C*

## 4.5. NUMERICAL MODELLING

### 4.5.1. Modelling Setup

The numerical modelling of the EME beams, as described in Section 3.7, was performed in order to investigate the initial tensile stresses created in the beams when loaded with a sinusoidal as well as a haversine waveform in the Four Point Beam Test (4PBT). As discussed previously, the reason for doing this is because premature breaking of the beams occurred in some cases where the beams were loaded with a haversine waveform. After investigating the output results from the 4PBT software, for the fatigue classification tests, it was possible to gather the elastic modulus, displacement (amplitude) and initial applied load data for both loading cases. This data was used to simulate the loading cases in ABAQUS FAE. The output results for the fatigue classification tests can be seen in Table 4-16 and Table 4-17, the "bad" data is indicated in red as it was not used to calculate the simulation properties.

*Table 4—16: Data output from 4PBT for haversine loading*

| **Haversine** | | | |
|---|---|---|---|
| Number | Elastic Modulus (MPa) | Initial applied load (N) | Vertical support displacement (mm) |
| S1-BA | 8646 | 1190 | 0.14 |
| S1-BB | 8506 | 1060 | 0.14 |
| S1-BC | 8566 | 1160 | 0.14 |
| S2-BA | 298 | 1500 | N/A |
| S2-BB | 276 | 1520 | N/A |
| S2-BC | 707 | 1480 | N/A |
| S3-BA | 8597 | 688 | 0.14 |
| S3-BB | 314 | 1460 | N/A |
| S3-BC | 8872 | 1360 | 0.14 |
| S4-BA | 5312 | 1450 | N/A |
| S4-BB | 5340 | 1490 | N/A |

*Table 4—17: Data output from 4PBT for sinusoidal loading*

| Sine | | | |
|---|---|---|---|
| Number | Elastic Modulus (MPa) | Initial applied load (N) | Vertical support displacement (mm) |
| S5-BA | 9564 | 870 | 0.14 |
| S5-BB | 7407 | 855 | 0.14 |
| S5-BC | 7862 | 701 | 0.14 |
| S6-BA | 9848 | 1130 | 0.14 |
| S6-BB | 13511 | 349 | 0.14 |
| S6-BC | 9223 | 831 | 0.08 |
| S7-BA | 12051 | 758 | 0.14 |
| S13-BA | 8748 | 927 | 0.14 |
| S13-BB | 8811 | 833 | 0.14 |
| S15-BB | 9509 | 1130 | 0.14 |

ABAQUS FAE software call for the user to define material properties in the form of Young's Modulus and Poisson's ratio for the investigated material. The Young's Modulus for the EME material were calculated by taking the average value of the Elastic Modulus for both loading cases, as presented in Table 4-16 and Table 4-17. The "bad" data, indicated in red, were not used in this calculation. The result for the Young's Modulus and the assumed Poisson's ratio, as used in the modelling can be seen in Table 4-18.

*Table 4—18: Material properties as used in ABAQUS FAE software*

| | Young's Modulus (MPa) | Poisson's ratio (-) |
|---|---|---|
| **Haversine** | 8845 | 0.44 |
| **Sine** | | |

In order to model the two loading cases, the amplitude for both cases had to be define. When considering the vertical support displacement data in Table 4-16 and Table 4-17, it can be seen that the peak to peak displacement for both cases were 0.14 mm. The amplitude for the haversine case was therefore set to be 0.14 mm, and for the sinusoidal case half of the peak to peak displacement, yielding 0.07 mm. The loading profiles for three cycles, as used for the modelling, can be seen in Graph 4-15 and Graph 4-16 respectively.

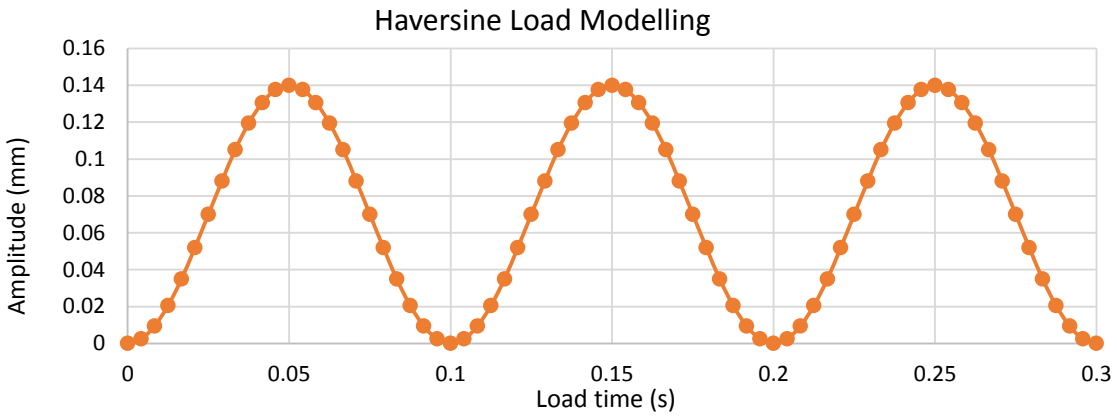


*Graph 4—15: Haversine load modelling profile*

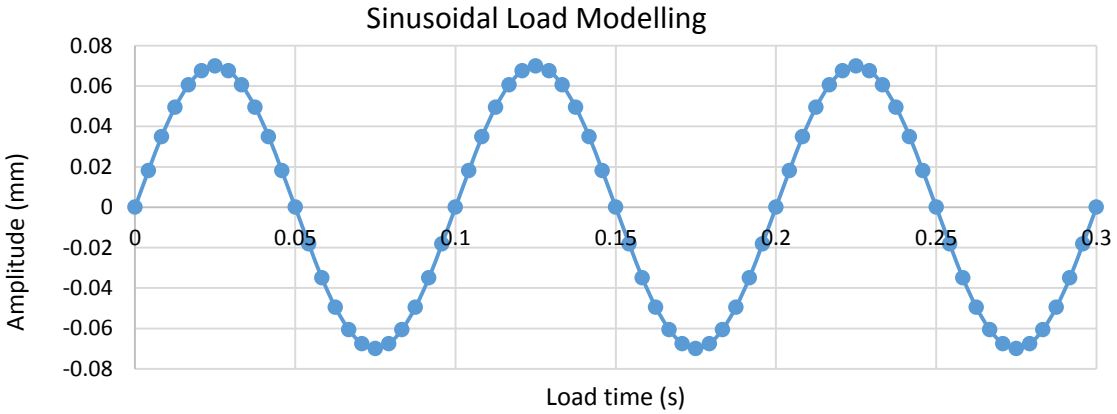


*Graph 4—16: Sinusoidal load modelling profile*

### 4.5.2. Modelling Results

After running the simulated 4PBT setup for the EME material in ABAQUS FAE, the tensile stress results for both loading cases could be investigated. These tensile stresses at the top of the beam specimen can be seen in Figure 4-6 and Figure 4-7, for the haversine and sinusoidal load cases respectively. The maximum tensile stresses are indicated in red, with the blue representing the compressive stresses. These stresses are all measured in the S11 or x-direction (parallel to the length of the beam).

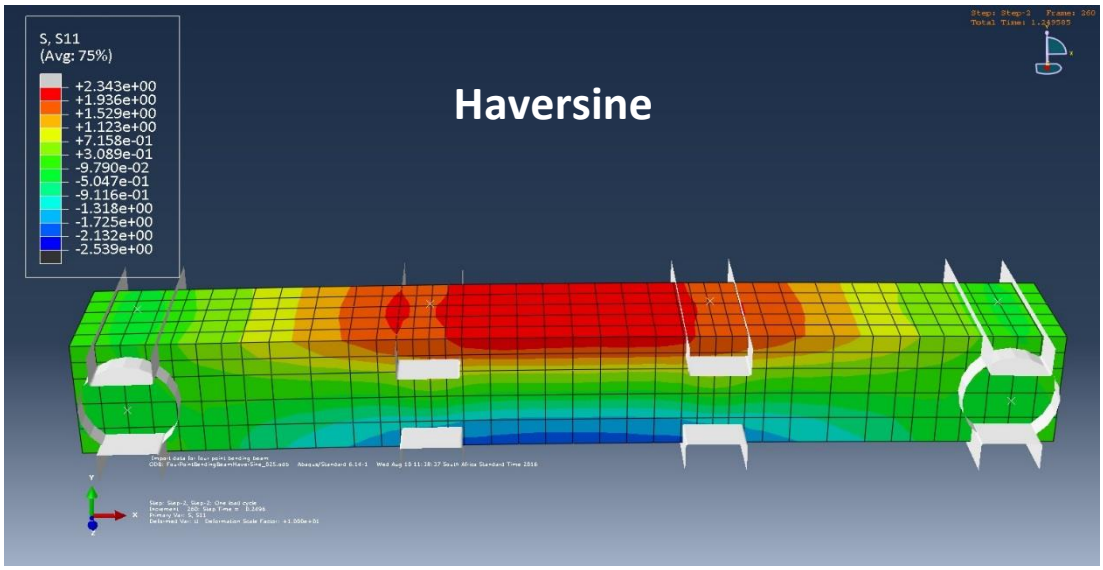


*Figure 4—6: Visual illustration of tensile stresses with haversine loading*

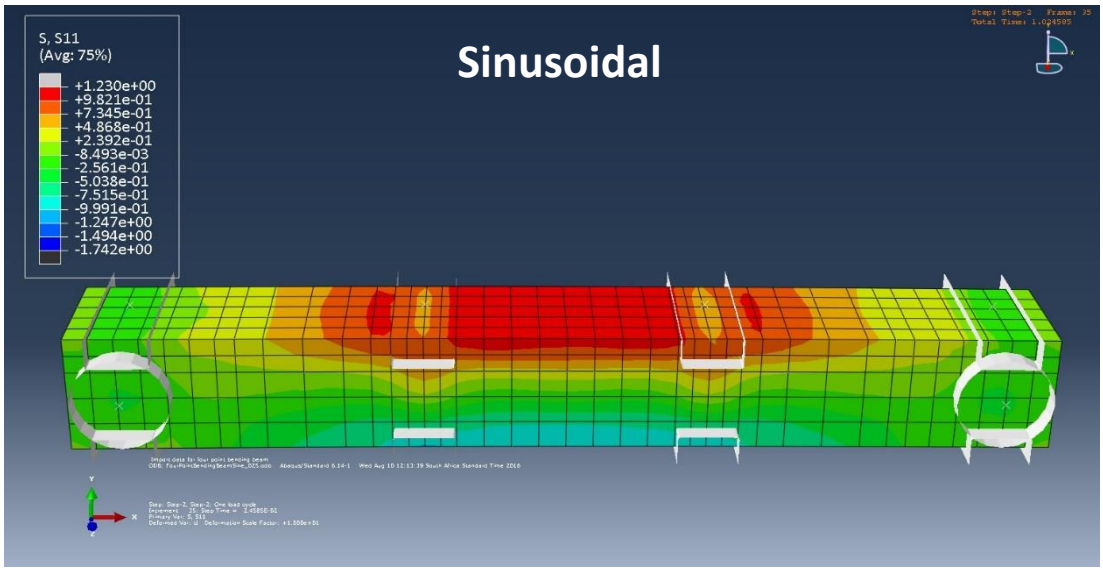


*Figure 4—7: Visual illustration of tensile stresses with sinusoidal loading*

The tensile stiffness results were gathered from the centre point of the investigated nodes, as illustrated in Figure 4-8.

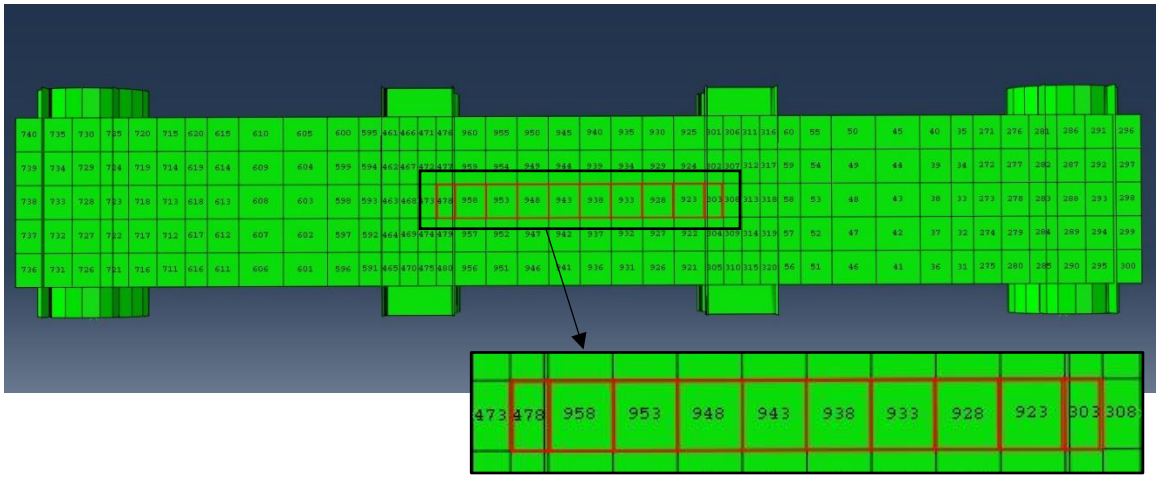


*Figure 4—8: Nodal configuration*

The tensile stiffness results at these nodes, for the haversine and sinusoidal loading cases, can be seen in Table 4-19.

*Table 4—19: Tensile stress results from ABAQUS FAE*

| | Tensile stress (kPa) | |
|---|---|---|
| **Node Number** | **Haversine** | **Sinusoidal** |
| 478 | 2178 | 992 |
| 958 | 2312 | 1197 |
| 953 | 2349 | 1236 |
| 948 | 2297 | 1190 |
| 943 | 2232 | 1132 |
| 938 | 2225 | 1128 |
| 933 | 2275 | 1180 |
| 928 | 2314 | 1219 |
| 923 | 2262 | 1172 |
| 303 | 2106 | 957 |

As expected, the haversine loading case yielded higher tensile stresses than the sinusoidal loading cases. This higher tensile stress may explain the premature failure to a number of beams loaded with a haversine waveform.

### 4.5.3. Manual Validation of Modelled Results

This section will aim to validate the tensile stress results from ABAQUS FAE, by manually calculating the maximum tensile stresses. The maximum tensile stresses were calculated using the following equation together with the average initial applied load as listed in Table 4-16 and Table 4-17:

$$\sigma_t = \frac{0.357P}{bh^2} \qquad \textbf{Equation 4-2}$$

where,

$P$ = load applied by actuator (N)
$b$ = average beam specimen width (m)
$h$ = average beam specimen height (m)

The manually calculated maximum tensile stress results can be seen in Table 4-20.

*Table 4—20: Manually calculated maximum tensile stress*

| **Haversine** | | | |
|---|---|---|---|
| P | b | h | Maximum Tensile Stress |
| 1305 N | 0.063 m | 0.05 m | 2959 kPa |
| **Sine** | | | |
| P | b | h | Maximum Tensile Stress |
| 838 N | 0.063 m | 0.05 m | 1900 kPa |

The manually calculated maximum tensile stress values for both loading cases yielded slightly higher values than the results from the numerical modelling procedure. The overall trend however remains the same for the manually calculated tensile stress values as well as the results from the numerical modelling procedure.

# CHAPTER FIVE

# 5. CONCLUSIONS AND RECOMMENDATIONS

## 5.1. INTRODUCTION

In this, the final chapter, conclusions and recommendations are made based on the research done and results obtained during the study. The conclusions are drawn from the laboratory evaluation and analysis of the test data as presented in chapter four. In addition, where applicable, recommendations are provided based on the findings of this thesis and will aim to assist possible further research on the topic at hand.

The conclusions are summarised with the original primary objective of the study in focus, in order to address the need for a fundamental understanding of EME asphalt as a pavement engineering material.

The recommendations serve as a vital part of the research, as EME testing in South Africa has not yet been conducted on the scale in which it is covered during this study. The recommendations would thus be helpful with regards to future testing and research on the subject.

## 5.2. CONCLUSIONS

The conclusions are structured in the format of the laboratory results, as it was presented in chapter four, starting with the flexural stiffness test followed by the fatigue tests and all of its components.

### 5.2.1. Flexural Stiffness

The following conclusions were drawn with regards to the flexural stiffness tests:

- The EME, as in the case of asphalt pavements, show a stiffness modules increase with decreasing temperature and increasing loading frequency.

- In terms of Master Curve development, Arrhenius equation was sufficient in shifting the frequency-temperature sweep data into a continues curve, with a constant C = 15580 K and at a reference temperature of $T_{ref}$ = 20˚C.

### 5.2.2. Fatigue Behaviour

#### 5.2.2.1. Fatigue Classification

The following conclusions were drawn with regards to the fatigue classification testing:

- Firstly, it can be concluded that the deflection input with regards to the haversine waveform, as used in the ASTM D7460 method, remains haversine throughout the test but as predicted, based on literature, a shift in the neutral axis is found. Because of the shifted position of the neutral axis, the developed strain and stress pulses change to an effective sinusoidal waveform after a few cycles. For this reason, it appears unnecessary to use a haversine waveform in the 4PBT.
- The fatigue testing protocols, as defined in AASTHO T321, can be concluded to be the best approach to the 4PBT. This approach is also prescribed by Sabita Manual 33, as it utilises a sinusoidal waveform.
- It was concluded that the void percentage of a beam sample has an effect on the pavement life. In the cases where the beams were loaded with a haversine loading waveform, premature failure to the beams occurred at low void percentages (between 2.06% and 2.49%) as a result of stress concentration that is created in the beam specimens due to the low void percentages. The highest number of load cycles were encountered at a void percentage of 2.92%.
- From the sinusoidal loading case results, it was concluded that at low void percentages the beams yielded the best pavement life (voids between 2.92% and 3.69%)

#### 5.2.2.2. Fatigue

The following conclusions were drawn with regards to the fatigue tests:

- The failure criteria of 50% fatigue reduction is not appropriate and too strict in terms of EME. In most cases, after 4000000 load cycles, the fatigue experienced did not reach close to the 50% fatigue reduction point.

#### 5.2.2.3. Endurance limit and Transfer functions

The following conclusions were drawn with regards to the endurance limit and transfer functions for EME at 10˚C as well as 40˚C:

- As mentioned, the endurance limit can be concluded to be a certain strain limit below which no fatigue will occur. The EME showed that a probable endurance limit exists at a strain value of 100 με, for the 10˚C case. However, the exact strain value at which the endurance limit is located will have to be refined with further testing.
- At a temperature of 40˚C, no sign of a possible endurance limit was found. However, the percentage fatigue at termination (4 000 000 load cycles) decreased substantially as the strain level got lower.
- At both temperature intervals (10˚C and 40˚C), the illustrated transfer functions for the fatigue cases, cannot be seen as reliable design transfer functions, as it only represents a function between two strain points. This can be attributed to the fact that at two out of the four investigated strain cases, an endurance limit was encountered. In this regard, for future testing, it would be advisable to refer to the recommendations made on this subject.
- It can be concluded that the endurance limit be regarded as function of the damage. This is due to the fact that the fatigue experienced decreased as the testing strain values got closer to the probable endurance limit strain value.

## 5.3. RECOMMENDATIONS

### 5.2.1. Flexural Stiffness

In terms of the frequency-temperature sweeps and the Master Curve development, it will be recommended that additional frequency-temperature sweep tests be done at lower frequencies or at higher temperatures.

### 5.2.2. Fatigue Behaviour

#### 5.2.2.1. Fatigue Classification

For fatigue classification purposes it is recommended that the protocols, as defined in AASTHO T321, be followed. This is also defined in Sabita Manual 33: *Interim Procedure for the Design of High Modulus Asphalt (EME)*.

#### 5.2.2.2. Fatigue

For the fatigue tests it would be recommended to review the 40˚C testing temperature, or preferably to add an intermediate testing temperature of around 20˚C. At the 40˚C testing temperature, no noteworthy tensile strains are developed in the asphaltic layer in a pavement structure, generally only compression strains. This is due of the fact that at 40˚C, the material stiffness of the asphaltic material tends to be close to that of the underlying layer i.e. a modular ratio close to one.

#### 5.2.2.3. Endurance limit and Transfer functions

Based on the transfer function graphs, and the shortcomings that were experienced with regards to the strains at which fatigue tests were done, it will be recommended future testing be done at intermediate strain values. It will also be recommended that at least three tests be done at the primary strain values. If the main objective of future tests were to be the setup of transfer function for EME design purposes, it would be recommended to consider the test matrix, illustrated in Table 5-1:

*Table 5—1: Recommended test matrix for Transfer Function development*

| Strain Value (με) | Number of tests |
|---|---|
| 100 | 3 |
| 130 - 140 | 2 |
| 175 | 3 |
| 200 - 210 | 2 |
| 250 | 3 |
| 280 - 300 | 2 |

The recommended testing matrix is set up with the assumption that the amount of beams available for testing is not a constraint, as 15 beams are required. The idealized transfer function graph will look like the example illustrated in Graph 5-1.

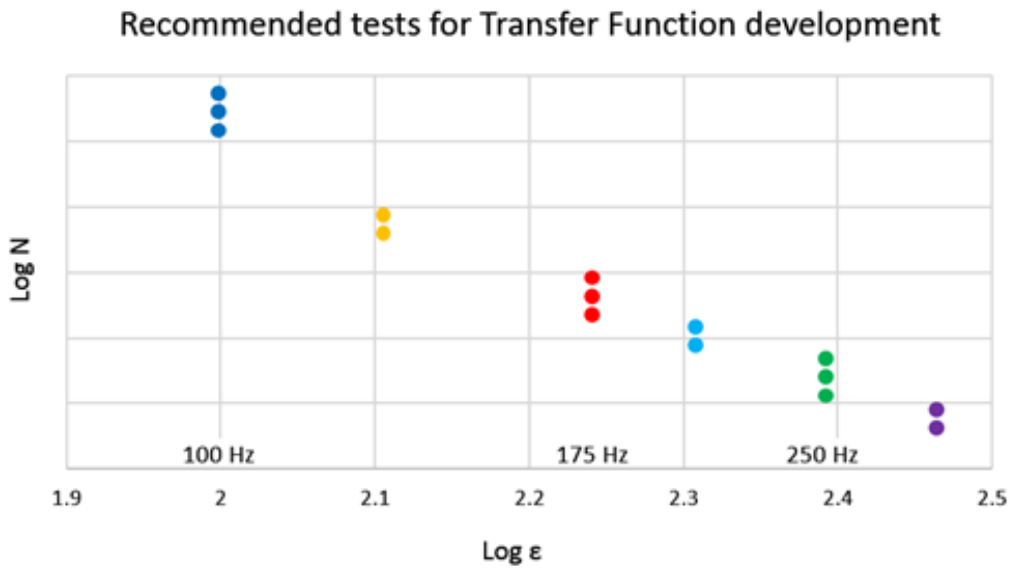


*Graph 5—1: Recommended tests for Transfer Function development*

# REFERANCES


1. Adhikari, S., Shen, S. & You, Z., 2009. Evaluation of Fatigue Models of Hot-Mix Asphalt Through Laboratory Testing. *Journal of the Transportation Research Board,* Issue 2127, pp. 36-42.

2. Airey, G., 1995. *Fatigue Testing of Asphalt Mixtures Using a Third Point Loading Fatigue Testing System,* South Africa: University of Pretoria.

3. ASTM International, 2010. *Standard Test Method for Determining Fatigue Failure of Compacted Asphalt Concrete Subjected to Repeated Flexural Bending - D760-10,* Pennsylvania, United States: ASTM International.

4. Ayers, M., 2006. *Status of the Mechanistic - Emperical Pavement Design Guide (M-EPDG),* Washington, DC: American Concrete Pavement Association.

5. Baladi, G., 1989. Fatigue life and permanent deformation characteristics of asphalt concrete mixes. *Transportation Research Record,* Volume 1227, p. 75–87.

6. Barksdale, R., 1978. Partical application of fatigue and rutting tests on bituminous base mixes. In: 47, ed. Minneapolis: Asphalt Paving Technol, p. 115–159.

7. Bonnaure, F., Gravois, A. & Udron, J., 1980. A New Method of Predicting the Fatigue Life of Bituminous Mixes. *Proceedings of Association of Asphalt Paving Technologists,* Volume 49, pp. 499-529.

8. Brown, E. et al., 1996. *Hot Mix Asphalt Materials, Mixture Design and Construction,* Maryland, USA: National Centre For Asphalt Technology (NCAT).

9. Brown, S., 1973. Determination of Young's Modulus for Bituminous Materials in Pavement Design. *Highway Research Record ,* Volume 431, pp. 38 - 49.

10. Carpenter, S., Ghuzlan, K. & Shen, S., 2003. Fatigue Endurance Limit for Highway and Airport Pavements.. *Transportation Research Record: Journal of the Transportation Research Board,* pp. 131-138.

11. Castelo, B. et al., 2008. Fatigue Analysis of Asphalt Mixtures Independent of Mode of Loading. *Journal of the Transportation Research Board, No. 2057,* pp. 149-156.

12. Cloete, R., 2015. *FATIGUE PERFORMANCE OF SEALS,* Stellenbosch: Stellenbosch University.

13. Corté, J.-F., 2001. *Development and Uses of Hard-Grade Asphalt and of High-Modulus Asphalt Mixes in France,* Washington: Transportation Research Circular.

14. Denneman, D. E. & Petho, D. L., 2013. *EME Technology Transfer to Australia: An Explorative Study,* Sydney: Austroads Ltd.

15. Denneman, D. E., Petho, D. L., Beecroft, A. & Griffin, J., 2014. *High Modulus High Fatigue Resistance Asphalt (EME2) Technology Transfer,* Sydney: Austroads Ltd..

16. Denneman, E., 2011. *High Modulus Asphalt (HiMA) trial Mix & pavement design,* Pretoria: CSIR.

17. Department of Transport and Main Roads, 2015. *TN 142 High Modulus Asphalt (EME2) Pavement Design,* Queensland: State of Queensland.

18. ENGEN, 2009. *Engen Penetration Grade Bitumens.* [Online] Available at: http://www.engen.co.za/downloads/products_and_services/chemicals_sp/products/bitumen/penetration_grades.pdf
[Accessed 2 June 2016].

19. Epps, J. & Monismith, C. L., 1971. *Fatigue of asphalt concrete mixture-summary of existing information,* Philadelphia: ASTM.

20. Francken, L. & Clauwaert, C., 1988. Characterization and Structural Assessment of Bound Materials for Flexible Road Structures. *Proceedings 6th International Conference on the Structural Design of Asphalt Pavements,* University of Michigan(Ann Arbor, MI, USA), pp. 130-144.

21. Goddard, R. T. N., Powell, W. D. & Applegate, M. W., 1978. *Fatigue resistance of dense bitumen macadam: the effect of mixture variables and temperature,* Crowthorne, UK: Transport and Road Research Laboratory.

22. Heukelom, W., 1966. Observations on the rheology and fracture of bitumens and asphalt mixes. *Association of Asphalt Paving Technologies,* Volume 35, pp. 358-399.

23. IPC (Industrial Process Control Ltd), 1998. *Beam fatigue apparatus,* Boronia, Australia: Reference Manual.

24. Jacobs, M., 1995. *Crack Growth in Asphaltic Mixes,* Netherlands: Delft University of Technology.

25. Jaoude, A., 2015. Analytic and linear prognostic model for a vehicle suspension system subject to fatigue. *Systems Science & Control Engineering: An Open Access Journal,* pp. 81-98.

26. Jenkins, K., 2000. *Mix Design Considerations For Cold and Half-Warm Bituminous Mixes with Emphasis on Foamed Bitumen,* South Africa: University of Stellenbosch.

27. Lytton, R. et al., 1993. *Development and Validation of Performance Prediction Models and Specifications for Asphalt Binders and Paving Mixes,* Washington DC, USA: SHRP Report A-357.

28. Mashaan, N. S. et al., 2014. Evaluation of Fatigue Life of CRM-Reinforced SMA and Its Relationship to Dynamic Stiffness. *The Scientific World Journal,* Volume 2014(Article ID 968075).

29. Mbaraga, A., 2011. *MASTER CURVE AND FATIGUE TESTING OF WARM MIX ASPHALT,* South Africa: Stellenbosch University.

30. Medani, T. & Huurman, M., 2003. *Constructing the Stiffness Master Curves for Asphaltic Mixes ,* Delft: Delft University of Technology.

31. Medani, T. & Molenaar, A., 2003. *Estimation of fatigue characteristics of asphalt mixes using simple tests,* The Netherlands: Wegbouwkundige werksdagen.

32. Molenaar, A., 2007. Prediction of Fatigue Cracking in Asphalt Pavements. *Journal of the Transportation Research Board,* 10.3141/2001-17(Transportation Research Record 2001), pp. 155-162.

33. Monismith, C., Epps, J. & Finn, F., 1985. Improved Asphalt MixDesign. *Journal of the Association of Asphalt Paving Technologists,* Volume 55, pp. 347-406.

34. NCHRP Report 646, 2010. *Validating the Fatigue Endurance Limit for Hot Mix Asphalt,* WASHINGTON, D.C.: NATIONAL COOPERATIVE HIGHWAY RESEARCH PROGRAM.

35. Pavement Interactive, 2007. *Penetration Grading.* [Online] Available at: http://www.pavementinteractive.org/article/penetration-grading/ [Accessed 30 May 2016].

36. Pavement Interactive, 2007. *Viscosity Grading.* [Online] Available at: http://www.pavementinteractive.org/article/viscosity-grading/ [Accessed 30 May 2016].

37. Pavement Interactive, 2008. *Asphalt.* [Online] Available at: http://www.pavementinteractive.org/article/materialsasphalt/ [Accessed 30 May 2016].

38. Pavement Interactive, 2008. *Superpave Performance Grading.* [Online] Available at: http://www.pavementinteractive.org/article/superpave-performance-grading/ [Accessed 31 May 2016].

39. Pavement Interactive, 2011. *Flexural Fatigue.* [Online] Available at: http://www.pavementinteractive.org/article/flexural-fatigue/ [Accessed 1 June 2016].

40. Pell, P. S. & Cooper, K. E., 1975. The Effect of Testing and Mix Variables on the Fatigue Performance of Bituminous Materials. *Journal of the Association of Asphalt Paving Technologists,* Volume 44, pp. 1-37.

41. Pell, P. S. & Cooper, K. E., 1975. The Effect of Testing and Mix Variables on the Fatigue Performance of Bituminous Materials. *Journal of the Association of Asphalt Paving Technologist,* Volume 26, p. 5618–5622.

42. Raithby, K. D. & Ramshaw, J. T., 1972. *Effects of secondary compaction on the fatigue performance of a hot-rolled asphalt,* Crowthrone: Transport and Road Research Laboratory.

43. Raithby, K. & Sterling, A., 1972. *Some effects of loading history on the fatigue performance of rolled asphalt, Laboratory Report 496,* Crowthorne: Tranport and Road Research Laboratory.

44. Read, J., 1996. *Fatigue cracking of bituminous paving mixtures,* Nottingham: University of Nottingham.

45. Read, J. M. & Collop, A. C., 1997. Partical fatigue characterisation of bituminous paving mixture. *Journal of the Association of Asphalt Paving Technologist,* Volume 66, pp. 74-108.

46. Read, J. & Whiteoak, D., 2003. *The Shell Bitumen Handbook.* 5th ed. Shell Bitumen UK: Thomas Telford Publications.

47. Roberts, F., Kandhal, P., Brown, E. & Lee, D. a. K. T., 1996. *Hot Mix Asphalt Materials, Mixture Design, and Construction..* 2nd Edition ed. Lanham: National Asphalt Pavement Association Education Foundation. .

48. Roberts, F. L. et al., 1991. *Hot Mix Asphalt Materials, Mixture Design and Construction.* Maryland: National Asphalt Paving Association.

49. Sabita Manual 33, 2013. *Interim design procedure for high modulus asphalt,* South Africa: Sabita.

50. Sanders, P. & Nunn, M., 2005. *The application of Enrobés à Module Elevé in flexible pavements,* UK: TRL Limited.

51. Shen, S. & Carpenter, S., 2005. Application of the Dissipated Energy Con-cept in Fatigue Endurance Limit Testing.. *Transportation Research Record: Journal of the Transportation Research Board,* pp. 165-173.

52. Shen, S. & Carpenter, S., 2007. Development of an Asphalt Fatigue ModelBased on Energy Principles.. *Journal of the Association of Asphalt PavingTechnologists,* pp. 525-574.

53. SHRP, 1994. *Fatigue Response of Asphalt-Aggregate Mixes,* Strategic Highway Research Program: National Research Council.

54. Tangella, R., Claus, J., Deacon, J. & Monismith, C., 1990. *Summary Report on Fatigue Response of Asphalt Mixtures,* University of California, Berkeley, California, USA: Strategic Highway Research Project A-003-A: TM-UCB-A-003-A-89-3.

55. Theyse, H., 2015. *South African Road Design System - Recursive Performance Simulation,* South Africa: SANRAL.

56. Tuate, A., Verhaeghe, B. & Visser, A., 2001. *Interim Guidelines For Design of Hot Mix Asphalt in South Africa,* Pretoria, South Africa: CSIR.

57. Twagira, E., 2006. *Characterization of Fatigue Performance of Selected Cold Bituminous Mixes,* South Arica: University of Stellenbosch .

58. Walubita, L. & Ven, M. v. d., 2000. *STRESSES AND STRAINS IN ASPHALT-SURFACING PAVEMENTS ,* South Africa: South African Transport Conference.

59. Witczak, M., Mamlouk, M., Souliman, M. & Zeiada, W., 2013. *Laboratory Validation of an Endurance Limit for Asphalt Pavements (NCHRP REPORT 762),* WASHINGTON, D.C.: NATIONAL COOPERATIVE HIGHWAY RESEARCH PROGRAM.

# APPENDIX A